Multidentate NHC complexes of Group IX metals featuring carbon-based tethers: synthesis and applications

Estefan van Vuuren, Frederick P. Malan,* Marilé Landman*

Department of Chemistry, University of Pretoria, Hatfield, Pretoria, South Africa, 0002

Highlights

•Synthesis and properties of Co, Rh and Ir NHC complexes with carbon-based tethers.

•Imidazolylidene ligands and derivatives as frameworks in metallacyclic complexes.

•Twelve different homogeneous catalytic applications employing these complexes.

•Photochemical and biological applications of the complexes in this study.

Abstract

Incorporation of N-tethers to N-heterocyclic carbene ligands to form a powerful class of multi-dentate, responsive ligand frameworks that have proven to be more than just ancillary ligands with reported success and usefulness in a multitude of applications. NHC complexes of group IX transition metals (Co, Rh, Ir) have enjoyed considerable research interest over the last two decades, owing to their vast range of accessible oxidation states, favourable stabilities and

---

Abbreviations: A, Ampere; acac, acetylacetonate; ad, adenyl; BODIPY, boron dipyrromethene; bpin, pinacolboryl; coe, cyclooctene; cod, 1,5-cyclooctadiene; Cp, cyclopentadienyl; Cp*, cyclopentadienyl; DCE, dichloroethane; DCM, dichloromethane; DFB, 2,6-difluorobenzene; DPEPO, bis[2-(diphenylphosphino)phenyl]ether oxide; Dipp, diisopropylphenyl; IDipp, bis(diisopropylphenyl)imidazolylidene; IMes, bis(mesityl)-imidazolylidene; KHMDS, Potassium bis(trimethylsilyl)amide; Mes, mesityl; napht, naphthalene; nbd, 2,5-norbornadiene (bicyclo[2.2.1]hepta-2,5-diene); NHC, N-heterocyclic carbene; PGM, platinum group metal; SCXRD, Single Crystal X-Ray Diffraction; SIDipp, bis(diisopropylphenyl)imidazolinylidene; ^{t}AmOH, *tert*-amyl alcohol; TOF, turnover frequency (h^{-1}); TON, turnover number; TlCp, cyclopentadienyl thallium; TSPO1, diphenyl-4-triphenylsilylphenylphosphine oxide; VT-NMR, variable temperature nuclear magnetic resonance.

* Corresponding author.

E-mail address: marile.landman@up.ac.za (M. Landman); frikkie.malan@up.ac.za (F.P. Malan)

reactivities, as well as multi-functional use. The inclusion of carbon as a secondary binding atom has been extremely useful to help enable the resulting metal complex for complex C-H activation, small molecule fixation and activation, and unusual migratory insertion reactions. This comprehensive review communicates results that demonstrate the versatility of this carbon-based multidentate ligand series through inclusion of synthetic routes available to access the metal-NHC complexes, their associated stability and reactivity pathways, as well as advances made in several different applications, most notably homogeneous catalysis.

Graphical abstract

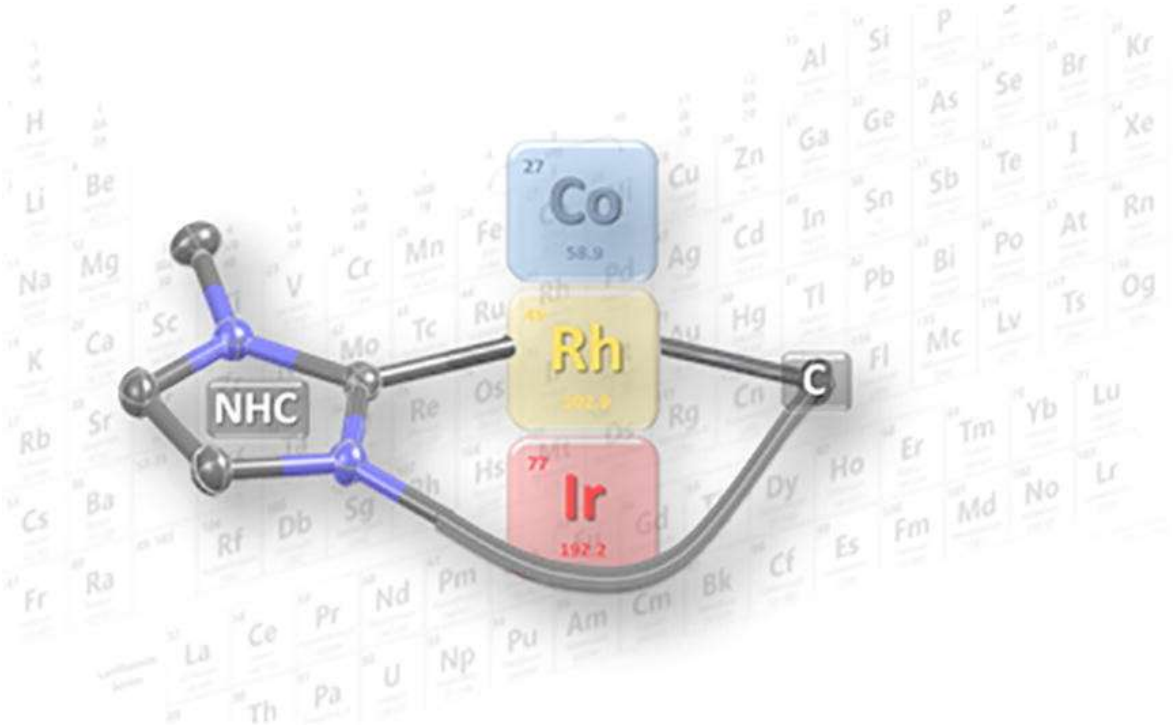

Keywords: N-heterocyclic carbene; cobalt; rhodium; iridium; cyclometallated

Contents

1. Introduction

N-heterocyclic carbenes (NHCs) are integral to modern coordination chemistry and have proven to be more than spectator ligands. Several extensive libraries containing different functionalised N-heterocycles have been developed over the past 20 years [1-3]. NHCs' easy accessibility, steric and electronic tunability as well as the relatively high degree of stability of their metal complexes have allowed NHCs to be tailored for use in a wide range of applications including catalysis [4], electrochemistry [5], photophysics [6,7], materials science [8] and medicinal chemistry [9].

During the last decade, various new and interesting classes of NHCs have been reported and notably include cyclic amino alkyl carbenes (CAACs) [10], ring expanded NHCs [11], NHCs containing multiple heteroatoms [12], abnormal (aNHC) [13,14] or mesoionic carbenes (MICs) [13,15], and ditopic carbanionic carbenes [14], each with their own associated structural and electronic properties, bonding characteristics, stability, and reactivity. Mesoionic carbenes are dipolar compounds whereas normal and abnormal NHC's are neutral. The inherent nature of the imidazolylidenes, the most common class of NHC ligands, allows for pre- [16-18] and post-coordination [19] functionalisation in order to incorporate a plethora of functional groups that could confer extra stability or exhibit favourable interactions with the metal core. These functional groups often provide an additional means for (reversible) secondary coordination, an attractive feature that has proved useful in catalysis [12]. This favourable property of "smart" ligands [20] is often described as hemilability, which may be an important factor in improving catalyst activity [21,22] through dissociation from the metal centre on command, followed by rapid re-coordination for metal complex stabilisation.

With respect to transition metal complexes incorporating NHC ligands, a wide range of group IX complexes have been reported which include examples of the earth-abundant cobalt, as well as the highly catalytically active and versatile Rh and Ir metals (Chart 1). These three metals

exhibit a rich oxidation state chemistry, ranging from -1 to +4 for cobalt, -1 to +5 for rhodium, and impressively from -3 to +9 for iridium [23-27]. Therefore, a diverse range of catalytic transformation reactions, including carbon-carbon coupling [28,29], hydrogenation [17,30-34], transfer hydrogenation [17,35-40], hydrosilylation [41], secondary alcohol oxidation [42], water oxidation [4,43-45], amination [46], and hydroformylation [47-49] are feasible with complexes of group IX metals as catalysts.

Chart 1. Number of published articles per year on NHC complexes of group IX metals.[a]

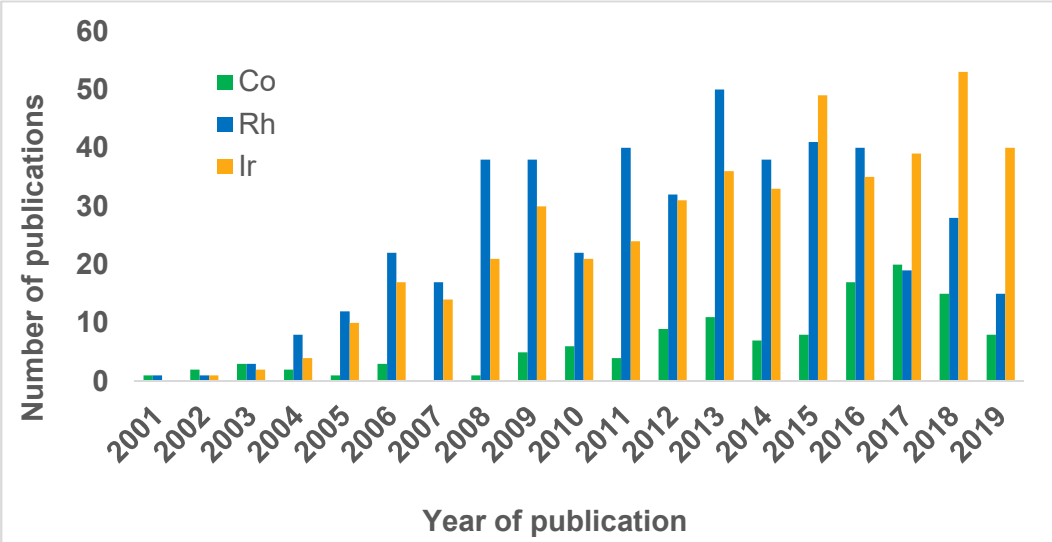

[a] Search was conducted using the Scopus database (2020) with keywords "NHC" and "carbene" and either "cobalt", "rhodium", or "iridium" featuring in the title, abstract or keyword descriptions.

Of particular interest in this review is the incorporation of neutral and anionic carbon-based tethers on the NHC ligand, capable of stabilising a range of Group IX metal complexes in a range of different oxidation states. The set of ligand motifs reviewed has been restricted to the 2- and 4-imidazolylidenes (normal and abnormal varieties) and 2-imidazolinylidenes, as most examples reviewed are based on these skeletal groups. Therefore, ligands that are of interest include NHCs where secondary bonding through an olefin alkene tether (η^2-type bonding, Figure 1 **A**) features as a class of LL-type ligands. Many NHC ligands with hydrocarbon moieties in the vicinity of a metal cation are susceptible to nucleophilic attack upon which cyclometallation occurs (Figure 1 **B**, LX-type). This is a common feature with N-mesityl substituents on IMes (bis-mesityl imidazolylidene) ligands and other long-chain aliphatic substituents. Classical cyclometallated metal-arene systems (LX-type) qualify as a third category (Figure 1 **C**). A unique class of L_2X-type ligands featuring an NHC ligand and an appended cyclopentadienyl-based group is illustrated in Figure 1 **D**. In this review, examples

of multi-carbenes (where the second NHC may qualify as a C-donor tether) is excluded to avoid extensive overlap with several outstanding published reviews [2,50-52] exclusively covering the chemistry of mono- and poly-NHC complexes of transition metals. However, some bis-NHC ligands which bind simultaneously in either a monometallic or bimetallic manner are also included only if an additional carbon-coordinated fragment exists within the ligand structure. There are also several detailed reviews [2,53,54] covering transition metal complexes with functionalised NHC ligands – their syntheses, characteristics and applications, where some focus specifically on cobalt- [55], rhodium- [56] and iridium-NHC complexes [4,54], cyclometallated Ir(III) and Rh(III) complexes with a few NHC examples [57,58], and oxygen-functionalized metal NHC complexes [4].

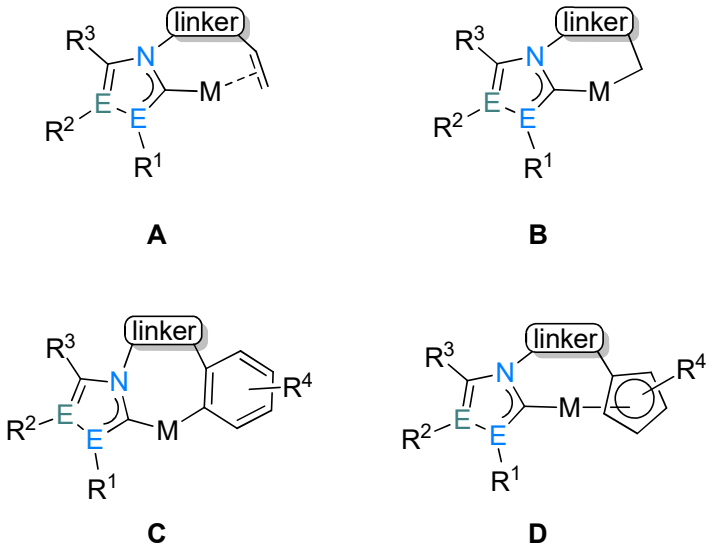

Figure 1. Multi-dentate imidazolyl-based NHC's binding *via* a carbon tether. R^1 – R^4 = alkyl, arene; E = C(R^x), N. Linker = aliphatic/arene-based moieties.

This up-to-date review is unique in highlighting the rich chemistry of M-C (M = Co, Rh, Ir) bonds incorporated in different carbon-tethered NHC ligand scaffolds, and the interesting stability, reactivity, and application possibilities associated with these. In unique and unusual cases, the structural features of the metal complexes are explored. Concerning the complex application sections, unusual transformation reactions of the NHC metal complexes, the underlying mechanisms, as well as the associated catalytic implications have been emphasised.

2. Synthesis and characterisation of Cobalt NHC complexes

While cobalt is the most earth abundant group IX metal, it is interesting to note that a significantly smaller contribution of work relevant to this review is found for cobalt as compared to the popularly studied rhodium and iridium metals. In the following examples, the most common oxidation states of Co are +1, +2, and +3 (in that order). This part is organized into sections according to the type of carbon-based tether present in an NHC ligand. The synthetic and reactivity routes and characterisation of each of the complexes are described in each section.

2.1. Carbene complexes with alkene-based tethers

This class of ligands are based on the alkene tethered NHCs from class **A** (Figure 1). This series of complexes remained unexplored until very recently when the group of Kunz [59] reported the first two examples. Two unique synthetic routes were identified in which the bis(imidazolylidene)carbazolide cobalt(I) complex (**2**) could be synthesised. The first route involves the direct transmetallation of the lithiated biscarbene ligand with $CoCl(PPh_3)_3$, whereas the second is a two-step process. Transmetallation with $CoCl_2$ is followed by reduction of Co(II) to Co(I) (Scheme 1). During the two-step process, the paramagnetic, brown Co(II)-NHC intermediate **1** is formed, where only one alkene tether is coordinated to the cobalt centre. Reduction of Co(II) to Co(I) in complex **1** is then mediated by KC_8 to form the red, diamagnetic complex **2**. The molecular structures of both complexes **1** and **2** were fully elucidated to illustrate their distorted trigonal bipyramidal geometries with the NHC moieties in the axial positions.

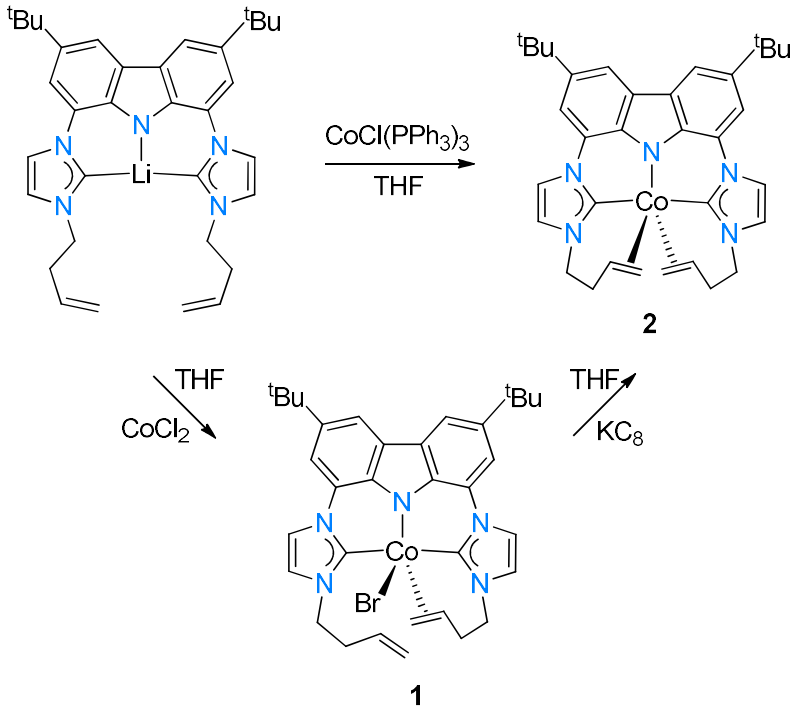

Scheme 1. Synthesis of **2** *via* two synthetic routes.

2.2 Cyclometallated carbene complexes with alkyl-based tethers

In this section, bidentate NHC scaffolds of type **B** (Figure 1) will be discussed. Carbon-based tethered carbene complexes of Co remain relatively limited, with the first case of C-H activated cyclometallation of an NHC ligand only reported in 2015. Deng and co-workers [60] reported that the three-coordinated cobalt(0) complex featuring an IMes ligand undergoes cyclometallation with a methyl group of the IMes ligand upon reaction with 2,6-dimesitylphenyl azide ($DmpN_3$) (Scheme 2) to form the Co(II) complex **3**. Use of the bulkier IDipp (bis(diisopropylphenyl)imidazolylidene) analogue failed to provide the desired cyclometallation product but formed the linear Co(II) imido complex adduct instead. Gao *et al.* [61] reported a paramagnetic cobalt(I)-NHC complex that was able to react with $LiCH_3$, $LiCH_2SiMe_3$, or NaCp to result in NHC-based cyclometallated Co(I) and Co(II) products **4-6** (Scheme 2). From the X-ray crystallographic studies of complexes **4-6**, the Co-C_{NHC} bond distances (1.869(4)-1.939(2) Å) were shorter than the corresponding Co-$C_{Ad/Mes}$ bond distances (1.934(9)-2.032(2) Å).

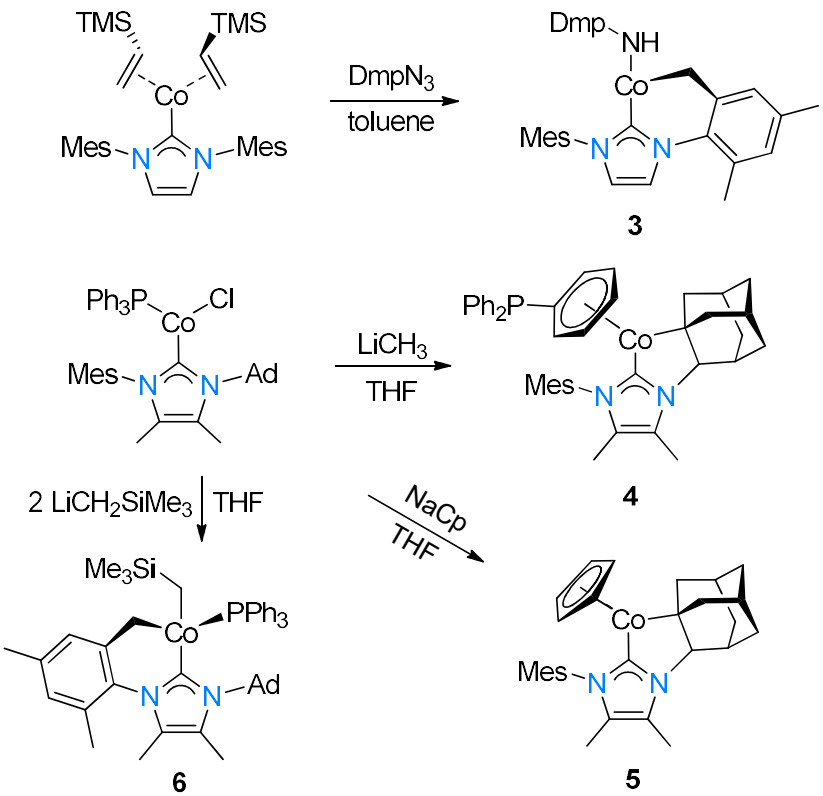

Scheme 2. Cyclometallation of Co(0) and Co(I) complexes to give **3**-**6**.

Other notable examples also emanate from studies by the group of Deng and Wang [62-67], who reported on similar cyclometallation reactions observed for monocarbene Co-NHC complexes as discussed above, but in this case for biscarbene complexes. As part of their aim to expand on Co(0)-NHC biscarbene complexes, they reported that the reduction reaction of [CoCl(IMes)$_2$] with Na/Hg amalgam (in the absence of an alkene) initiated C-H activation at the formed Co(0) centre, and subsequently yields the red bis-cyclometallated NHC complex **7** (Scheme 3) in moderate yield (60%). A later report [64] showed that **7** could also be directly accessed from the free imidazolylidene ligands (two equivalents), $CoCl_2$, and two equivalents of Na/Hg amalgam. The authors [63] reported that cyclometallation involving only one NHC ligand could be mediated by reaction of the precursor complex [CoCl(IMes)$_2$] with organolithium ($LiCH_3$, $TMSCH_2$) or Grignard reagents (p-MePhMgBr), with concomitant N_2 fixation when performed under an atmosphere of N_2 (1 atm.) (**8**). The long N-N distance of the coordinated N_2 ligand in **8** (from the SCXRD molecular structure) in addition to the stretching frequency of 2006 cm^{-1} indicated that the N_2 is weakly coordinated to the Co(I) centre. The migratory insertion reactivity of the cyclometallation products was studied with the aim of discovering the possibility of cobalt-mediated C(sp^3)-H bond functionalisation [63]. It was found that **7** reacts with 2,6-Me$_2$-PhO-COCHN$_2$, 2,6-Me$_2$-PhNHC, and an excess of CO gas to

yield the novel N- or C-inserted cobalt complexes **9-11** (Scheme 3). Complexes **9** and **10** did not react further with additional equivalents of diazo or isocyanide compounds, which was proposed to be due to steric congestion.

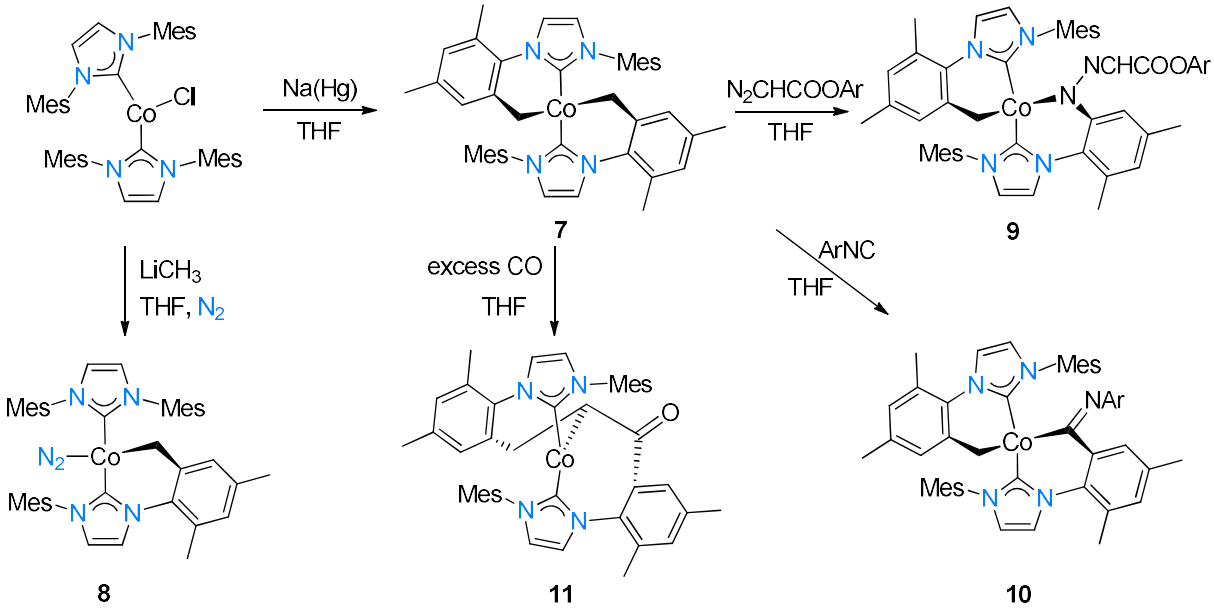

Scheme 3. Synthesis and reactivity of mono- and bis-cyclometallated cobalt NHC complexes **7-11**.

The first silyl-donor functionalised NHC complex featuring a cobalt metallacycle was reported in 2013 by the group of Deng [64]. They observed that addition of one equivalent of $PhSiH_3$ to a benzene solution of **7** at room temperature resulted in a gradual colour change of dark-brown to green, with evolution of gas (H_2). The silyl-donor-functionalised NHC complex **12** was isolated as yellow-green crystals in moderate yield (63%) (Scheme 4). The reaction of **7** with either $PhMeSiH_2$ or Ph_2SiH_2 in benzene occurs slowly at room temperature, and faster (4 hours) at 70 °C to give corresponding yellow-green complexes **13** and **14**. In a later report [66] they showed that the cyclohexyl NHC derivative of **14** could also be accessed by reacting the Co(0) complex $[Co(IMesCy)_2(CH_2CH(TMS))]$ (analogue shown in Scheme 2) with H_2SiPh_2 to form the silyl complex $[CoH(HSiPh_2)(IMesCy)_2]$, which then spontaneously converts to the cyclometallated derivative **14** at room temperature. Complex **7** was unreactive when treated with either $(EtO)_3SiH$ or Ph_3SiH at room temperature, which after subsequent heating of the reactions to 70 °C resulted in pale-yellow suspensions from which no isolated products could be recrystallized. SCXRD diffraction studies confirmed that all the complexes **12-14** exhibited distorted square-planar cobalt(II) centres with two anionic bidentate ligands, with the $[IMesSi]^-$

ligand fragment leading to the formation of a boat-shaped seven-membered ring with a bite angle of almost 90° (88.5(1)-91.5(1)°). Deng and co-workers [62] continued to investigate the reactivity of **14** (Scheme 4): Reaction of **14** with one equivalent of $[Cp_2Fe][BPh_4]$ in Et_2O resulted in a red suspension from which the diamagnetic hydrido complex $[(CSiC)CoH(OEt_2)][BPh_4]$ was isolated. The latter complex, bearing no Co-C bonds other than the two Co-C_{NHC} bonds, exhibit a characteristic high-field ^{1}H NMR peak at -33.36 ppm. Upon further reaction of the complex $[(CSiC)CoH(OEt_2)][BPh_4]$ with $LiBEt_3H$ (1 equivalent) under N_2 atmosphere in Et_2O the complex $[(CSiC)Co(N_2)]$ (**C1**), bearing a coordinated N_2 molecule, is formed. The authors found that complex **C1** acts as a highly reactive cobalt(I) species because it can undergo oxidative addition reactions with C-H, N-H and O-H bonds. This high reactivity of the complex was attributed to the strong electron-donating character of the C-Si-C pincer ligand that chelates with the cobalt centre. For example, the reversible C-H bond oxidative addition behaviour of **C1** was observed by the presence of the corresponding cyclometallated complex [CoH(CSiCMes')] (**15**) (Scheme 4). SCXRD analysis of **15** confirmed the C-Si-C pincer ligand scaffold, along with the cyclometallative bond (Co-C = 2.032(2) Å), and hydrido ligand (Co-H = 1.39(3) Å). Additionally, the ^{1}H NMR spectrum of **15** exhibited a high-field signal at -29.21 ppm (Co-H).

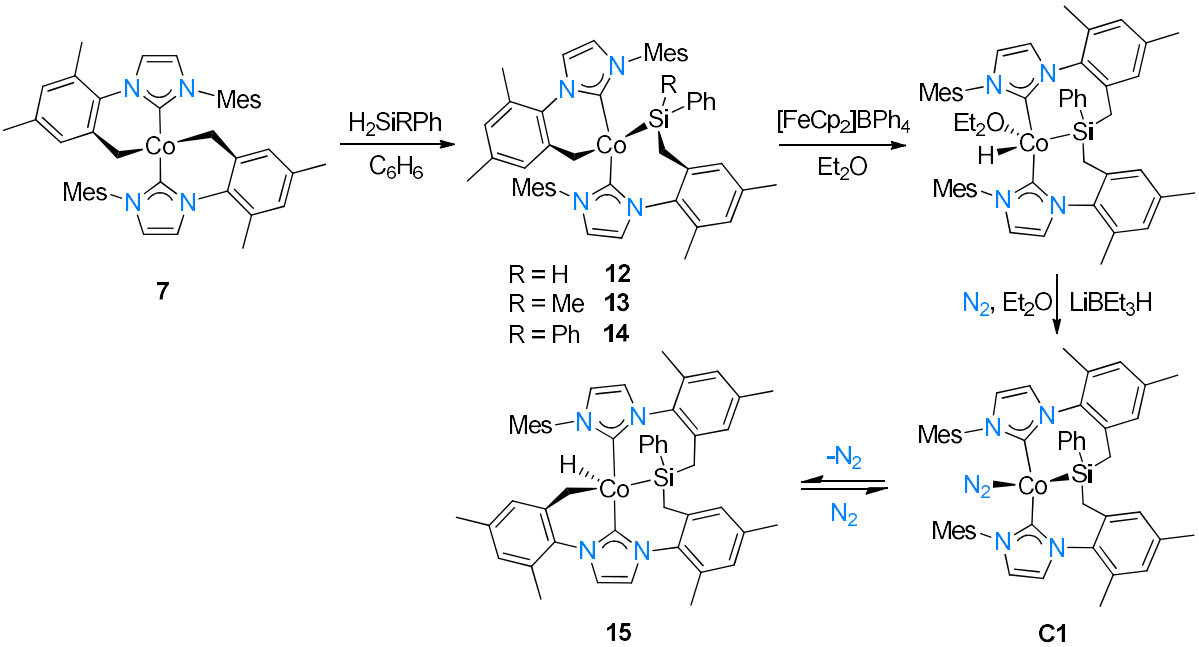

Scheme 4. Synthesis of silyl-donor-functionalised Co-NHC complexes **12-15**.

2.3 Cyclometallated carbene complexes with arene-based tethers

This popular series of arene-cyclometallated complexes of type **C** (Figure 1) usually feature bis-NHC ligand frameworks. Most examples in this category include complexes with two coordinated imidazolylidene moieties connected by a phenyl group, which results in this ligand class to be classified as CCC pincer type ligands [3,30,62,68-71]. Monoanionic bis-NHC pincer complexes featuring cobalt (I-III) were investigated by a variety of groups, most notably by Fout and co-workers [3]. Complexes **16** and **17** were formed (⩾ 80%) by the sequential addition of $LiN(SiMe_3)_2$, $Co(N(SiMe_3)_2)_2(py)_2$, and an equivalent of $ClCPh_3$ (oxidant) to the precursor benzimidazolium salts in THF, followed by stirring at room temperature overnight [3]. Characterisation of the low spin complexes **16** and **17** was done using ^1H NMR spectroscopy and SCXRD. The authors observed that both cobalt carbene bond lengths of 1.958(2) and 2.000(2) Å of **16**, as well as those of **17** (1.961(4) and 1.958(4) Å respectively), were comparable to related complexes previously reported. For the synthesis of **19** (Scheme 5) the authors modified the method for the synthesis of **17**, using no oxidant, to successfully yield a Co(II) centre instead of a Co(III) centre. Interestingly, this modification failed for the mesityl derivative (**16**). The authors found that the addition of half an equivalent of 9,10-dihydro-9,10-anthracendiyl-tris(THF)magnesium to a THF solution of **16** gave **18** in a low yield (28%). As part of evaluating reactivity patterns for **18**-**21**, a series of reactions were conducted where interconversions among these and new complexes were established (Scheme 5): (i) The Co(III) centre in **16** may be reduced to Co(II) by reaction of **16** with 9,10-dihydro-9,10-anthracendiyl-tris(THF)magnesium ($Mg(C_{14}H_{10})\cdot 3THF$, Path **A**) to form **18**. Oxidation of **18** back to **16** is feasible by reaction of **18** with $ClCPh_3$ at room temperature (Path **B**). (ii) A similar strategy is applicable to the Co(II) (**17**) and Co(I) (**19**) Dipp-NHC derivatives. Reduction occurs by reaction of **17** with Na/Hg at room temperature (Path **C**) to form **19**, whereas oxidation of **19** to form **17** occurs again by route **B**. (iii) The dinitrogen adduct of **19**, namely $[Co(^{Dipp}CCC)(N_2)]$ (**20**) is attainable by reacting $Mg(C_{14}H_{10})\cdot 3THF$ with a frozen solution of **19** in benzene. The FT-IR spectrum of **20** showed an N_2 frequency at 2063 cm^{-1}. (iv) The subsequent reaction of **20** with PPh_3 in the presence of N_2 gives the phosphane adduct **21** with a N_2 frequency of 2117 cm^{-1}. (v) The mesityl derivative of **21**, namely **22**, is attainable directly from **16** *via* route **C** (in the presence of added PPh_3). Similar to that of **20** and **21**, FT-IR spectroscopy of **22** revealed an intense stretching band at 2112 cm^{-1}, indicating the presence of a bound, unactivated dinitrogen molecule. The authors hypothesised that the presence of the dinitrogen ligand, as

well as the steric demands of the ligated triphenylphosphine, would ensure that **22** remains monomeric. This hypothesis was proven to be correct by characterisation of the complex *via* X-ray crystallography. A square pyramidal species with the N_2 molecule bound *trans* to the Co-C_{aryl} bond, similar to the structure of **20**, was revealed (Figure 2).

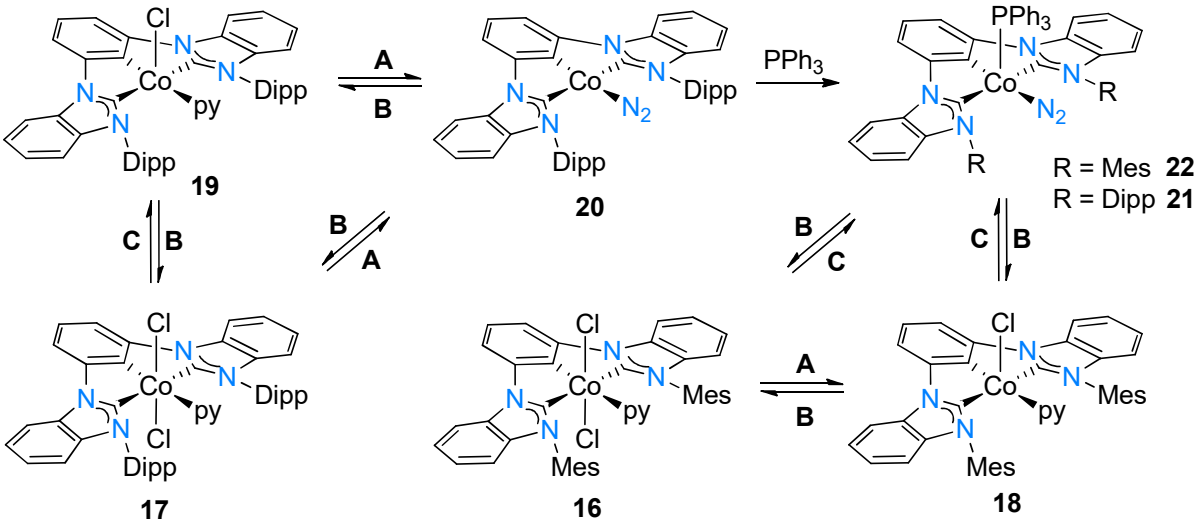

Scheme 5. The interconversion between complexes **16-22** reported by Ibrahim *et al*. [3]. Experimental conditions: **A** = $Mg(C_{14}H_{10})\cdot 3THF$, C_6H_6, -35 °C, 4h; **B** = py, $ClCPh_3$, THF, rt, 3h; **C** = Na/Hg, THF, rt, 18h.

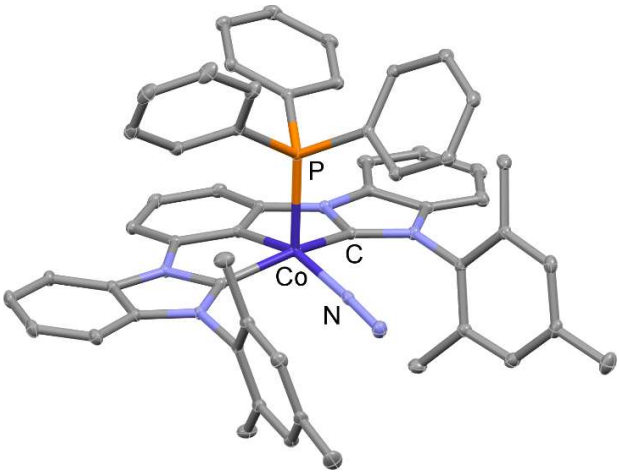

Figure 2. ORTEP plot of **22**. Thermal ellipsoids are drawn at 50% level. For clarity, the hydrogen atoms have been omitted.

Fout and co-workers [30] continued to study the reactivity of **22** and found that **22** is able to fixate dihydrogen to form the cobalt dihydrogen complex **24** supported by a pincer bis-NHC

ligand, ^{Mes}CCC (^{Mes}CCC = bis(mesityl-benzimidazol-2-ylidene)phenyl) (Scheme 6). Subjecting a THF solution of complex **22** to H_2 (4 atm.) at room temperature, resulted in an immediate colour change from dark red to red-orange. The authors confirmed the diamagnetic nature of **24** using ^{1}H NMR spectroscopy where, apart from noticeable shifts in the mesitylene proton signals, a broad singlet was observed at -5.56 ppm. This integrated for two protons, confirming the formation of **24**. The reaction was found to be reversible when **24** was exposed to N_2 (1 atm.), again giving a dark red solution which was indicative of the reformation of **22**. To confirm that **24** was indeed the dihydrogen complex, the authors exposed **22** to 4 atm. of D_2(g) which subsequently resulted in the formation of a red-orange diamagnetic compound exhibiting the same ^{1}H NMR mesityl resonances as previously observed in **24**. In addition, the previously broad peak at -5.56 ppm was absent, thus confirming that the dihydrogen gas was the source of the peak. The same set of reactions also held valid for the more basic PMe_3 analogue (**23**), to provide (reversible) access to the corresponding complex **25**, albeit in slightly lower yield (60%). Complex **23** was synthesised by reduction of [$CoCl_2$(^{Mes}CCC)(py)] (**16**) with KC_8 in the presence of PMe_3.

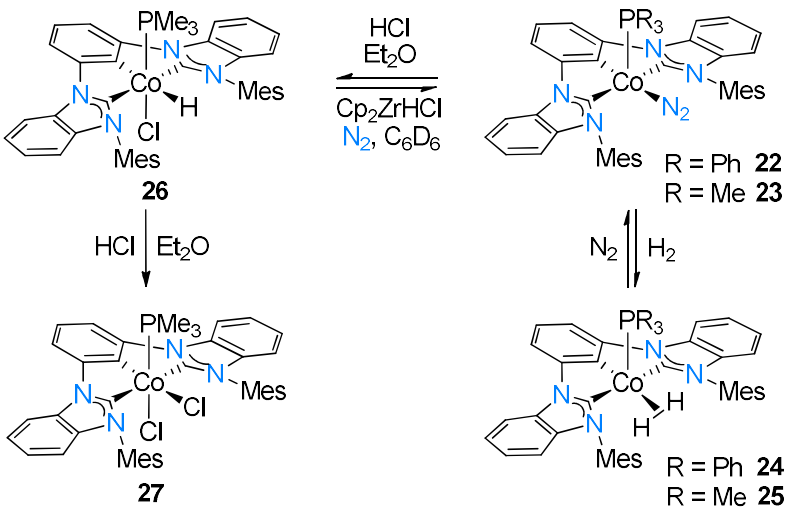

Scheme 6. Synthesis of Co(I)-dihydrogen (**24**, **25**), Co(II)-hydride (**26**), and Co(II)-dichloride (**27**) NHC complexes, and the interconversion between the different complexes.

The stoichiometric reactivity of **23** with HCl was also investigated: The authors theorized that H-H bond cleavage is likely due to the previously observed hydrogen-deuterium scrambling. To test this, an equivalent of HCl was added to a diethyl ether solution of **23**, which yielded an orange solid **26**. The ^{1}H NMR spectrum of **26** (in C_6D_6) revealed similar resonances than **23**

except for a doublet resonance that was observed at -10.0 ppm, which integrated for one hydrogen. This signal was confirmed to be due to a hydride ligand, for which the large associated *J* coupling constant of 109 Hz suggested that the hydride is substituted in a *trans* fashion with respect to the phosphine substituent. This finding was also supported by the molecular structure obtained from SCXRD data [30].

As part of a mechanistic study, Fout and co-workers [31] continued to derivatise the Co(II) complex **16**. They found that the reaction of **16** with two equivalents of the reductant KC_8 in THF yielded the corresponding diamagnetic, square planar Co(I) complex **28** in 80% yield (Scheme 7). The molecular structure of **28** was confirmed using SCXRD. Complex **28** was found to readily react with 4-methoxybenzonitrile to form the nitrile adduct (**29**) by pyridine substitution. The corresponding square pyramidal Co(I) complex **30** is attained by reaction of **29** with PPh_3. It was found that the dinitrogen Co(I) complex **22** could be reacted with benzonitrile to form the corresponding square pyramidal nitrile adduct **31** by facile N_2 substitution.

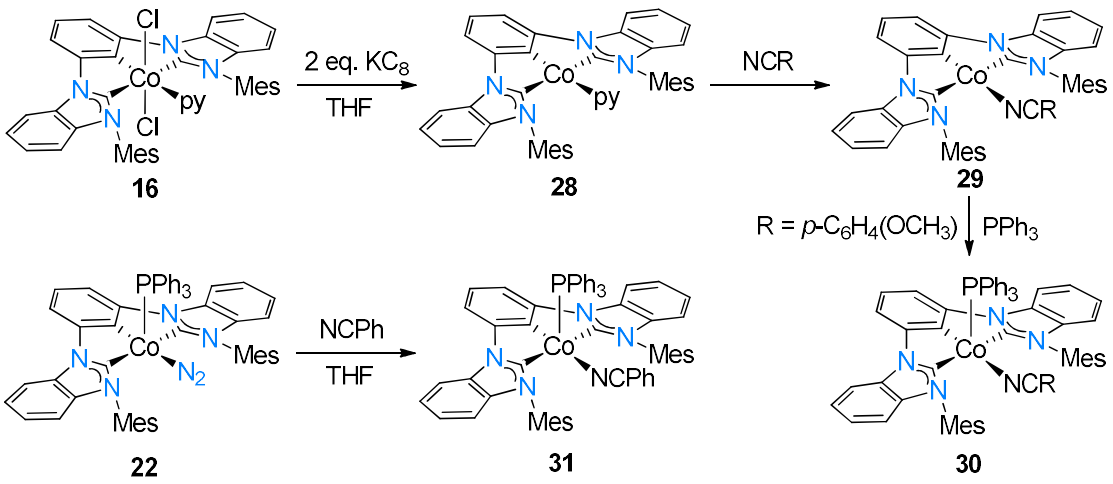

Scheme 7. Substitution reactions of **16** and **22** to form nitrile adducts **29-31**.

Hollis and co-workers [69,72] contributed to the chemistry of CCC-NHC pincer cobalt complexes through the use of zirconium-CCC complexes as transmetallation agents. Initially they found that the *in situ* generated zirconium complex, $[ZrI(^{Bu}CCC)(NMe_2)_2]$, could successfully transmetallate the ^{Bu}CCC NHC ligand (Scheme 8) to Co(III) using $Co(acac)_3$, albeit with a lack of selectivity. A complex mixture of products were obtained, of which three complexes (**32-34**, including a tetracarbene complex) were identified (Route **B**, Scheme 8). The products included mixed halogen salts of the tetracarbene complex **32**, the dichlorido

cobalt complex, $[CoCl_2(HNMe_2)(_{Bu}CCC)]$ (**33**) (from exchange in dichloromethane), as well as the acetylacetonato cobalt complex $[CoI(acac)(^{Bu}CCC)]$ (**34**). Subsequent re-evaluation of the reaction showed that reaction of the corresponding (*in situ* formed) chlorido zirconium complex, $[ZrCl(^{Bu}CCC)(NMe_2)_2]$, gave the air-stable chloride salt of the tetracarbene complex **32** as the only product (Route **A**). It was also found that reaction of the pre-isolated Zr complex, $[ZrI_2(^{Bu}CCC)(NMe_2)]$, with $Co(acac)_3$ in toluene gave the iodido derivative of **34** (Route **C**), which was structurally confirmed by means of SCXRD. A later report of the same reaction by the authors found that elevated temperatures (100 °C) and longer reaction times (18 hours) now forms the iodido salt of the tetracarbene complex **32** as a second (major) product, apart from the minor complex **34**. They also found that reaction of the Zr complex $[ZrI_2(^{Bu}CCC)(NMe_2)]$ with $CoCl_2$ in THF formed complex **32**, having the tetrahedral cobalt complex, $[CoCl_3(THF)]^-$, as the anion.

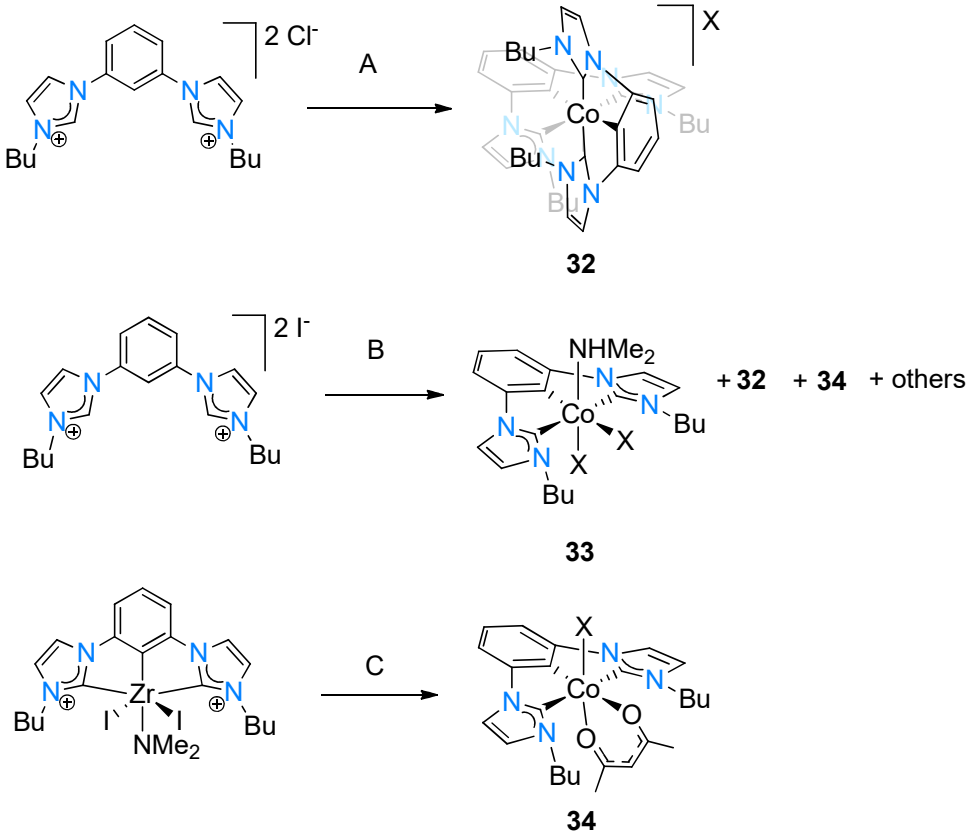

Scheme 8. Syntheses of Co(II) and Co(III) bis- and tetracarbene complexes **32-34** *via* transmetallation of ^{Bu}CCC-NHC Zr complexes. Route **A**: Bisimidazolium diiodido salt, 2.5 eq. $Zr(NMe_2)_4$, 1.1 eq. $Co(acac)_3$, DCM, rt, 12h. Route **B**: Bisimidazolium dichlorido salt, 1.01 eq. $Zr(NMe_2)_4$, 1.1 eq. $Co(acac)_3$, DCM, rt, 6h. Route **C**: $[ZrI_2(^{Bu}CCC)(NMe_2)]$, 1 eq. $Co(acac)_3$, toluene, 100 °C, 18h.

3. Synthesis and characterisation of Rhodium NHC complexes

With rhodium featuring as the significantly more expensive, less abundant, and often equally reactive analogue of cobalt, insight into many catalytic mechanisms was obtained by experimentally isolating and identifying Rh-based catalytic intermediates [56]. After the isolation and successful application of what is now known as Wilkinson's catalyst, $[RhCl(PPh_3)_3]$, research and interest into rhodium-based complexes was met with the rapid development of a wide range of stabilising ligand systems, including NHCs, tailored to both the electronic requirements of the metal and application. Rhodium is one of the most studied platinum group (PGM) metals to feature as part of catalyst design in homogeneous catalysis, as evidenced by the examples reviewed below. The most common oxidation states of Rh are +1 and +3, which also feature as the predominant oxidation states of the catalytic intermediates of most catalytic transformation reactions. This section is organised according to the carbon-based tether of the carbene ligand. Various similar complexes have been clustered together where distinct differences in the synthetic routes and reactivity patterns of these complexes were highlighted.

3.1 Carbene complexes with alkene-based tethers

In this section complexes of type **A** (Figure 1) is included. The first examples of a Rh(I)-NHC complex featuring a chelating alkene ligand was reported by the group of Bergman and Ellman in 2002 [73,74]. They were able to isolate the catalyst resting state, $[RhCl(PCy_3)(NHC\text{-}alkene)]$ (**35**), as part of a mechanistic study. A series of Rh catalysts were found to be catalytically active in a C-C bond formation reaction through Rh(I)-catalysed C-H activation of aromatic and heterocyclic compounds with sequential intramolecular coupling to an alkene. The reaction of a THF solution containing stoichiometric quantities of the imidazole ligand precursor, the Rh(I) dimer, $[RhCl(coe)_2]_2$, and PCy_3 formed the protic Rh(I)-NHC complex, with the alkene chelating to the square planar Rh centre, in moderate yield (64%, Scheme 9). Complex **35** showed a downfield singlet (12.0 ppm) in its ^{1}H-NMR spectrum, owing to the protonated nitrogen moiety of the NHC. Later, in 2011, Li *et al.* [75] reported a similar alkene-tethered Rh(I) derivative, **36**. Complex **36** was synthesised by treating stoichiometric amounts of $[RhCl(cod)]_2$ with the imidazolium carboxylate salt precursor at room temperature for 40 minutes to give yellow solids in high yield (93%) after workup. The success of the reaction is

due to the energetically favourable release of CO_2 from the air- and moisture stable zwitterionic carboxylate salt upon reaction with the rhodium precursor.

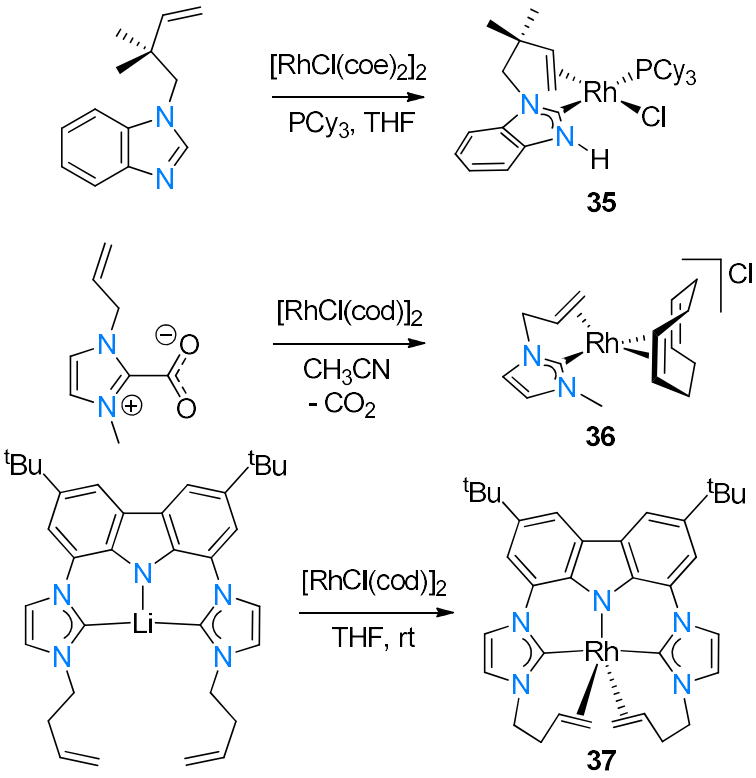

Scheme 9. Synthesis of alkene-tethered Rh(I) complexes **35-37**.

Following a similar protocol as with the cobalt analogue (**2**), the group of Kunz [76] reacted the bis-imidazolium salt with 1.3 equivalents of LiHMDS in THF, followed by half an equivalent of $[RhCl(cod)]_2$ at room temperature to give the desired complex **37** in quantitative yield (^{13}C NMR carbene signal observed at 185.5 ppm), along with concomitant formation of LiCl and LiBr. An effective alternative route was to use KHMDS in THF at -30 °C instead. Tamm and co-workers [77] observed a side-on (η^2) intramolecular interaction of an N-aryl group from an anionic NHC ligand in a Rh(I) complex. Treatment of the lithiated NHC borate ligands with $[RhCl(cod)]_2$ in toluene gave the yellow crystalline zwitterionic complex **38** in 50% yield (Scheme 10). The molecular structure of **38** was furthermore confirmed by SCXRD which revealed the dipp substituent adjecent to the borate moiety to exhibit an arene-rhodium interaction. The resultant effect was seen in the carbene ligand being twisted to one side (Rh-C_{NHC}-N_{NHC} = 105.70(14)°), to allow for sufficient interaction of the arene moiety with the rhodium centre. The same result was observed employing the dimer $[RhCl(CO)_2]_2$ in a similar reaction to form analogous complex **39** (Scheme 10). A strong *trans* effect was observed

experimentally, where the carbonyl ligand *trans* to the NHC exhibited a longer Rh-C_{CO} bond length of 1.936(2) Å compared to the *cis* carbonyl ligand (1.8379(19) Å), highlighting the strong electron donor property of the NHC ligand. Interestingly, complex **38** could not be converted to **39** by exposure to CO gas and NEt_4Cl. The square planar complex $[RhCl(CO)_2(NHC)]$, **38b**, without an arene interaction, was formed instead.

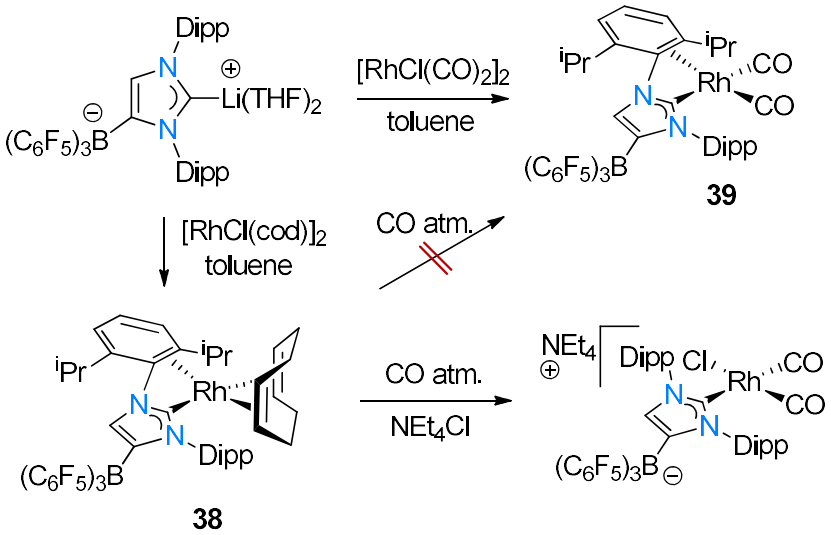

Scheme 10. Synthesis and reactivity of zwitterionic Rh(I)-NHC complexes **38** and **39**.

The group of Castarlenas [78] observed interesting chemistry when focussing on the pentacoordinated Rh(I) complexes featuring coumarin-functionalised biscarbene ligands. They found that reaction of two equivalents of bis-(benz)imidazolium salts with one equivalent of the $[Rh(OMe)(cod)]_2$ dimer in the presence of NaOMe in THF under reflux for 24 hours affords the corresponding white biscarbene complexes **40-45** in low to moderate yields (38-66%) (Scheme 11). However, for the allyl-functionalised coumarin-NHC ligand, the reaction produces complex **46** which instead chelates *via* the allyl ligand as opposed to the alkene from the coumarin moiety as seen in complexes **40-45**. Complexes **40-46** were all characterised using elemental analysis, NMR spectroscopy, and SCXRD (**41**, **44**, and **46** only).

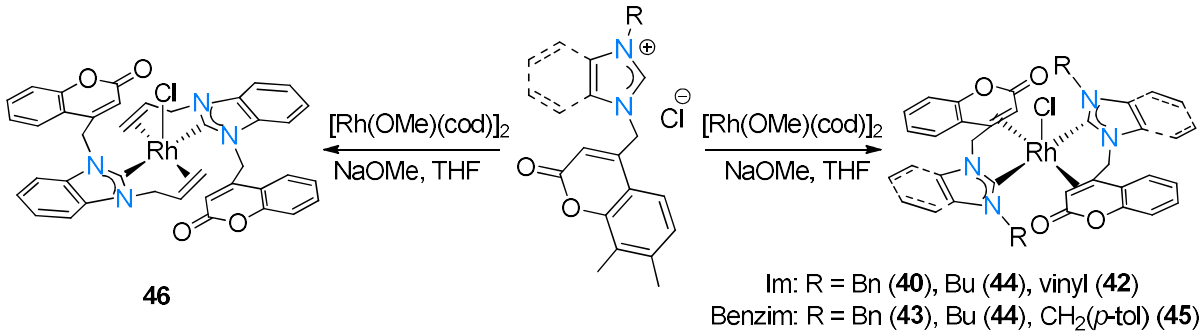

Scheme 11. Formation of alkene-coordinated biscarbene complexes of Rh(I) (**40-46**).

3.2 Cyclometallated carbene complexes with alkyl-based tethers

The rhodium-NHC compounds described here are more commonly encountered as multidentate NHCs that bind through a σ-alkyl carbon tether (class **B**, Figure 1). The examples reviewed differ in the rhodium oxidation state, the resultant geometry of the rhodium centre, the number of NHC moieties present, the relative size of the NHC ligand(s), as well as the type of ancillary ligands – and as a result have been grouped accordingly within this section.

Various groups of Crudden [79], Nolan [80], Glorius [81], and Chauvin [82] were all able to synthesise Rh-NHC complexes featuring σ-alkyl anionic tether groups. Crudden [79] found that the dimer $[RhCl(H_2C{=}CH_2)_2]_2$ reacts with two equivalents of free SIDipp (under N_2) to form the Rh-NHC dimer, or with four equivalents of free SIDipp (under N_2) to form the Rh-N_2 adduct complex (Scheme 12). Each of these complexes is heat sensitive, which upon heating either complex to 80 °C sees the formation of the biscarbene complex **47**, bearing an alkyl tether. A similar complex was formed by Nolan [80] through the reaction of the dimer $[RhCl(coe)_2]_2$ with four equivalents of free IMes in THF at room temperature to rapidly give a crystalline orange solid after workup. This complex was identified to be the orthometallated Rh hydride complex **48**, both from an SCXRD structure elucidation, as well as ^{1}H-NMR spectroscopy, where a high upfield hydride signal at -27 ppm was observed. The group of Glorius [81] tentatively showed, using NMR spectroscopy, how intramolecular C-H activation takes place in an unsymmetrical NHC to form complex **49** from Wilkinson's catalyst, $[RhCl(PPh_3)_3]$ (Scheme 12).

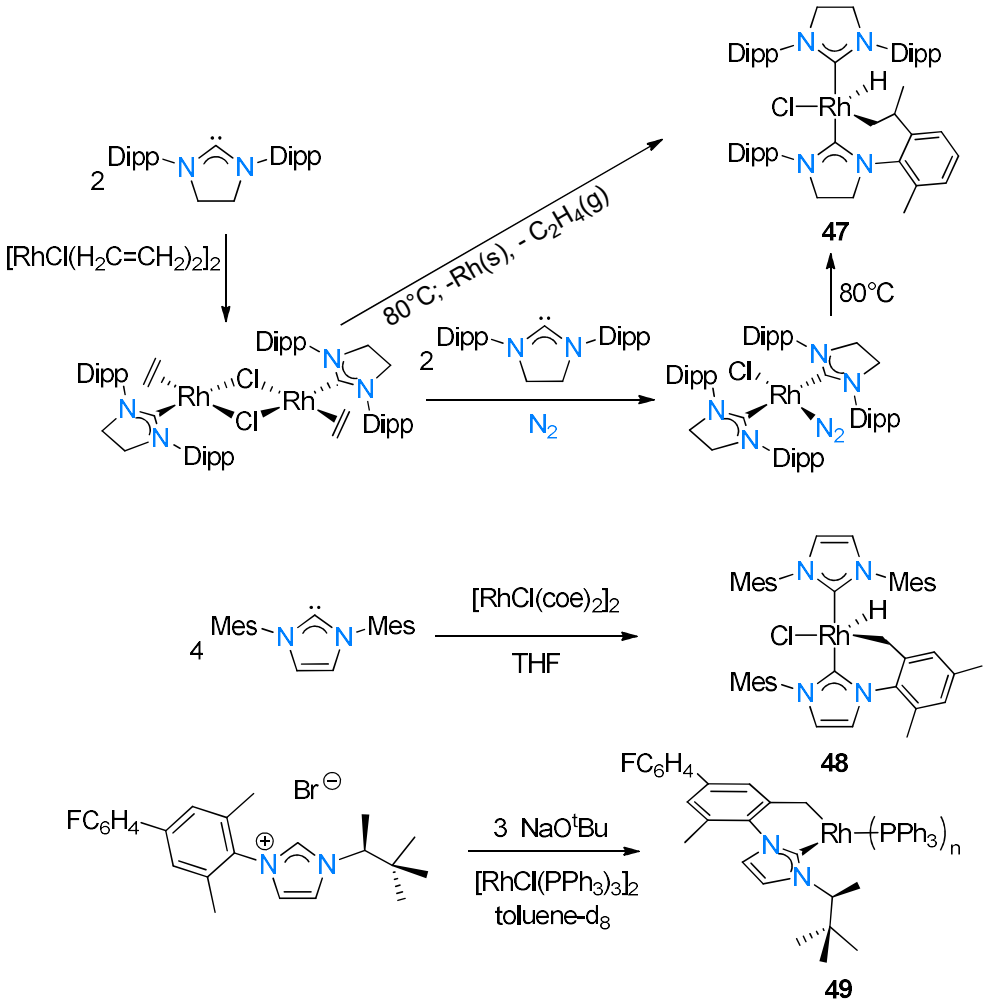

Scheme 12. Synthesis of alkyl-cyclometallated complexes **47-49**.

Chauvin [82] was able to selectively synthesise ylide phosphonium Rh-NHC complexes in a stepwise fashion: Reaction of half an equivalent of $[RhCl(cod)]_2$ with the dicationic NHC salt in the presence of NEt_3 gave the Rh-NHC complex. After treatment with potassium *tert*-butoxide, the methyl functionality of the phosphonium group was deprotonated, thereby forming the NHC-phosphonium ylide complex **50** in 92% yield (Scheme 13). Subsequent treatment of **50** with CO (1 atm.) substitutes the cod ligand for two CO ligands to form complex **51**.

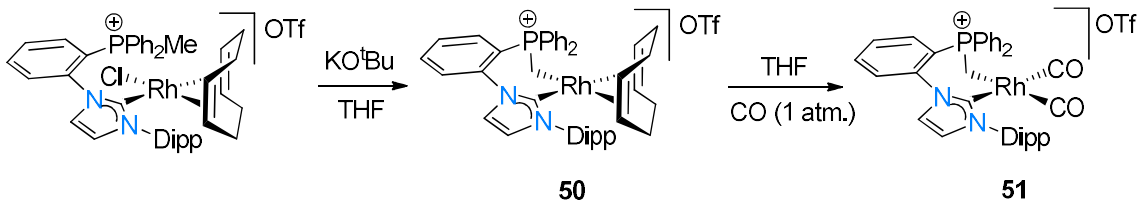

Scheme 13. Synthesis of cyclometallated Rh(I)-NHC complexes **50** and **51**.

Several examples of biscarbene complexes featuring two separate bidentate NHC ligands coordinated to a Rh(I) metal centre have been investigated by the groups of Nolan [83,84] and Castarlenas [78]. Nolan observed different reactivity when two equivalents of the free bis(*tert*-butyl) imidazolylidene is reacted with half an equivalent of $[RhCl(coe)]_2$ in either hexane or benzene. In hexane oxidative addition, involving one *tert*-butyl group of one NHC, occurs to yield the yellow hydrido Rh(III) bis-NHC complex **52**, featuring one cyclometallated NHC, and the other involved in an agostic hydrogen interaction with the rhodium centre (Scheme 14). The ^{1}H NMR spectrum of **52** exhibits a broad signal at -22.93 ppm confirming the presence of the hydride ligand, as well as a overlapped signal at 2.1 ppm integrating for two protons showing cyclometallation of the *tert*-butyl group has occurred. When the reaction is performed in benzene, the dark-yellow bis-cyclometallated Rh(III) complex **53** forms.

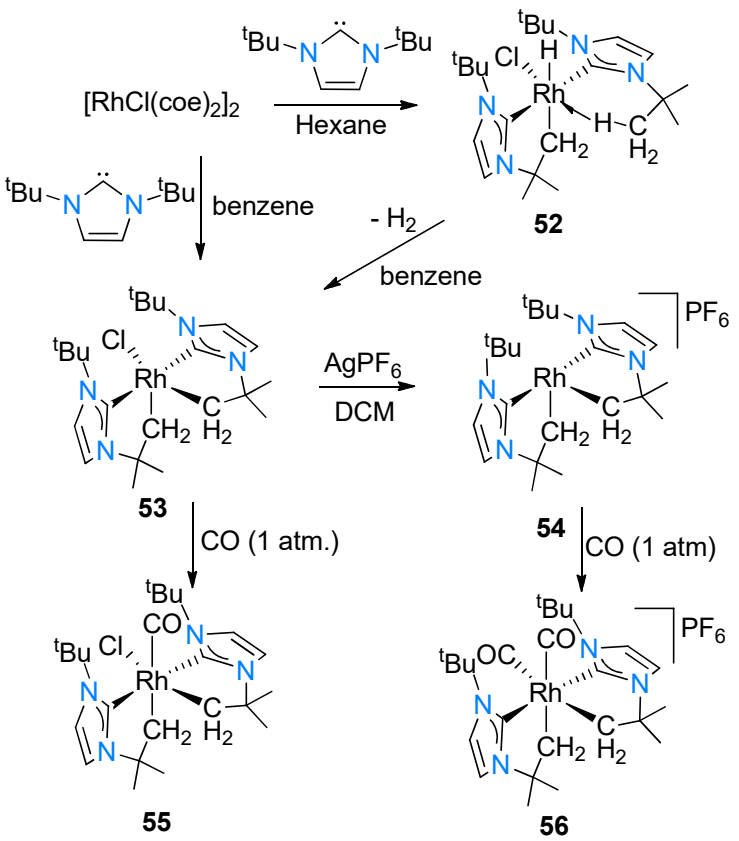

Scheme 14. Formation of 14- and 16-electron cyclometallated Rh(III) biscarbene complexes **52-56**.

NMR experiments also confirmed the formation of **53** from **52** in C_6D_6 with concomitant loss of H_2(g). Complex **53** may react further with $AgPF_6$ in DCM to form the 14-electron complex **54**. Both coordinatively unsatured complexes **53** and **54** readily react with CO (1 atm.) to give

the white and colourless complexes **55** and **56**, respectively, in almost quantitative yields (Scheme 14). FT-IR revealed one υ_{CO} = 2015 cm^{-1} for complex **55** and two υ_{CO} = 2093 and 2058 cm^{-1} for complex **56**. Complexes **52-56** were fully characterised, including by SCXRD, which confirmed ligand connectivities and complex geometries.

3.3 Cyclometallated carbene complexes with arene-based tethers

The class of arene cyclometallated Rh-NHC complexes (Figure 1 **C**) has been considerably expanded since the report of the first example by the group of Cross [85]. The authors reported the formation of a cyclometallated Cp*Rh-NHC complex **57** (40%) from the reaction of $[Cp^*RhCl_2]_2$, an amine-functionalised NHC salt, and NaOAc over the course of 5 days at room temperature (Scheme 15). In contrast to the expected secondary coordination of the amine moiety (six-membered metallacycle), spontaneous aromatic C-H activation occurs to form the five-membered metallacycle (Scheme 15).

The use of other bases (Ag_2O, KO^tBu) leads to lower yields of **57**. The groups of Choudhury [86-90] and Wang [91] were also successful in isolating several examples of (hetero)arene-cyclometallated Rh-NHC complexes as part of ongoing studies into Rh-catalysed intermolecular C-H activation/annulation reactions of imidazolium salts to form a variety of functionalised benzo[ij]imidazo[2,1,5-de]quinolizines. As part of their studies, they found that the reactions of $[Cp^*RhCl_2]_2$ with unsymmetrical imidazolium iodide salts, in the presence of excess sodium acetate, forms the cyclometallated Rh(III)-NHC complexes **58-63** (Scheme 15). Interestingly, in reaction with the N-2-pyridyl imidazolium salt, cyclometallation persists to rather activate the *ortho*-position of the pyridyl moiety to form the neutral Rh(III)-NHC complex **60**. In the case of the N-4-pyridyl imidazolium salt, cyclometallation again occurs, although secondary coordination by a second Rh(I) centre occurs to form the binuclear Rh(I)-NHC complex **61**. Similarly, for alkene-functionalised NHC ligands: cyclometallation occurs on the alk-2-ene position to form five-membered rhodacycles **62** and **63**.

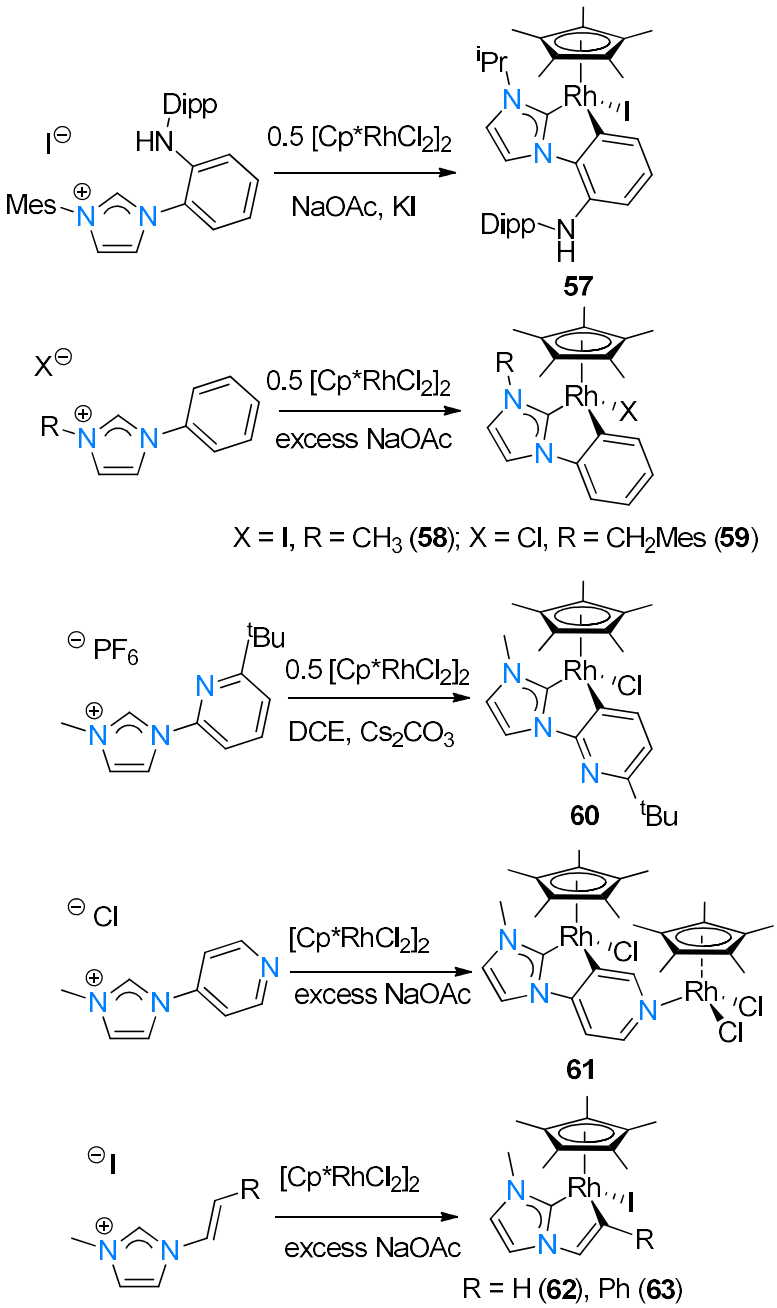

Scheme 15. Arene- and alkene-cyclometallated Rh(III) complexes **57**-**63**.

As part of the study in isolating organometallic intermediates of the catalytic reaction, the mono-annulated imidazolium salts were reacted with $[Cp^*RhCl_2]_2$: Cyclometallated mono-carbene complex **64** was formed when using excess of NaOAc as the only base [87], whereas prior treatment of the imidazolium salt with AgOTf, followed by the rhodium precursor and excess NaOAc formed the biscarbene complex **65** instead [91] (Scheme 16). Apart from NMR spectroscopy, complexes **58**-**65** were also structurally characterised using SCXRD.

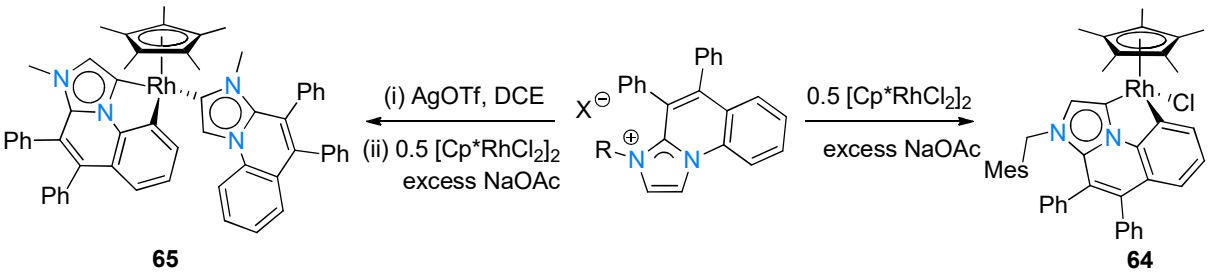

Scheme 16. Formation of abnormal Rh(III)-NHC complexes **64** and **65**.

The group of Peris [92] observed preferential (non-selective) C-H activation in pyridyl-containing NHC ligands to form a mixture of cyclometallated Rh(III)-NHC complexes (Scheme 17): The reaction of the pyridyl-NHC salt with $[Cp^*RhCl_2]_2$ in the presence of NaOAc and KI in CH_3CN gives a mixture of **66-68** (38%, 16%, and 25% yields, respectively). Similarly, treatment of the C(2)-protected NHC analogue with Cs_2CO_3 gives **69** as the only product (60%). Complex **69** is formed from the reductive coupling between the Cp* and pyridinium groups, which results in the imidazolylidene ring to be bound to the metal *via* the activated C(2)-CH_3 group. All complexes **66-69** were characterised using NMR spectroscopy, mass spectrometry and SCXRD (except **67**). The ^{1}H NMR spectrum of **68** suggests Cp* activation by the appearance of four inequivalent methyl signals (2.26, 2.22, 1.85, and 1.36 ppm), with the two diastereotopic CH_2 linker protons appearing at 3.61 and 3.44 ppm (doublets with $^3J_{HH}$ = 15 Hz each). The ^{13}C NMR spectrum of **69** shows two doublets at 66.5 ($^1J_{RhC}$ = 15 Hz, pyridinyl) and 1.8 ppm ($^1J_{RhC}$ = 27 Hz, methyl), implying the presence of two unique metallated carbon atoms. The authors speculated that the formation of the Cp*-activated complexes **68** and **69** occurs *via* a Rh-tetramethylfulvene intermediate, which is then prone to nucleophilic attack.

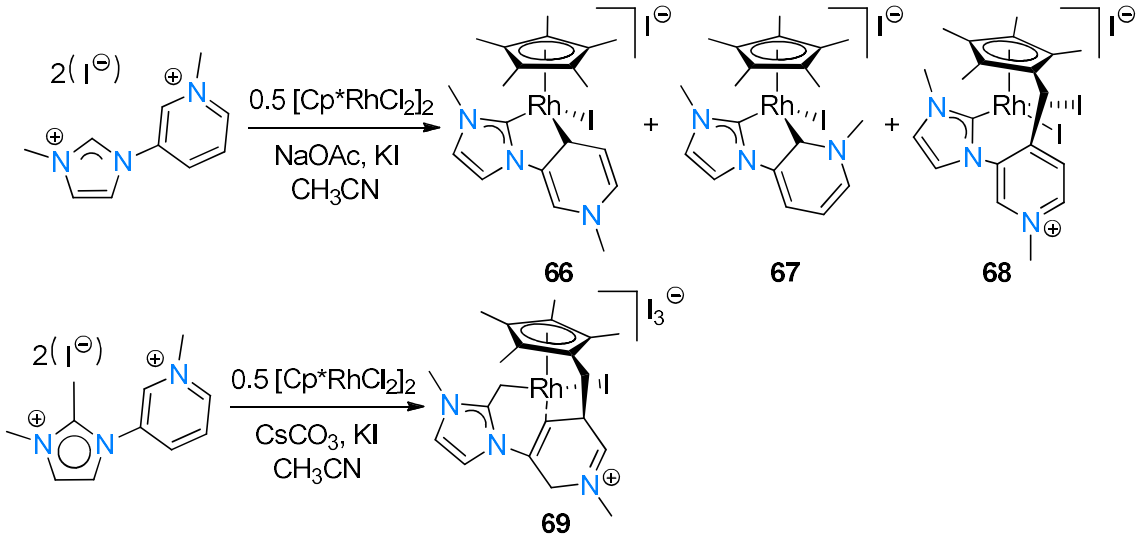

Scheme 17. C-H activation of pyridyl-NHCs to form biscarbene Rh(III)-NHC complexes **66-69**.

Colbran and co-workers [93] found that blocking of the *meta*-position of the pyridyl group in a related NHC forms the expected monodentate NHC ligand in the Rh(I)-NHC complex which, after exposure to air, selectively cyclometallates the *ortho*-position of the pyridyl ring (Scheme 18). They found that a solution containing the Rh(I)-NHC complex, $[RhI(cod)(NHC^{+})]PF_6$, exposed to air at room temperature, gradually converts to the Rh(III)-cyclometallated complex **70** (70% yield). If the reaction is repeated with the imidazolium salt, $[RhCl(cod)_2]_2$, and carboxylate salts of sodium, the octahedral Rh(III) complexes **71-73** are formed. In the case of using sodium acetate, two additional dinuclear paddlewheel Rh(III)-NHC complexes (**74**$_S$ (*syn*) and **74**$_A$ (*anti*)) are also formed.

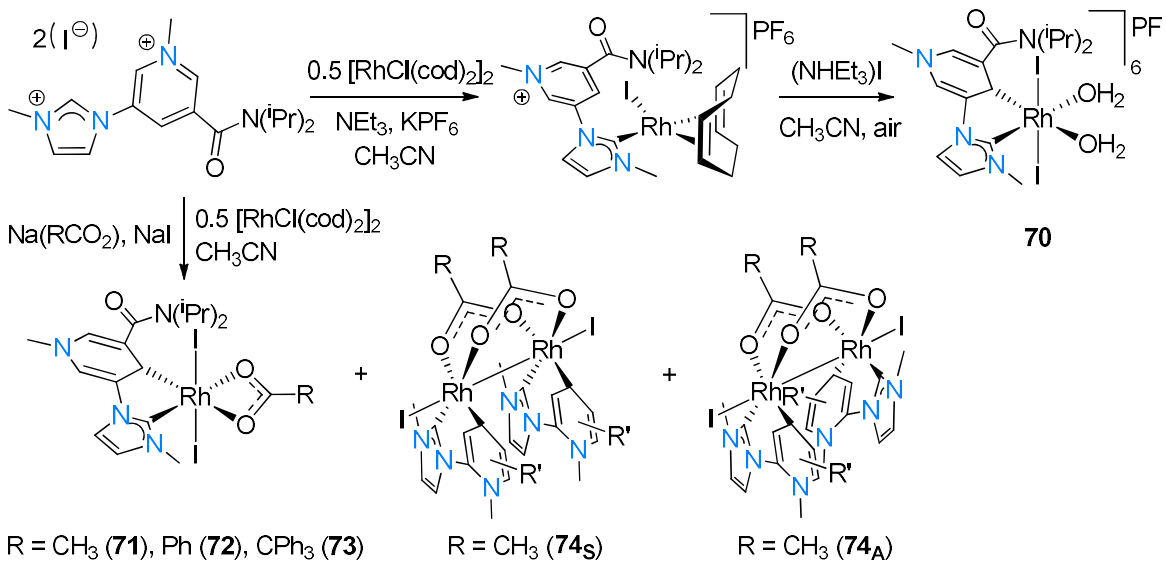

Scheme 18. C-H activation of pyridyl-NHCs to form mono- and multinuclear Rh(III)-NHC complexes **70-74**.

The groups of Hahn and Peris [94] were successful in isolating a series of heterobimetallic Rh(III)-NHC complexes featuring Pd(II), Ir(I), Au(I), and Ru(II) metal moieties. Starting from an N-benzimidazolium-imidazolium diiodide salt, NaOAc, KI, and $[Cp^*RhCl_2]_2$, the corresponding cyclometallated Cp*Rh-NHC complex **75** was first isolated in 85% yield (Scheme 19). Complex **75** was then reacted with Ag_2O in DCM, after which the respective metal precursor and KI was added, to yield (*via* silver transmetallation) the corresponding heterobimetallic complexes containing Pd(II) (**76**, 61% yield), Ir(I) (**77**, 39% yield), Ru(II) (**78**, 49% yield), and Au(I) (**79**, 40% yield) in moderate yields. Crystal structure elucidation was performed for complexes **75** and **77-79** (Figure 3). The carbenic carbon signal in the ^{13}C NMR

spectra of complexes **76-79** (182-183 ppm ($^1J_{RhC}$ = 52-55 Hz)) was shifted only slightly downfield from the corresponding signal in complex **75** (180.3 ($^1J_{RhC}$ = 54 Hz) ppm), indicating a limited perturbation in electron donation experienced by the rhodium centre by the different organometallic-substituted NHC ligands.

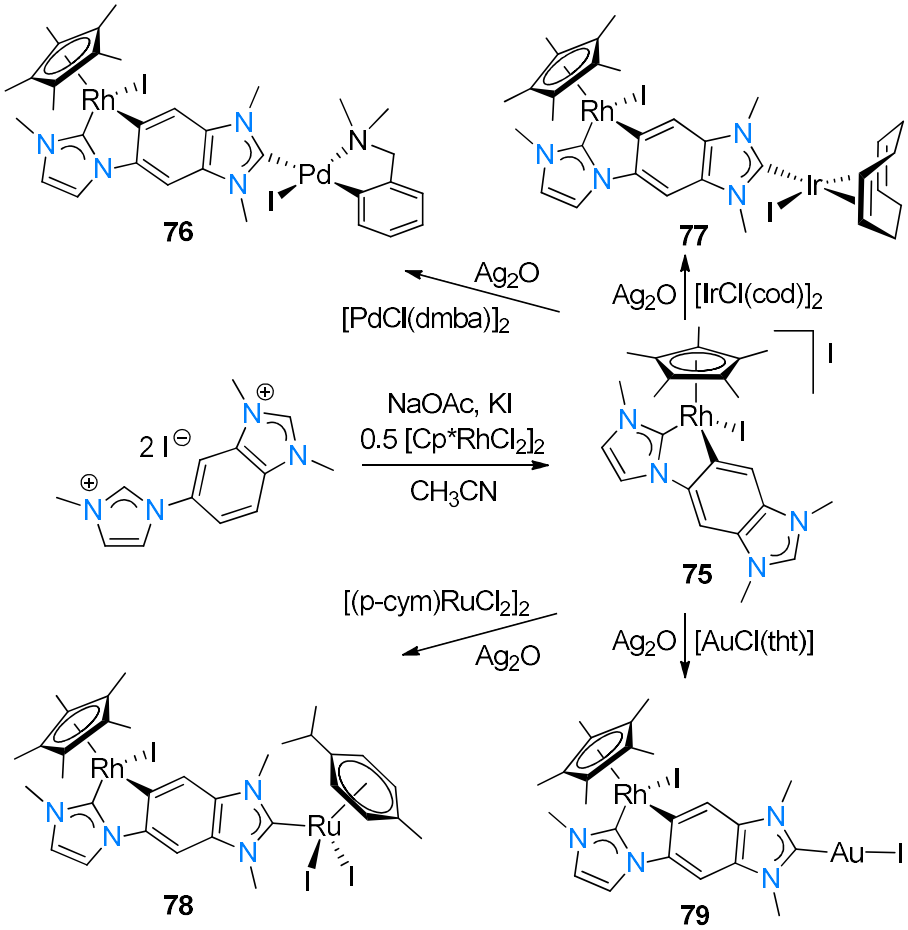

Scheme 19. Synthesis of heterobimetallic Rh(III)-NHC complexes **75-79**.

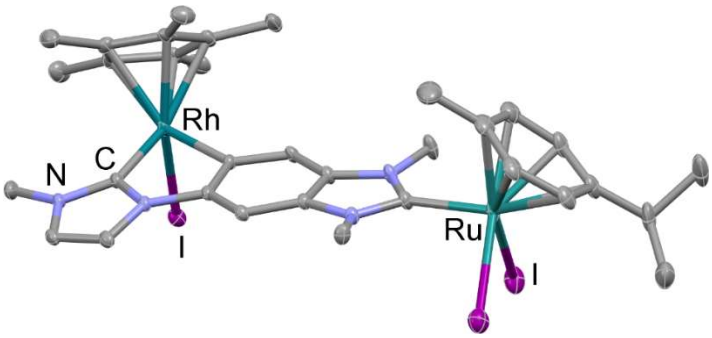

Figure 3. ORTEP plot of **78**. Thermal ellipsoids are drawn at 50% level. For clarity, the hydrogen atoms have been omitted.

The same groups of Hahn and Peris [94,95] also reported the synthesis of cyclometallated Cp*Rh-NHC and heterobimetallic Cp*Rh/Au complexes (Scheme 20). Reaction of either the 1,4- or 1,3-dibriged phenylimidazolium diiodide salts with Cs_2CO_3, NaOAc, KI, and $[Cp^*RhCl_2]_2$ in acetonitrile gave the corresponding cyclometallated Cp*Rh-NHC imidazolium iodide salt complexes **80** (91% yield) and **81** (90% yield), respectively. Complexes **80** and **81** may then be reacted first with Ag_2O to form the silver carbene adduct. The subsequent transfer-metallation to gold using [AuCl(tht)] in the presence of KI gave corresponding complexes **82** (21% yield) and **83** (26% yield) in low yield. Complex **84** is synthesised in a similar manner to **82-83** except $[Pd(dmba)]_2$ is added as the second metal reagent, **84** was isolated in a low yield (47%).

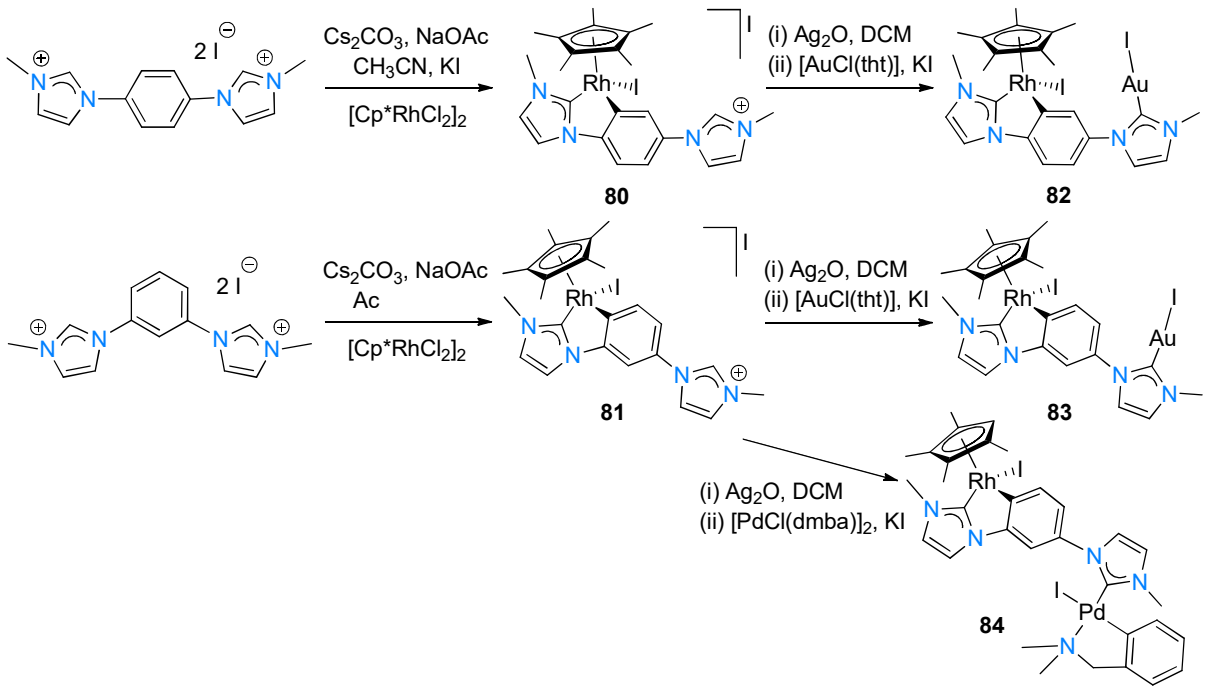

Scheme 20. Synthesis of cyclometallated Cp*Rh-NHC complexes **80-84**.

Hahn and co-workers [96] also reported the synthesis of bis- and triscarbene rhodium complexes **85** and **86** from the respective tris-imidazolium salt, Cs_2CO_3, and $[Cp^*RhCl_2]_2$ in acetonitrile (Scheme 21). Biscarbene complex **85** was obtained (66% yield) directly from the tris-imidazolium salt featuring a PF_6^- anion. **86** was obtained (53% yield) from the tris-imidazolium salt bearing a bromido anion using Cs_2CO_3, following a subsequent treatment of Ag_2O and an additional half an equivalent of $[Cp^*RhCl_2]_2$ to yield the tris-cyclometallated complex **86**. The ^{13}C NMR spectra of **85** revealed two doublets at 180.7 ($^1J_{RhC}$ = 54 Hz) and 182.7 ppm ($^1J_{RhC}$ = 52 Hz) for the inequivalent carbene carbon atoms, while the equivalent

carbenic carbon atoms in the C_3-symmetric complex **86** all appeared as one doublet at 177.7 ppm ($^1J_{RhC}$ = 53 Hz).

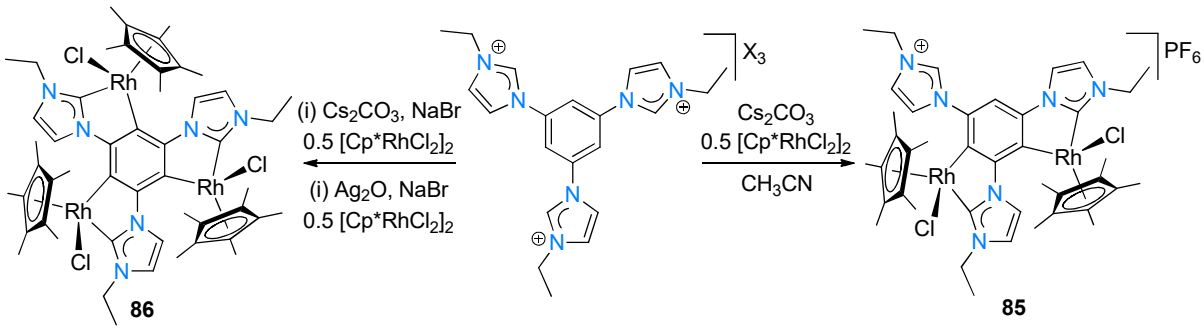

Scheme 21. Synthesis of bis- and triscarbene Cp*Rh complexes **85** and **86**.

The group of Fryzuk [97] showed that a thermal rearrangement reaction of Rh(I)-NHC complexes featuring a pincer NHC ligand (PCP type) leads to a ligand rearrangement process as a result of intramolecular P-C bond cleavage. The initial Rh-NHC complexes were prepared by usual methods, *i.e.* reaction of the free NHC ligand with $[RhCl(cod)]_2$, to give the corresponding square planar Rh(I)-NHC complex $[RhCl(PC_{NHC}P)]$. The latter complex was then treated with either $KBEt_3H$ in benzene, or $LiCH_3$ in toluene to yield the corresponding hydride and methyl complexes of $[RhH(PC_{NHC}P)]$ and $[Rh(CH_3)(PC_{NHC}P)]$, respectively. Thermolysis at 60 °C of either the methyl or hydride complexes result in P-C bond cleavage to form cyclometallated complexes **87** and **88** (Scheme 22). The ^{31}P NMR spectra of both **87** and **88** exhibited a pair of doublet of doublets (ABX pattern) indicative of two inequivalent phosphorus nuclei coupled *cis* to one another and to ^{103}Rh. The molecular structures of both **87** and **88** have been elucidated using SCXRD. Saunders and co-workers [98] reported on the tethering of a pentamethylcyclopentadienyl ligand to an NHC by intramolecular 1,4-addition to a polyfluorophenyl substituent of a coordinated NHC ligand. The authors synthesised **89** by reaction of the mono-carbene Cp* rhodium complex with Ag_2O over 24 hours to cleanly form **89** (Scheme 22). A crystal suitable for SCXRD study was grown and the structure revealed the 1,4-addition of the rhodium centre with concomitant loss of aromaticity of the severely distorted pentafluorophenyl group (Figure 4). It was proposed that the reaction occurs by abstraction of a chloride ligand with silver(II) oxide to generate a metal cation, which in turn increases the acidity of the Cp* protons. In the presence of a base, proton abstraction occurs to form a zwitterionic 16-electron complex that possesses a nucleophilic methyl carbon atom and

a Lewis acidic metal centre. Complex **89** is then formed by a concerted or stepwise 1,4-addition onto the metal centre.

As part of the group of Oro's mechanistic studies [99] of Rh-catalysed hydrosilylation of acetophenone with $HSiMe(OSiMe_3)_2$, they were able to identify proposed intermediates of the catalytic cycle. The reaction of the complex [RhCl(cod)(NHC)] (featuring a free N-anisole functional group) with $HSiMe(OSiMe_3)_2$ was monitored using ^1H NMR spectroscopy. After eight hours at 90 °C, signals relating to the precursor complex disappeared with the appearance of several signals that suggested the presence of the hydrido-bridged binuclear Rh complex (**90**) (Scheme 22). The upfield triplet resonance at -10.10 ppm ($^1J_{RhH}$ = 26 Hz) in the ^1H NMR spectrum is assigned to the bridging hydride ligands, whereas the ^{13}C NMR spectrum featured two doublet resonances at 183.1 ($^1J_{RhH}$ = 26 Hz, C_{NHC}) and 155.8 ppm ($^1J_{RhH}$ = 39 Hz, C_{arene}) and provided evidence for the presence of *ortho*-cyclometallated NHC ligands. Upon employing the silane $HSiEt_3$ a similar outcome was observed: Analogous complex **91** was obtained and showed similar resonances in the ^1H and ^{13}C NMR spectra.

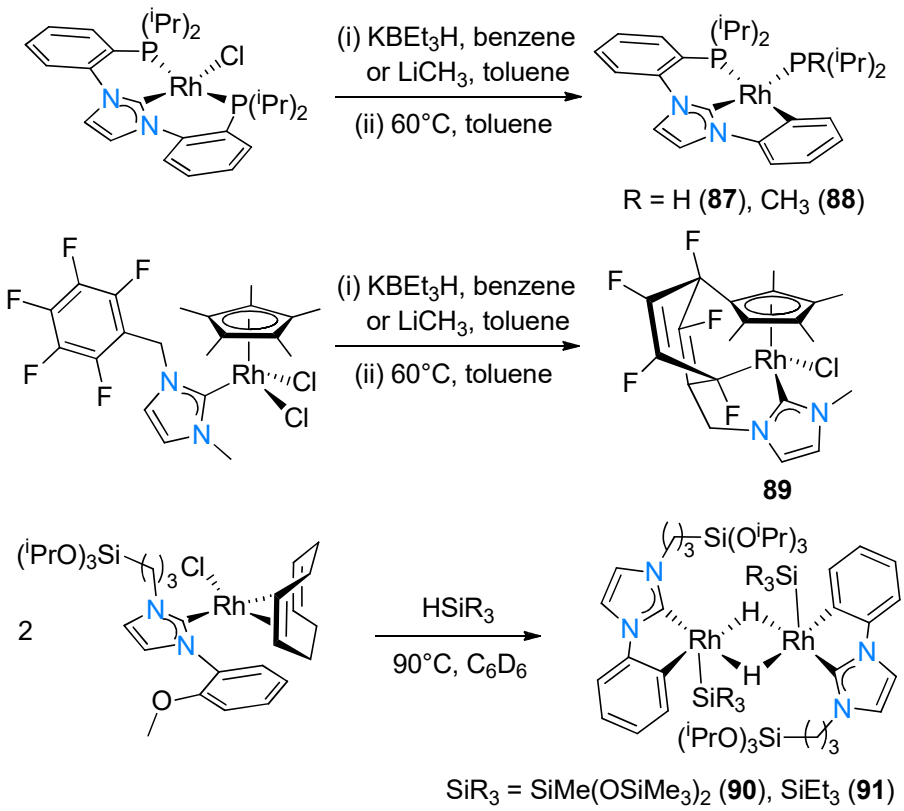

Scheme 22. Synthesis of cyclometallated Rh(III)-NHC complexes **87-91**.

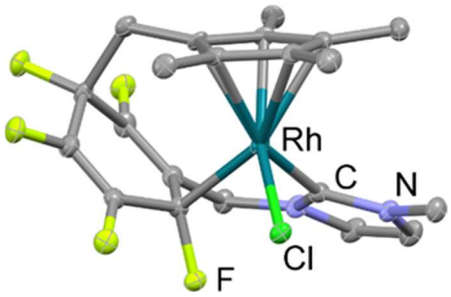

Figure 4. ORTEP plot of 89. Thermal ellipsoids are drawn at 50% level. For clarity, the hydrogen atoms have been omitted.

The group of Dyson [100] reported on the alcohol-induced C-N bond cleavage of bis-NHC systems to form cyclometallated Cp*Rh-NHC complexes. The reaction of the bis-imidazolium salts with $[Cp^*RhI_2]_2$ in the presence of bases (such as NEt_3 and NaOAc) in a variety of solvents including DCM, THF, CH_3CN, acetone and $HNEt_2$, forms the expected biscarbene complexes in good yields (> 60%) (Scheme 23). However, when methanol is employed as solvent, the ligand is cleaved to form phenylimidazole, the phenylimidazole adduct $[Cp^*RhI_2(PhIm)]$, and the cyclometallated complex **92** in 33, 22, and 42% yields, respectively. The cyclometallated complex **92** features an $N\text{-}CH_2OR$ substituent from the alcohol (MeOH). Repetition of the reaction in the alcoholic solvents EtOH, ^{i}PrOH, BnOH all gave the same outcome to produce corresponding complexes **93-95** (Scheme 23). Hahn and co-workers [101] reported on asymmetric Cp*Rh biscarbene complexes that feature two different NHC donor ligand sets obtained *via* mild NaOAc mediated C-H activation. Employing a hybrid method utilising silver oxide to coordinate the one imidazolylidene ring to the rhodium centre as an intermediate, subsequent addition of NaOAc in acetonitrile forms the red C-H activated monocarbene complex **96**, [Cp*RhCl(NHC-Im)], featuring the cyclometallated imidazole ring. Alternatively, addition of two equivalents of NaOAc to the bis-imidazolium salts gave the cyclometallated complexes **96-98** in a one pot reaction in high yield (81-92%). Subsequent reactions of complexes **97** and **98** with either an acid ($HBF_4 \cdot Et_2O$) or an alkylating agent (Et_3OBF_4) forms the corresponding red-orange N-substituted biscarbene complexes (Scheme 24). Sets of two unique doublets at 177-178 ppm ($^1J_{RhC}$ = 55 Hz), and 159-162 ppm ($^1J_{RhC}$ = 47-48 Hz) appeared in the ^{13}C NMR spectra of complexes **96-98** that confirmed the presence of the carbene and imidazolyl moieties, respectively. Further work on complex **98** by Hahn

[102] showed how polynuclear tetracarbenes could be formed by post-synthetic modification using **98** and *E*-1,4-dibromobut-2-ene.

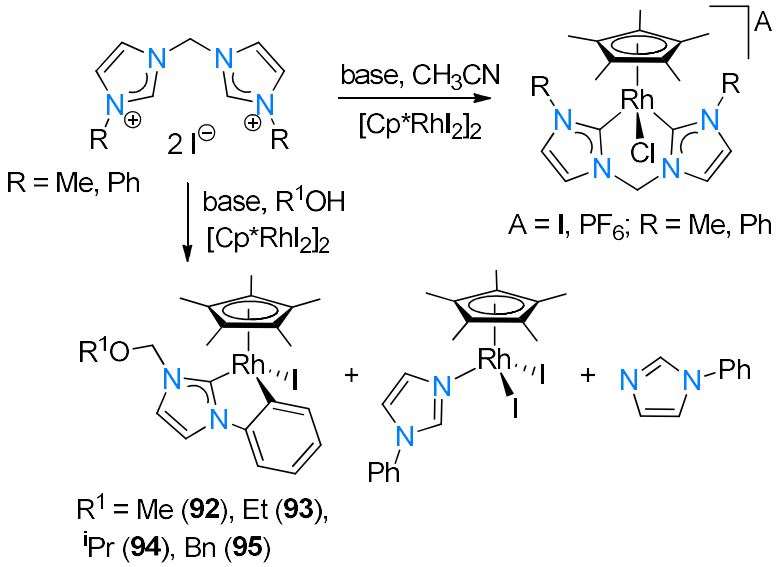

Scheme 23. Alcohol-mediated C-N cleavage in cyclometallated Cp*Rh(III)-NHC complexes.

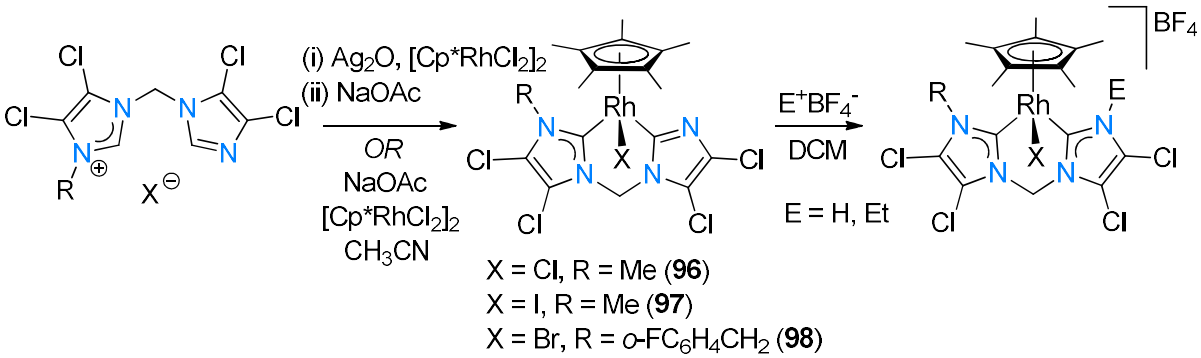

Scheme 24. Synthesis of asymmetric biscarbene precursors Cp*Rh(III) **96-98**.

The group of Hollis [103-105] investigated tridentate CCC biscarbene complexes of Rh(I) by making use of a zirconium transmetallation strategy. Treatment of the bis-imidazolium salt with $Zr(NMe_2)_4$ in DCM at room temperature, followed by the addition of $[RhCl(cod)]_2$ in a 1:1 ratio gave the orange Rh(III)-CCC complex **99** in 90% yield (Scheme 25). Slow evaporation of a chloroform solution of **99** formed a new Rh(III) complex, **101**. It was concluded that the ammine complex **99** and the iodido-bridged dimer complex **101** were in equilibrium and that the $NHMe_2$ was lost during slow evaporation to give crystals of **99**. Upon

employing THF as solvent, an inseparable mixture of **99** and its chlorido analogue (**100**) is obtained.

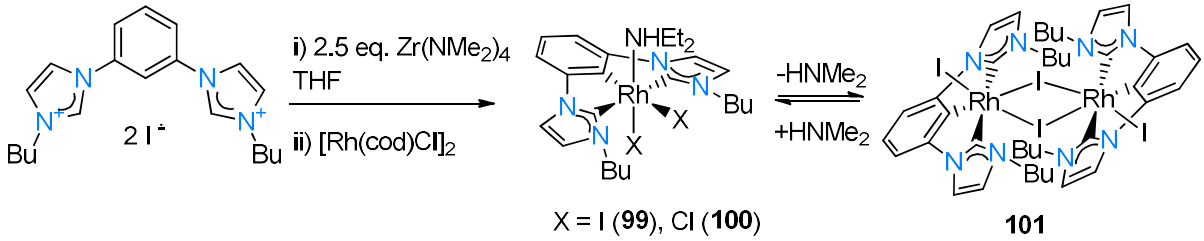

Scheme 25. Synthesis of tridentate Rh(III) biscarbene complexes **99-101**.

Ito *et al.* [106] synthesised cyclometallated Rh(III) complexes employing NHC-oxazoline CCN-type pincer ligand frameworks: Reactions of the precursor imidazolium pre-ligands with NEt_3 and $RhCl_3.3H_2O$ leads to C-H activation of the aryl group to form the corresponding Rh(III)-CCN complexes **102** and **103** (22-27% yield) (Scheme 26). In a third reaction employing the N-^{i}Pr and C-^{i}Pr-substituted CCN ligand, no mononuclear complex was formed, but instead complex **104**, a dimeric Rh(III)-CCN complex, was isolated in low yield (13%). The molecular structures (SCXRD) of the monomeric (**99** and **103**) and dimeric (**101** and **102**) complexes were elucidated and confirmed the distorted pseudo-octahedral rhodium geometries, each featuring a meridional pincer ligand. The structures of the dimeric compounds each showed two Rh-NHC being connected by bridging halide ligands, where each rhodacycle showed variable degrees of distortion due to steric repulsion of the NHC linker and substituents.

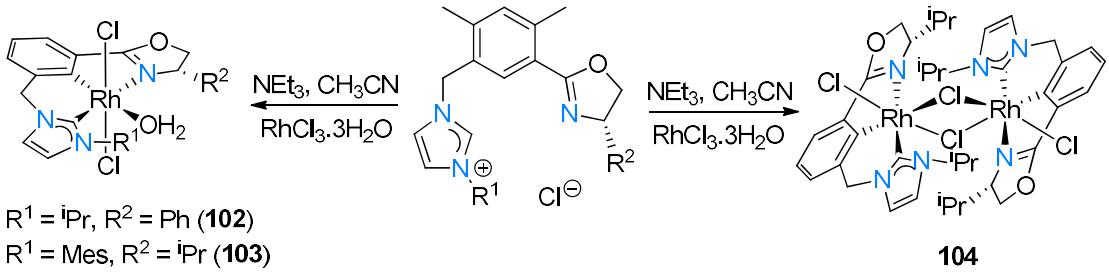

Scheme 26. Synthesis of Rh(III) cyclometallated complexes **102-104**.

The group of Willans [107] investigated the versatile modes of rhodium coordination when employing N-heterocyclic carbene carboranes. They employed two types of carborane-tethered NHC ligands: Starting from the N-ethyl-*ortho*-carborane-N-*tert*-butylimidazolium salt, reaction with Ag_2O and $[RhCl(cod)]_2$ in acetonitrile forms the seven-membered metallacycle containing the Rh(I) centre with the coordinated NHC and carborane ligands in high yield (**105**, 79%) (Scheme 27). The ^{13}C NMR spectrum exhibited a doublet at 70.6 ppm ($^1J_{RhC}$ = 53 Hz)

which indicates the presence of a Rh-carboranyl bonded carbon atom. Deboronation of the *closo*-carborane NHC salt is induced by addition of excess *tert*-butylimidazole to form the *nido*-carborane zwitterionic NHC ligand Reaction of this NHC salt with NaH, followed by addition of $[RhCl(cod)]_2$, forms the homo-bimetallic complex **106** featuring two Rh(I) centres. The NHC ligand is coordinated to one square planar Rh(I) centre, while the carborane is coordinated to the other Rh(I) centre in a η^5-fashion. This coordination involved a known 3,1,2 to 2,1,8 RhC_2B_9 cluster rearrangement, which is believed to occur due to steric crowding and the presence of an ancillary cod ligand [107]. Both complexes **105** and **106** were also structurally elucidated by means of SCXRD.

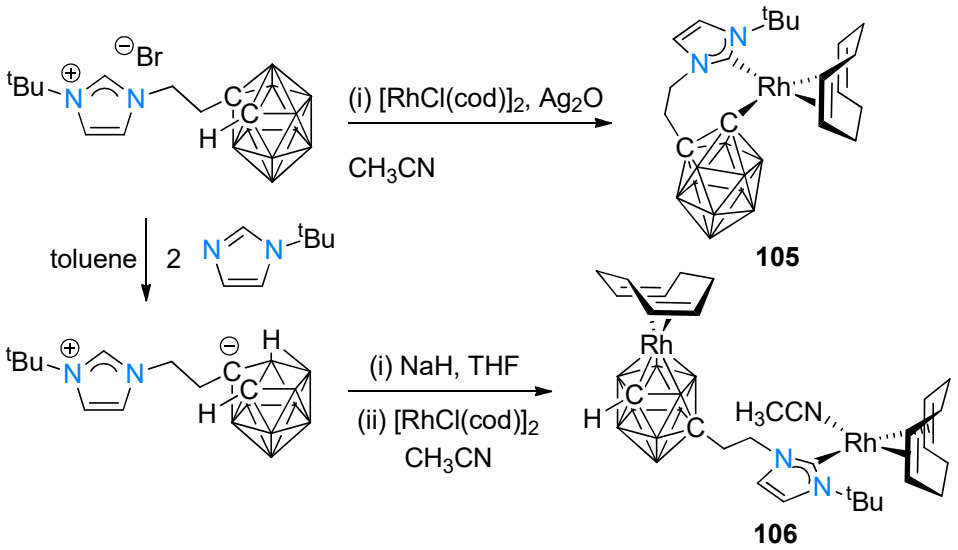

Scheme 27. Synthesis of carborane-functionalised Rh(I)-NHC complexes **105** and **106**. In the carborane, carbon atoms are highlighted as C with the rest being boron atoms.

3.4 Carbene complexes with cyclopentadienyl-based tethers

Several cyclopentadienyl-, fluorenyl-, and indenyl-appended NHC ligands that bind in a variety of ways (η^1-η^5) were also reported. Most of these examples belong to group **D** (Figure 1). César [108] observed a metal-assisted conversion of an N-ylide mesomeric betaine into its carbenic tautomer. The authors synthesised **107** in low yield (23%) by first double deprotonating the imidazolium salt with KHMDS in THF at -50 °C, followed by the subsequent addition of $[RhCl(cod)]_2$ (Scheme 28). The unusual NHC-containing four-membered metallacycle was confirmed using SCXRD and NMR spectroscopy, with the ^{13}C NMR spectrum showing the NHC carbene and the fluorenyl carbon atoms resonating as doublets at 160.8 ($^1J_{Rh\text{-}C}$ = 44.3 Hz)

and 63.5 ppm ($^1J_{Rh\text{-}C}$ = 10.7 Hz) respectively while the other quaternary carbons appear as singlets, thus providing further evidence for η^1-coordination.

Examples containing a ferrocenyl fragment was reported by the group of Labande [109,110]. They found that oxidation of a Rh(I) complex containing a ferrocene-based NHC ligand leads to an unexpected C-H activation on the ferrocenyl moiety to give the orange, air-stable complex **108**. They reasoned that the oxidation of Rh(I) to Rh(III) follows from the initial oxidation of ferrocene to ferrocenium, followed by electron transfer from the rhodium centre to the ferrocenium group. Complex **108** was furthermore reactive with 2,2'-bipy to give the red-orange bipyridine adduct complex **109**, as a mixture of two isomers (**109C** and **109T**, Scheme 28) as confirmed using ^{1}H and ^{31}P NMR spectroscopy. The relatively rigid nature of the facially ligated NHC tridentate ligand has been confirmed for **109** using SCXRD (one isomer, **109T**).

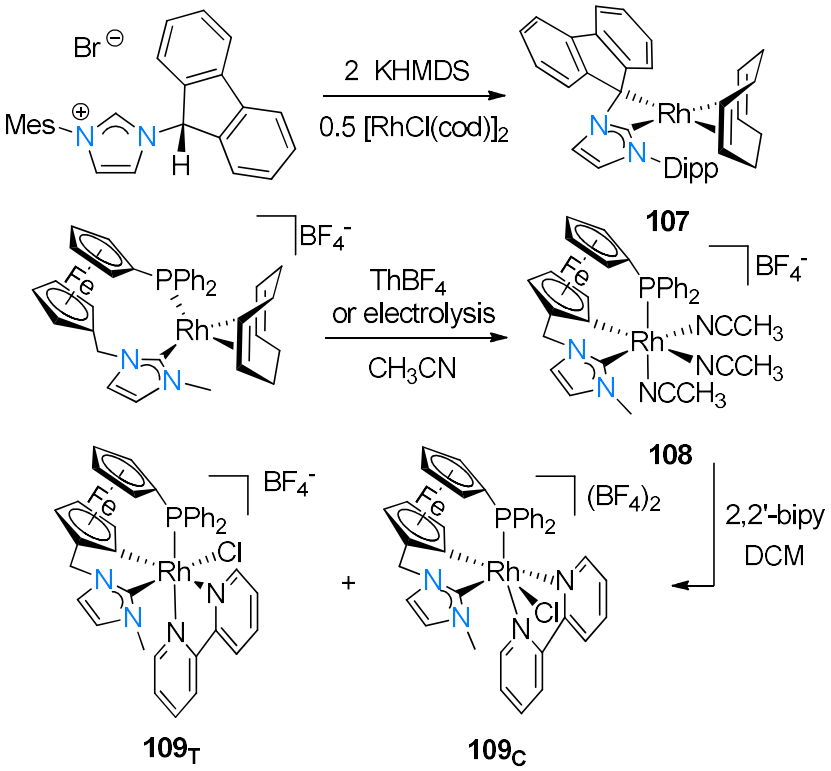

Scheme 28. Formation of fluorenyl- and ferrocenyl functionalised Rh-NHC complexes **107-109**.

The groups of Royo and Peris [111,112] reported on the facile design, synthesis, and ligation of Cp*-functionalised NHC systems to Rh(III) centres (**110-112**, Scheme 29). Initial reaction of either of the Cp*-NHC ligands with $[RhCl(cod)]_2$ *via* silver transmetallation gave the [RhCl(cod)(NHC)] species featuring a monodentate NHC ligand. After addition of acetic acid to the latter complexes, C-H activation of the Cp* fragment takes place to form Cp*-tethered

Rh(III)-NHC complexes **110-112** as red-orange solids in low to moderate yields (37%, 51%, and 30%, respectively). The groups of Danopoulos and Cole-Hamilton [113] also contributed to this series by isolating 16-electron indenyl-and fluorenyl-functionalised NHC complexes of Rh(III). The reaction of $[RuCl(cod)]_2$ with two equivalents of the potassium fluorenyl salt leads to an unexpected C-H activation reaction whereby a fulvene-like moiety is formed. In the resulting complex **113**, the rhodium centre binds to the NHC through its carbenic carbon atom, as well as to the severely distorted η^2-alkene bond of the fluorenyl group. The original η^4-cyclooctadiene group now binds to the rhodium centre as a η^3-cyclooctenyl group. In contrast, repeating the latter reaction with the potassium indenyl NHC salt and $[RhCl(CO)_2]_2$ retains the η^5-nature of the indenyl moiety, leading to Rh(I) complex **114** in good yield (80%) (Scheme 29); no products due to ligand C-H bond activation were observed. Finally, treatment of the Rh(I)-NHC complex [RhCl(cod)(NHC)] featuring the same indenyl moiety undergoes C-H activation when treated with half an equivalent of the dimer $[Ru(OMe)(cod)]_2$ to form the dinuclear monocarbene Rh-NHC complex **115**.

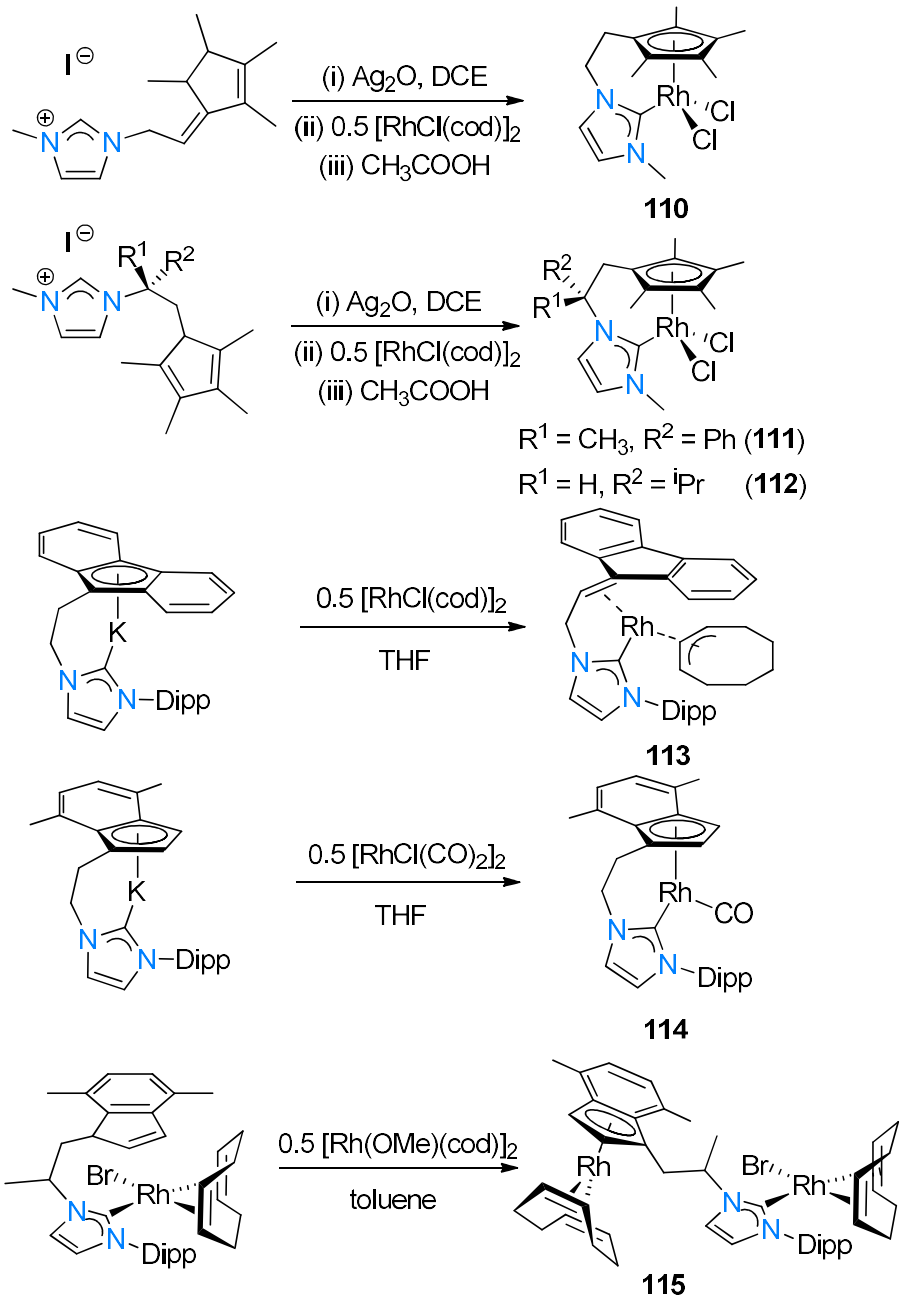

Scheme 29. Syntheses of cyclopentadienyl-, indenyl-, and fluorenyl-functionalised Rh-NHC complexes **110-115**.

The disappearance of the peak at 6.10 ppm in the ^{1}H NMR spectrum is characteristic of the deprotonation of the indene ring. Apart from NMR spectroscopy, all the products **113-115** were also structurally characterised (SCXRD).

4. Synthesis and characterisation of Iridium NHC complexes

While iridium is the least abundant metal of the group IX triad, there is a large contribution of work relevant to this review due to its unique reactivity and diverse application range. In the following examples, the most common oxidation states of Ir are 0, +1 and +3. While iridium complexes are known to mimic the reactivity and chemical properties of the lighter rhodium analogues, the inherent stabilities of the iridium complexes allowed for many mechanistic studies to be conducted in order to isolate important synthetic and catalytic intermediates. This section is organised into separate sections according to the type of NHC tether and the number of NHCs present in the complex.

4.1 Carbene complexes with alkene-based tethers

This section focuses on the use of tethers of class **A** (Figure 1), which enjoyed considerably more attention as compared to the cobalt and rhodium metal analogues. The first example in this ligand class, reported by Wolfgang Herrmann and co-workers [114] in 2000, features an unsymmetrically substituted Ir(III)-NHC complex obtained from a post-synthetic modification route *via* a C-H activation process. The authors initially synthesised the symmetrically substituted Ir(III) monocarbene complex, and in an attempt to substitute one methyl ligand with a triflate ligand, an immediate reaction with gas (CH_4 gas) evolution was observed upon which a pale yellow crystalline solid was obtained (**116**, Scheme 30). X-ray diffraction studies revealed that one of the cyclohexyl rings of the NHC showed a short C_5-C_6 distance, 1.400(8) Å, typical of η^2-coordinated double bonds, along with similar Ir-C bond distances of 2.145(5) and 2.177(5) Å. The authors theorised that the treatment of the monodentate carbene complex with trifluoromethylsulfonic acid results in methane elimination, proceeding through a possible cyclometallated intermediate **C2**, which likely undergoes *β*-hydrogen migration to yield the hydride complex **116**. The C-H activation/*β*-hydrogen migration process leads to the formation of four possible stereoisomers (chiral-at-metal, chiral ligand), which reduces to a pair of enantiomers based on the characterisation data and geometry considered.

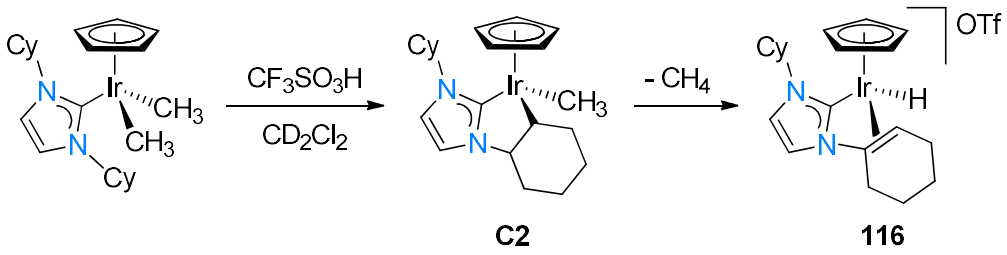

Scheme 30. Synthesis of the hydrido Ir(III)-NHC complex **116**.

Peris and co-workers [40] studied Cp*Ir(III) complexes with alkene-functionalised NHC ligands that were of a hemicleavable nature. Complexes **117-121** were synthesised *via* the well-known silver(I) oxide transmetallation reaction (Scheme 31). The authors noted that with longer alkene chain tethers (n = 3), a neutral complex forms, where the coordinated NHC is monodentate and has a free alkene chain. Through use of NMR spectroscopy and SCXRD, the authors confirmed the chelating mode of complexes **117-121**. NMR signals that correspond to coordinated alkenyls were observed, appearing further upfield as compared to the same signals in the corresponding imidazolium salts. For example, it was seen that the signals due to the allylic CH and CH_2 resonances of the imidazolium salt appear at 6.04 and 5.50 ppm, respectively, whereas for complex **117** they appear at 5.18, 3.89 and 3.60 ppm, respectively. The additional methylene signals observed are due to the diastereotopic carbon atoms that form upon coordination. X-ray diffraction studies confirmed the molecular structures of complexes **117-120**, as well as the chelating η^2-coordination of the NHC ligand. The authors noted that the biggest change due to the NHC backbone substitution of H atoms with Cl or CH_3 groups is the change in Ir-$C_{carbene}$ bond distance (**120**, H, 2.012(6) Å; **118**, Cl, 1.92(2) Å; **119**, CH_3, 2.029(8) Å). However, the Ir-$alkene_{midpoint}$ distance remained relatively consistent irrespective of the NHC backbone substituents, with distances in the range of 2.064-2.077 Å. The alkene chain length also resulted in a slight elongation of the Ir-$alkene_{midpoint}$ distance with 2.105Å observed in **120**.

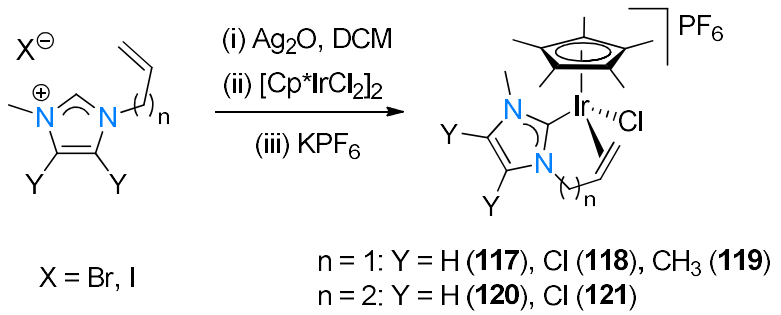

Scheme 31. Synthesis of Ir(III) hemicleavable NHC complexes **117-121**.

The groups of Hahn and Oro [17,115], Mata [116] as well as Kunz [59] reported several unique alkene-tethered mono- and dinuclear Ir(I) NHC complexes. Hahn and Oro devised a route to these complexes by reaction of the imidazolium halide salts with the metal precursor $[Ir(OMe)(cod)]_2$ in a 2:1 ratio in acetone to yield the five coordinate Ir(I) complexes **122**, **123**, **128**, and **129** (Scheme 32) as off-white solids. Mata made use of the silver transmetallation route using Ag_2O and the imidazolium salt, followed by addition of $[IrCl(cod)]_2$ to give complexes **124-127** in moderate to high yields (60-90%). The NMR spectra of **122** confirmed the η^2-coordination since the signals for the allylic protons have been shifted significantly upfield compared to those of the imidazolium salt. Mata also noted that complexes **124-126** show fluxional behaviour. They were able to obtain the activation barrier parameters of **124** by means of VT-NMR studies. The room temperature ^{1}H NMR spectrum of **124** confirms unique chemical environments for each of the two NHC backbone protons at 6.89 and 6.67 ppm, respectively. The coordination of the alkene fragment is inferred by these observations as well as upfield alkene peaks. The signals assigned to the olefinic protons at room temperature are broad, suggesting that a fluxional process that involves chemical exchange of the coordinated and uncoordinated olefins is present. X-ray diffraction studies of **122** showed that the equatorial Ir-C_{allyl} (2.145(6) and 2.138(5) Å) and Ir-C_{cod} (2.124(5) and 2.148(5) Å) bond distances are shorter than the Ir-C_{cod} bonds *trans* to the carbene ligand (Ir-C(1) 2.235(5) and Ir-C(2) 2.240(5) Å). The authors postulated that the carbene ligand acts predominately as a σ-donor, exerting a stronger *trans* influence compared to the ligands in the equatorial plane. Due to this, the Ir-C interaction of the olefin of the cod ligand in the *trans* position to the carbene ligand is weaker, leading to longer bond lengths. SCXRD studies also confirmed the molecular structures of complexes **123**, **129-131**, and **133**.

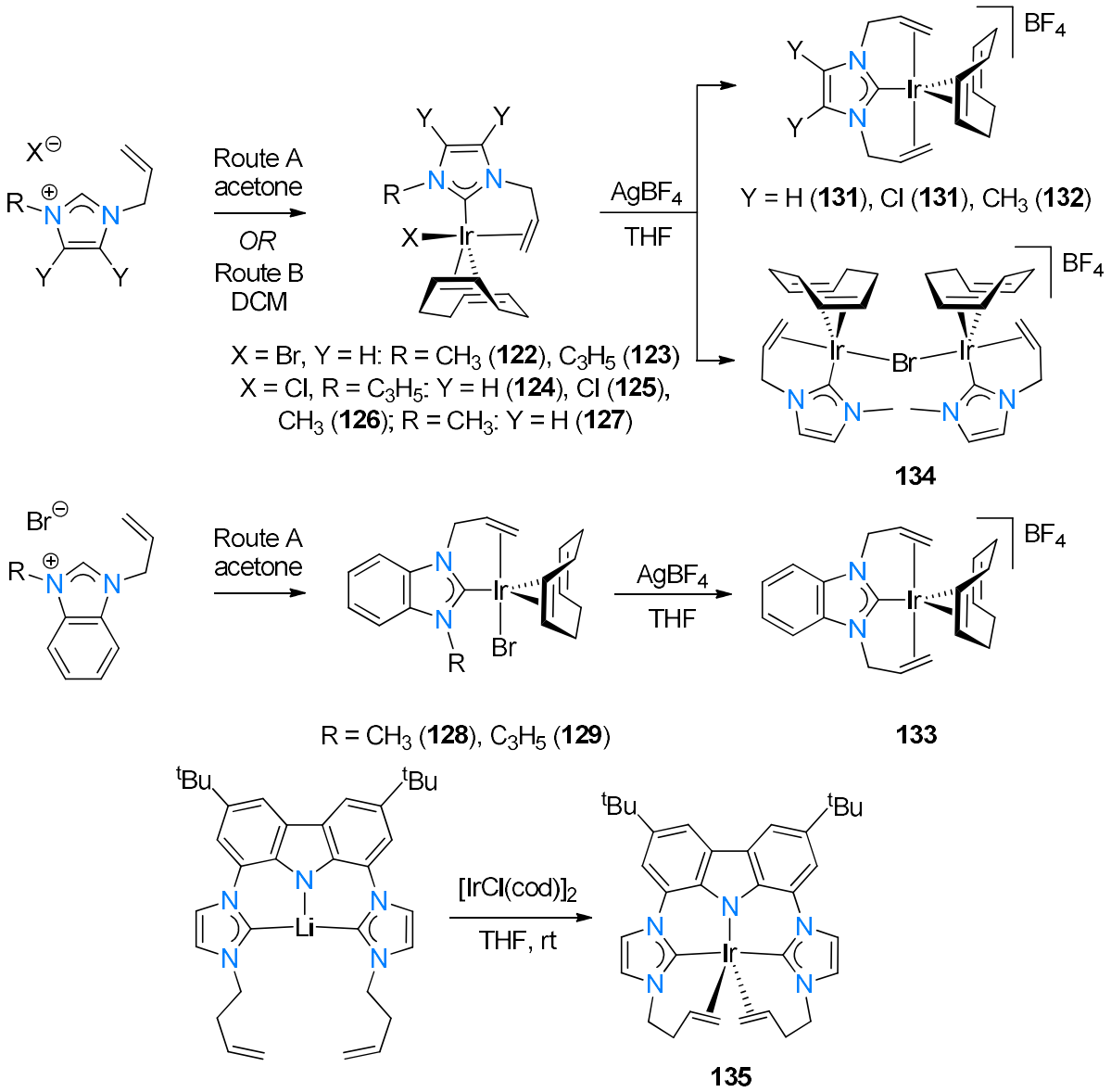

Scheme 32. Synthesis of the mononuclear Ir(I) NHC complexes **122-133** and **135**, as well as the dinuclear bridging Ir(I) NHC complex **134** by either routes A (direct reaction with $[Ir(OMe)(cod)]_2$) or route B (silver transmetallation using Ag_2O and $[IrCl(cod)]_2$).

In order to form the cationic iridium complexes, both groups made use of $AgBF_4$ that was added to solutions of **122-128** in CH_2Cl_2 (Scheme 32). Complexes **123-126** and **128** readily underwent anion exchange with $AgBF_4$ to form cationic complexes **130-133**, which feature both N-allyl substituents bound to iridium in a η^2-coordinated fashion. Conversely, reaction of **122** with $AgBF_4$ led to bromide abstraction and a bromido-bridged dinuclear complex **134** was formed, which was found to have an intense orange colour. Structural elucidation (SCXRD) of

134 confirmed the pentacoordinated iridium centre in a trigonal bipyramidal geometry (Figure 5). The bromido ligand is bridged along the equatorial position(s) of both iridium centres.

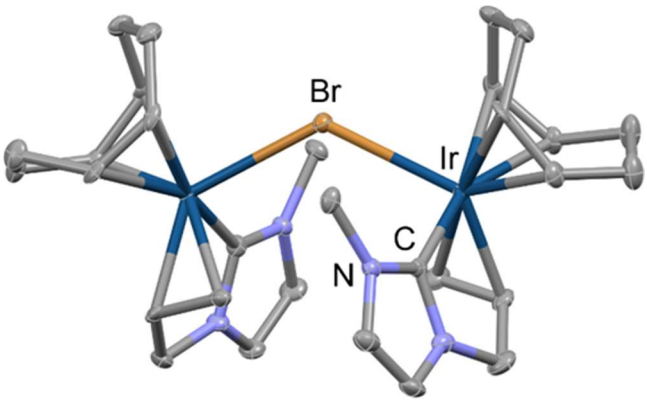

Figure 5. ORTEP plot of **134**. Thermal ellipsoids are drawn at 50% level. For clarity, a noncoordinating BF_4 anion, as well as hydrogen atoms are omitted.

Aldridge and co-workers [117-119] reported on sterically demanding NHC complexes of Ir(I). An interesting C-H activation was noted of an isopropyl group of the Dipp substituent forming an isopropene group during reaction of the HIDipp salt (in excess) with $[IrCl(coe)_2]_2$ at room temperature. After recrystallisation from pentane, a red crystalline solid (**136**) was obtained in 40% yield (Scheme 33). Activation of the isopropyl group was inferred from the ^{1}H NMR spectrum, which indicated three distinct isopropyl CH resonances in the ratio of 4:2:1, as well as a singlet methyl signal at 1.46 ppm. X-ray studies of **136** confirmed the structure of this biscarbene complex and thus that the alkene binds in a η^2-fashion. Both η^2-coordination and cyclometallation were observed. The authors found that **136** reacts with $Na[BAr^F{}_4]$ to generate the cationic complex **137** through chloride abstraction, accompanied by C-H bond activation of the previously inactivated NHC isopropyl moiety belonging to a second IDipp ligand. The ^{1}H NMR spectrum of **137** revealed a high-field peak at -46.6 ppm, which is not only diagnostic of C-H activation but also of a hydride *trans* to a vacant coordination site. The molecular structure determined from X-ray diffraction studies confirmed the structure, revealing a five-coordinate Ir(III) centre with two carbene donors, a η^2-coordinating allyl group, a cyclometallated σ-alkyl group, as well as a hydride ligand. Complex **137** is a rare example of an iridium complex containing the combination of alkene, alkyl and hydride ligands. Treatment of **136** with 4 atm. of H_2 yields the dihydride iridium(III) complex **138**. The ^{1}H NMR spectrum of **138** confirmed the presence of two hydride ligands with high-field signals observed as broad singlets at -25.69 and -24.97 ppm. The authors noted that further treatment of **136** with H_2 at 4

atm. results in hydrogenation of the alkene moiety, leading to bond cleavage to form the dihydride complex with two monodentate IDipp ligands.

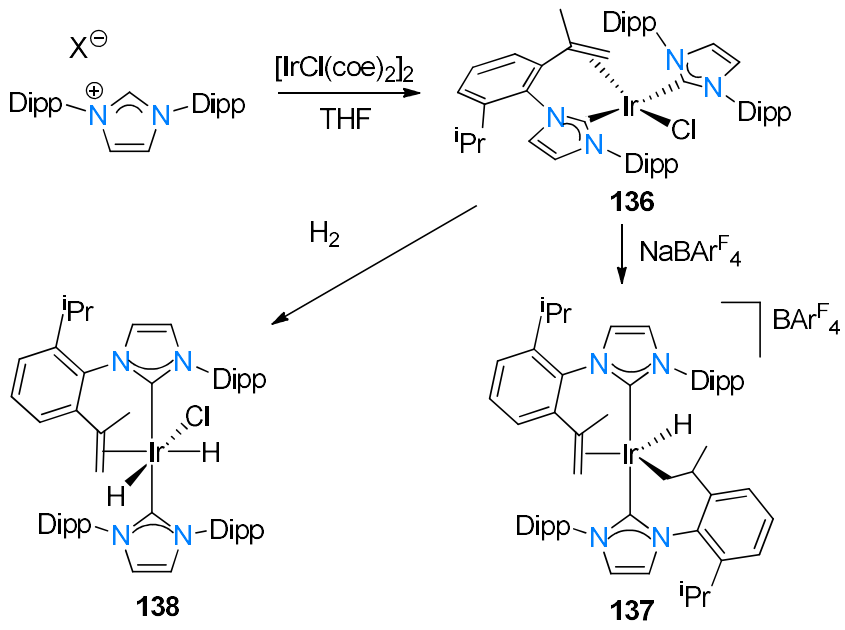

Scheme 33. Synthesis of Ir(I) (**136**) and Ir(III) (**137** and **138**) complexes.

Tamm and co-workers [32] investigated zwitterionic Ir(I) complexes with anionic NHC ligands for use in catalytic hydrogenation reactions. The authors initially synthesised the lithium-carbene complexes from the imidazolium salts and ^{n}BuLi, for use as transmetallation reagents. They proceeded to react the corresponding lithium salt with the metal precursor $[Ir(cod)Cl]_2$ in THF overnight to afford complexes **139-142** (50-74%) (Scheme 34). The authors found complexes **140** and **141** to be air-stable, complex **142** to be slightly air-sensitive and complex **139** to decompose rapidly, forming an unidentifiable mixture of products. The ^{1}H NMR spectrum of each complex revealed two distinct sets of signals for each aryl group, suggesting some dynamic interaction between the metal centre and one of the aryl groups. X-ray structural analysis of complexes **139-142** confirmed this interaction, where in all cases, intramolecular coordination of the arene ring is observed. This coordination of the arene ring results in a structural distortion and twisting of the NHC ligand. It was observed that there is a disparity between the M-C_{ortho} distances (e.g. Ir-C_{ortho} 2.706(3) Å *vs* Ir-C'_{ortho} 3.078(2) Å) which suggests that the arene bonded in a η^2-fashion. As part of their catalytic study, a brown, microcrystalline decomposition product (**143**) was isolated from the overnight reaction of **140** with H_2 (1 atm.). The ^{1}H NMR spectrum of **143** showed two separate ligand sets along with a characteristic

upfield (bridging) hydride resonance at -15.81 ppm integrating for a total of two ligands (one per iridium centre).

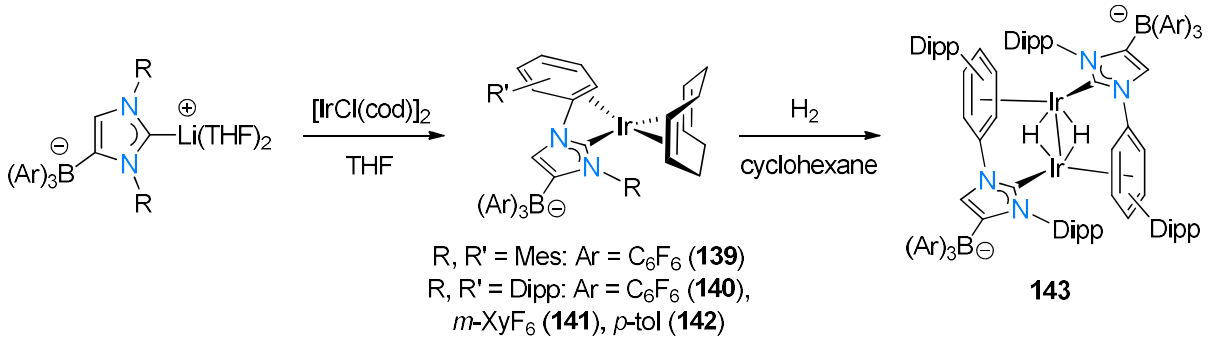

Scheme 34. Synthesis of Ir(I) NHC complexes **139-143**.

The group of Dorta [120-124] continued to investigate related formal 14-valence electron Ir(I) systems where pertinent aromatic interactions with the iridium centres exist. The reaction of square planar [IrCl(cod)(NHC)] complexes with $AgPF_6$ in DCM led to the formation of the deep-red, coordinatively unsaturated complexes **144-146**, each featuring a stabilising interaction from the adjacent wingtip of the N-arene (Scheme 35). SXRD of all three complexes confirmed the *syn*/*anti* geometry of the naphthyl wingtips and the slight sideways tilt of the Ir-NHC bond (Figure 6). Related halide abstraction experiments using $AgBF_4$ and $AgNTf_2$ expectedly gave analogous complexes **147** and **148**, respectively, of which the cation of the molecular structure (SCXRD) of each compared well with that of **146**. As part of evaluating the catalytic activity and selectivity of these complexes, chiral complexes **149-151**, each featuring Ph groups on the NHC backbone, were synthesised in a similar manner as in complexes **144-148**. The effect of the diene ligands were assessed by synthesizing analogues of complexes **144-151**, bearing the diene ligands tetrafluorobenzobarrelene (TFB), tetrachlorobenzobarrelene (TCB), and benzobarrelene (BB) in additionthe cod ligand. Of these new complexes **152-173** numerous complexes were found to be unstable both in the solid state and in solution, often showing signs of decomposition within the first few hours. Fortunately, all of the complexes **152-173** were fully characterised using among others NMR spectroscopy, with the molecular structures of an impressive nineteen of the twenty complexes fully elucidated by means of SCXRD. The ^{13}C NMR signals for the carbene carbon of complexes **144-172** were all comparable, ranging between 187.4-199.6 ppm. The effect of the non-coordinating anion was notable with an upfield shift from 196.0 ppm (*anti* **145**, PF_6) to 188.1 ppm (*anti* **148**, NTf_2) and 187.4 ppm (**147**, BF_4), respectively. The authors noted that **172** slowly decomposed in solution to form **174**, which could not be characterised by NMR,

however a single crystal suitable for X-ray diffraction was isolated. The molecular structure revealed a pincer complex whereby the two cylooctyl groups bind to the Ir centre in a square-planar geometry.

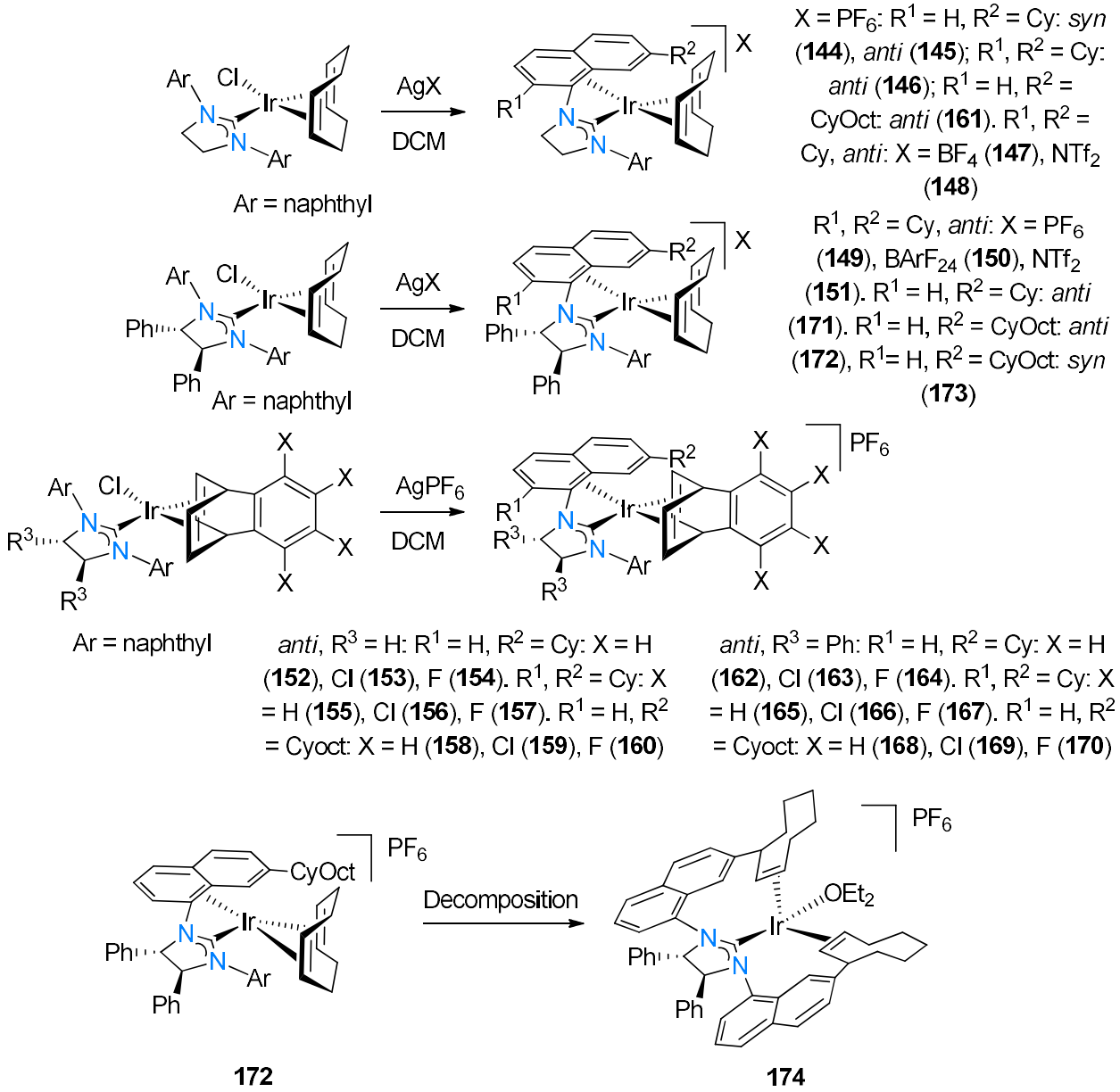

Scheme 35. Formation of naphthyl-stabilised Ir-NHC complexes **144-174**. Ar = 2,7-disubstituted naphthyl group. Substituents identical to the other coordinating N-group are shown in the figure.

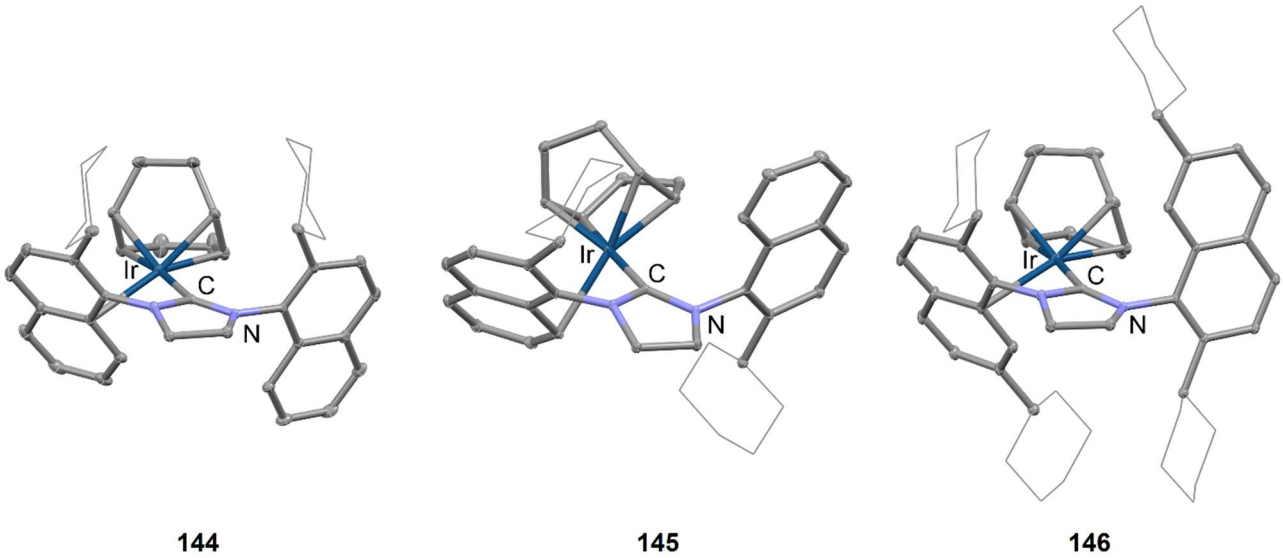

Figure 6. ORTEP plots of complexes **144**−**146**. Thermal ellipsoids are drawn at 50% level. For clarity, the cyclohexyl moieties are shown as wireframe presentations. DCM solvent molecules (**145** and **146**), noncoordinating PF_6 anions, and hydrogen atoms have been omitted.

4.2 Cyclometallated carbene complexes with alkyl-based tethers

This section reviews examples of class **B** (Figure 1) where chelating alkyl-NHC ligands feature on iridium complexes. The group of Yamaguchi [125,126] focussed on the use of alkoxide and triflate salts to facilitate facile intramolecular alkyl C-H activation reactions of Ir(III)-NHC complexes. Complex **175** formed (99% yield) by treating **C3** with sodium methoxide in isopropanol at room temperature (Scheme 36). The ^{1}H NMR spectrum of **172** revealed the non-equivalent geminal protons on the cyclometallated carbon with signals at 3.95 and 2.26 ppm ($^2J_{HH}$ = 10 Hz). Treatment of complex **175** with silver triflate and acetonitrile in dichloromethane gave complex **176**, having the chlorido ligand substituted for a nitrile ligand. Complex **176** is also attainable by first reacting **C3** with silver triflate in acetonitrile to form the bis-nitrile adduct **C4**, followed by treatment of either NaOMe in MeOH, or NEt_3 in CH_2Cl_2.

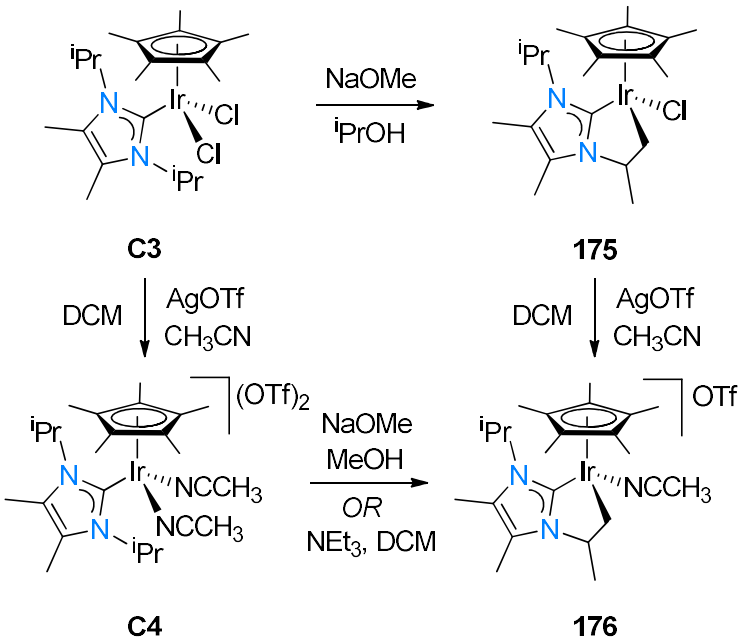

Scheme 36. Synthesis of cyclometallated Ir(III) complexes **175** and **176** *via* intramolecular C-H activation.

Additionally, the authors investigated similar reactions using an Ir(III)-NHC complex featuring a dimethylamine pendant cyclopentadienyl (Cp^N) ligand. The reaction of the diiodide complex **C5** with two equivalents of AgOTf in the presence of acetonitrile yielded complex **177** with 85% yield (Scheme 37). Like complex **175**, the ^{1}H NMR spectrum of **177** revealed the non-equivalent geminal protons on the cyclometallated carbon at 3.08 and 2.63 ppm ($^2J_{HH}$ = 11 Hz). Signals due to the carbene carbon, the nitrile carbon and the methyl carbon of the CH_3CN ligand were observed at 156.9, 117.3, and 4.0 ppm, respectively, on the ^{13}C NMR spectrum. The authors reasoned that the amino group might play an important role as a proton acceptor in the C-H bond activation mechanism. In order to remove a proton from the ammonium moiety of the $Cp^{N(H)}$ ligand in complex **177**, it was treated with $KOCH_3$ in THF at room temperature to form complex **178** in near quantitative yields. The ^{1}H NMR spectrum of **178** also exhibited the non-equivalent geminal protons of the cyclometallated carbon, with the additional non-equivalent methyl protons of the dimethylamino group appearing at 2.64 and 2.34 ppm, indicating intramolecular coordination of the dimethylamino group to the iridium centre.

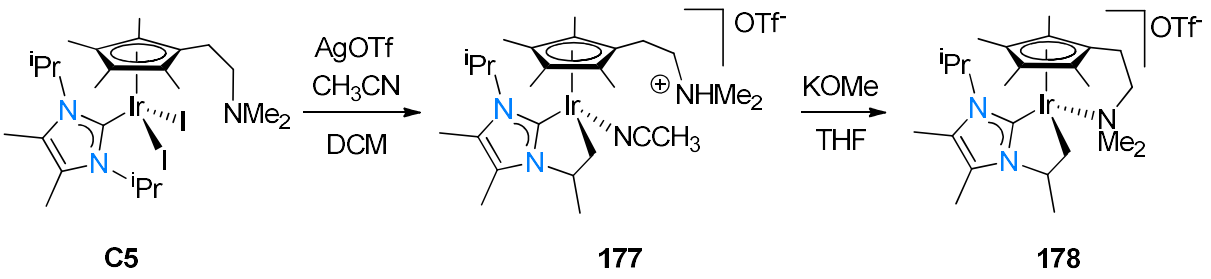

Scheme 37. Intramolecular alkyl C-H bond activation of Cp^{N}Ir-NHC complexes **177** and **178**.

Yamaguchi and co-workers [126] continued to investigate the cyclometallation of related NHC systems, and found that reaction of a **C3** analogue (**C3'**) with two equivalents of NaO^{i}Pr in ^{i}PrOH formed the cyclometallated Ir(III)-hydride complex **179** in 90% yield (Scheme 38). The hydride signal in the ^{1}H NMR spectrum of **179** appeared at -16.3 ppm. A similar reaction with excess NaOMe in ^{i}PrOH yielded analogous complex **180** (94%) that exhibited comparable NMR signals. Gradual chlorination of **179** was found to occur in chloroform at room temperature over a period of half an hour to give complex **181**, which in turn reacts readily with AgOTf in the presence of a neutral ligand (acetonitrile, pyridine) to give the corresponding ligand adduct complex salts **181** and **183** in high yield.

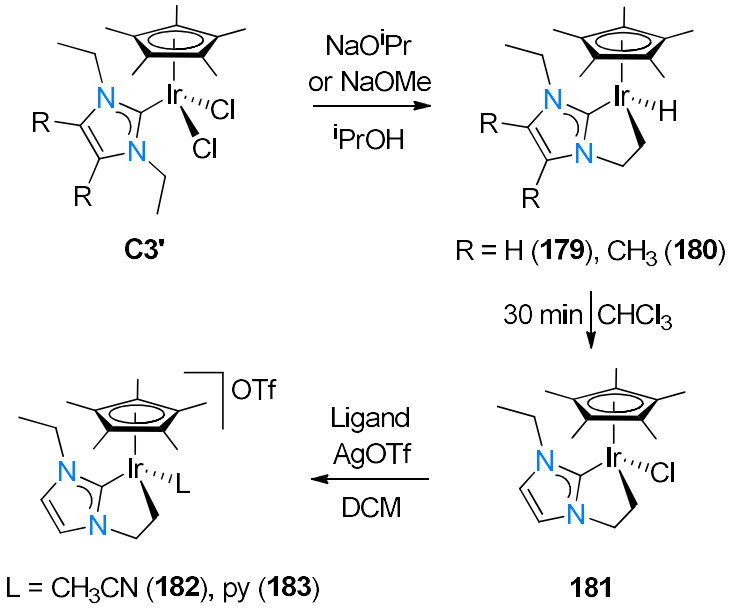

Scheme 38. Synthesis of cyclometallated Ir(III) complexes **176-180**.

Complementary to their previously mentioned work, Nolan and co-workers [84,127,128] synthesised the Ir(III) analogues to the Rh complexes mentioned previously (**52**, **53**) (Scheme

14, Scheme 39). Complex **184** revealed similar reactivity patterns as with its Rh analogue. It undergoes C-H activation to form the doubly cyclometallated complex **185**, which in turn could be transformed to the cationic derivative **186**. As before, both complexes **185** and **186** readily add CO to form corresponding complexes **187** and **188**, respectively. Nolan and co-workers [128] later reported a mechanistic study where it was found that complex **186** reacts with 1 equivalent of NH_3BH_3 in a D_2O/d_8-THF mixture (1:1) which yielded a mixture of products (complex **189** and a non-cyclometallated dihydride Ir-NHC complex). The authors noted an increase in the amount of **189** formed when the equivalence of NH_3BH_3 was increased twofold. Based on these results the authors investigated the reaction of **187** with NH_3 and found that **186** adds one equivalent of NH_3 to yield **190**. To confirm that the *ortho*-demetallation observed in complex **189** was due to the presence of H_2 in the reaction mixture, the authors placed **190** under 1.0 atm. of H_2, which unexpectedly yielded the dihydride complex with a loss of the bound NH_3. It was reasoned that *ortho*-demetallation might facilitate the loss of a weakly bound ammonia ligand.

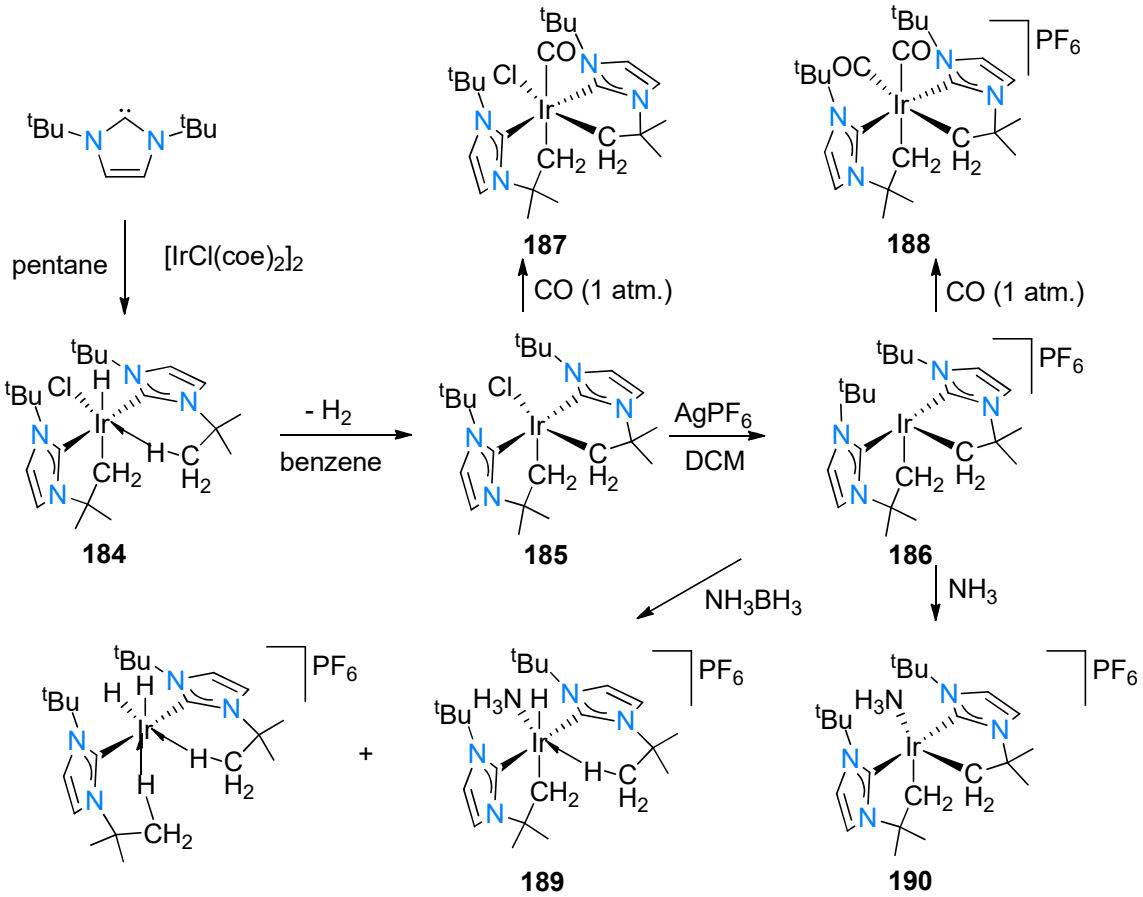

Scheme 39. Synthesis and reactivity of cyclometallated complexes **184-190**.

Aldridge and co-workers [129] investigated the related formation of the complex [IrCl(coe)(NHC)$_2$] from [IrCl(coe)$_2$]$_2$ and the free carbene IMes. The Ir(I) biscarbene spontaneously cyclometallates to form the five-coordinate complex **191** in 79% yield (Scheme 40). Complex **191** was also structurally characterised which in contrary to the structure of **184**, did not show any agostic hydrogen interaction of the neighbouring IMes ligand, and instead revealed an approximate planar coordination environment at the iridium centre (in the equatorial plane), with the hydride ligand effectively located *trans* to a vacant site. The ^{1}H NMR spectrum exhibited a hydride signal at -32.84 ppm, with ^{13}C NMR revealing two carbene carbon signals at 210.4 and 209.9 ppm, highlighting the two different NHC ligands in **191**.

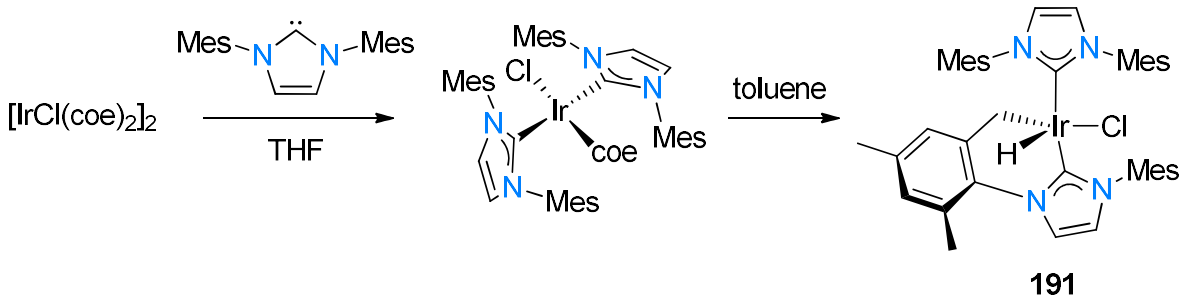

Scheme 40. Formation of complex **191**.

The group led by Sola [130,131] investigated NHC complexes of iridium with labile and cyclometallated ligand systems. The authors focussed on the hydrogenation reactions of dihydride-containing monocarbene Ir complexes (**C6**) and through these reactions discovered Ir(III)-NHC complexes featuring cyclometallated IMes ligands instead of the expected Ir(I) derivatives. The authors found that the reaction of the dihydride complex **C6** with an excess of a hydrogen acceptor (A = ethylene, propylene or PhC≡CPh) led directly to the formation of the cyclometallated complexes **194-196** (Scheme 41) *via* the intermediate hydride complexes **192** and **193**. However, to synthesise the intermediate complex **192**, the most effective method was bubbling propylene through solutions of the monocarbene complex. This is because of the facile nature of the reverse β-hydrogen elimination of **195** to form **192**, which, interestingly, could not be repeated using complexes **194** and **196**. A different reactivity profile of the phosphine derivative of **C6** (as compared to the acetonitrile analogue) was observed: reaction of the phosphine **C6** complex with an excess of a hydrogen acceptor (A = ethylene, propylene or PhC≡CPh) led to the formation of the intermediate **193** as the trapped product. The subsequent insertion reaction does not occur with complex **193**, which the authors contributed to possible thermodynamic reasons due to the associated steric properties of the P^{i}Pr$_3$ ligand.

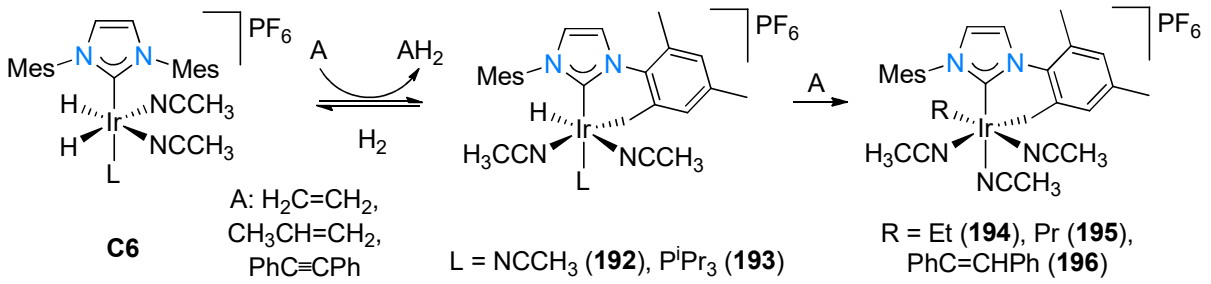

Scheme 41. Synthesis of cyclometallated Ir(III)-NHC complexes **192-196**.

In terms of iridium complexes featuring labile ligands, the group of Sola [130,131] found the optimal conditions for the synthesis of complexes **197-205** (Scheme 42) to be heating of propylene-saturated acetone solutions of the precursor arene complex (**C7**) at 328 K for several hours. Some complexes were also attainable from its derivatives using an appropriate reagent: for example, complex **198** is also accessible from the reaction of **194** in CH_3CN; and similarly, complex **199** from **198** and $NaBPh_4$. Interestingly, it was found that despite the ability of complexes **197-199** to generate coordination vacancies, they were unreactive to conventional sources of hydrogen to reverse the cyclometallation. Neither placing the complexes (**197-199**) under 60 bar of H_2 gas, nor other oxidative reagents such as triethylsilane, pinacolborane, or phenylacetylene showed any reaction. However, the phosphine derivative **200** was found to react with these reagents; reaction of **200** with phenylacetylene yielded complex **201**, which suggests the involvement of the Ir(IV) oxidation state as a possible intermediate or transition state. The authors theorised it would require an additional basic ligand such as a phosphine group, thus **200** reacts with HC≡CPh while **198** does not. Subjecting **200** to H_2 gas or excess triethylsilane cleaves the cyclometallated bonds to yield the corresponding dihydride complex. It is interesting to note that the reaction of the singly cyclometallated complex (**193**) with phenylacetylene yielded a different product to that of the doubly cyclometallated complex (**200**): reaction of **193** with phenylacetylene begins with a C-H reductive elimination step, which yields a hydride-alkynyl complex as the final product, while **200** incorporates the phenylacetylene into the cyclometallated IMes ligand. Even though the two complexes have similar structures, having singly or doubly cyclometallated IMes ligands led to different reactivities. Complex **202** is obtained *via* reaction of **C7** with TlCp (cyclopentadienyl thallium), subsequent reaction of **202** with triflic acid without solvent results in the formation of the intermediate **203** (isolated at below 270 K). In the presence of CH_3CN, reaction of **202** with

triflic acid yields **204**. Bubbling of ethylene through a solution of **202** in toluene with the addition of triflic acid results in the formation of **205**.

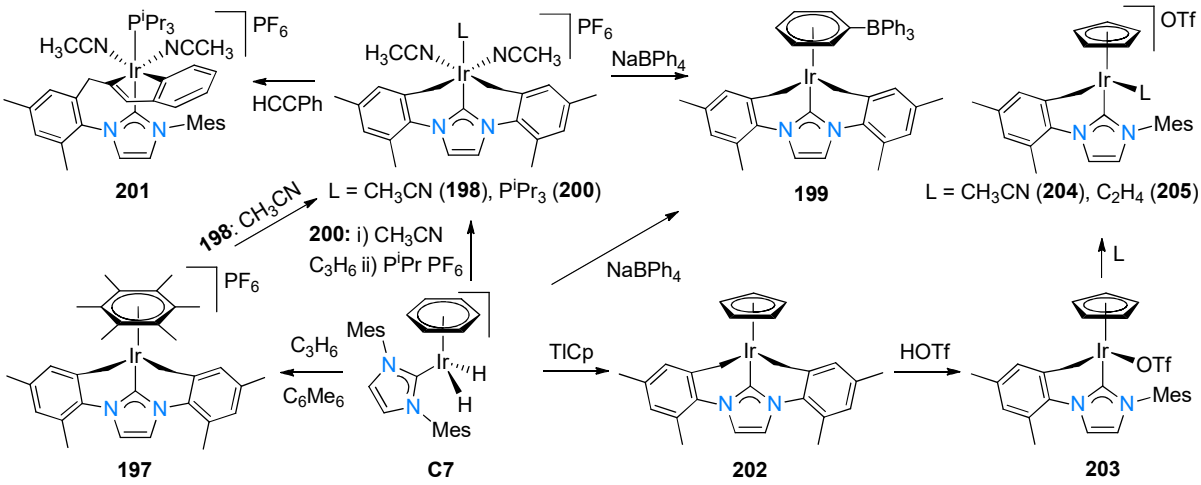

Scheme 42. Synthesis of doubly cyclometallated Ir(III) NHC complexes **197-205**.

The group of Chaplin [132] observed alkyl-based cyclometallation *via* an oxidative addition reaction upon subjecting an Ir(I)-NHC to deuterated acetonitrile. In this intramolecular C-H bond activation reaction, the cyclooctadiene ligand acts as an internal hydride acceptor, with the acetonitrile molecule coordination stabilizing the final cationic product **206** (Scheme 43). NMR and SCXRD studies collectively confirmed the meridional geometry that the cyclometallated NHC ligand adopts in **206**. The acetonitrile ligand in **206** is rapidly substituted for a molecule of CO upon exposure of an acetonitrile solution of **206** to carbon monoxide (1 atm.) to form complex **207**. Reaction of the precursor Ir(I)-NHC complex with diphenylacetylene as external hydride acceptor rendered the cyclooctadiene ligand a spectator ligand. Reacting the Ir(I)-NHC with diphenylacetylene at 318K results in non-reversible cyclometallation to form the complex **208**.

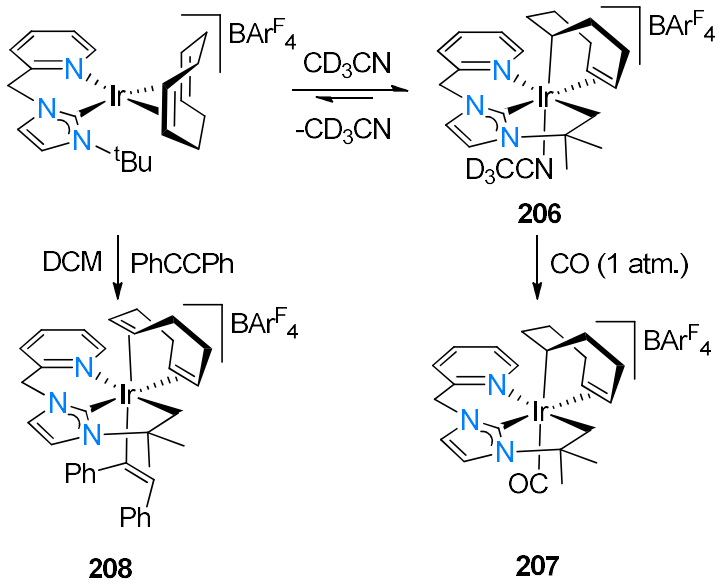

Scheme 43. Synthesis and reactivity of NCC pincer Ir(III)-NHC complexes.

The group of Peris [133-135] investigated the outcome of cyclometallation reactions with Cp*Ir(III)-NHC complexes featuring NHC ligands with activatable N-substituents (Scheme 44). For example, the hydroxyalkyl functionalised NHC ligands reacts with Ag_2O and KI, followed by addition of the dimer $[Cp^*IrCl_2]_2$ in a transmetallation reaction to yield the complexes $[Cp^*IrI_2(NHC)]$. The monocarbene complexes featuring hydroxyethyl substituents react further with Cs_2CO_3 in refluxing methanol to form the corresponding yellow cyclometallated complexes **209-211**, each now featuring a coordinated acyl group. Complexes **209-211** are also accessible directly from the imidazolium salt, $[Cp^*IrCl_2]_2$ and Cs_2CO_3 in methanol. Interestingly, a different outcome is achieved upon employing the monocarbene complex featuring a hydroxypropyl substituent: reaction with Ag_2O leads to intramolecular cyclometallation to form the yellow complex **212**, which now features a stereogenic carbon with a pendant ester functional group. This observed reaction was reasoned to occur due to the energetically more favourable five-membered iridacycle that forms, as is the case in the formation of complexes **209-211**. Complex **212** is also attainable from the imidazolium salt, $[Cp^*IrCl_2]_2$, Ag_2O and KI in MeOH, to form the intermediate ester-functionalised monodentate NHC iridium complex, followed by subsequent addition of Ag_2O to form **212**. ^{13}C NMR signals for the carbene carbon and cyclometallated carbon atoms of complexes **209-210** appeared at 162-165 and 222-223 ppm respectively, in comparison to the same atoms in **212** appearing at 158.5 and 184.0 ppm, respectively.

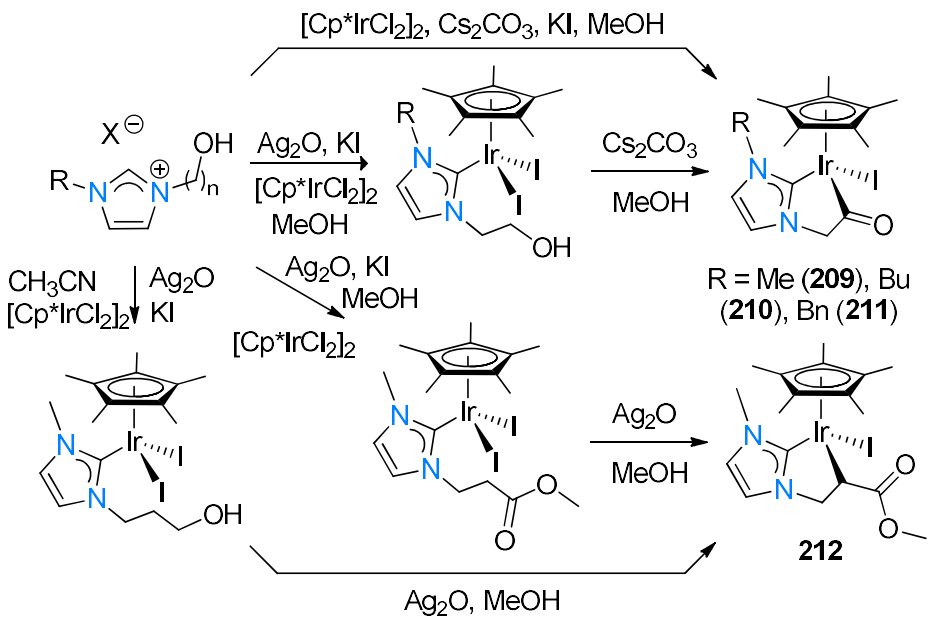

Scheme 44. Carbonyl-containing cyclometallated Ir(III) complexes **209-212**.

Peris [134-136] continued to investigate bis-imidazolium salts linked by methyl or ethyl tethers. Reaction of either ligand with $[Cp^*IrCl_2]_2$, NaOAc and KI, followed by KPF_6 gave the abnormal carbene complexes **213** (50% yield) and **214** (12% yield), each featuring a cyclometallated 2-alkylimidazole wingtip (Scheme 45). In the case of the ethyl-linked bis-imidazolium salt additional products formed, including the biscarbene complex (main product, 30%), and the dealkylated adduct (15%), making complex **214** the minor product formed in the reaction. ^{13}C NMR spectroscopy revealed signals for the two respective cyclometallated carbons at 29 ppm for **214** and an unusually high upfield value of -15 ppm for **213**. The molecular structure of **213** (SCXRD) confirmed the loss of symmetry associated with the NHC ligand post-ligation, as well as the geometry of the distorted seven-membered iridacyle.

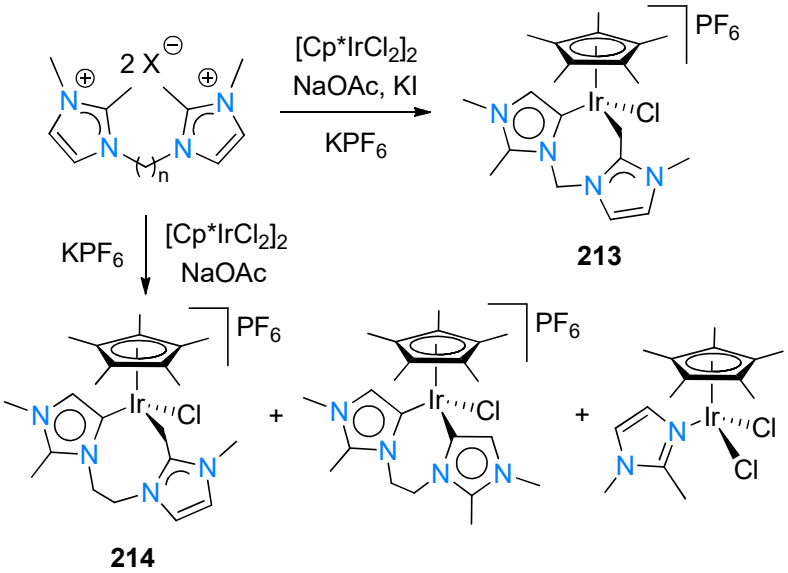

Scheme 45. Abnormal Cp*Ir(III)-NHC complexes **213** and **214**.

The same group also noted a competitive aliphatic versus aromatic intramolecular C-H activation process occurring in [Cp*Ir(NHC)] complexes [135]. During initial attempts at synthesising the (unstable) monodentate [Cp*IrX$_2$(NHC)] (X = Cl, I) complexes, facile C-H activation occurs within hours after formation of the monocarbene complexes to form the arene cyclometallated complexes **215-218** (Scheme 46). Alternatively, **215-218** could also be directly obtained from the reaction of the imidazolium salt, [Cp*IrCl$_2$]$_2$ and NaOAc (with the addition of NaI for **215** and **216**). ^{13}C NMR spectroscopy of the complexes revealed that both coordination of the NHC ($C_{Carbene}$ at 154-157 ppm) and *ortho*metallation ($C_{orthometallated}$ 141-145 ppm) have occurred. Complex **216** formed as a mixture of chiral complexes: four chiral complexes are obtained from two pairs of diastereomers evident from analysis of the ^{1}H NMR spectrum. The diastereomers could be easily separated by column chromatography. Crystals suitable for X-ray diffraction studies, were grown for both diastereomers and revealed unique Ir-NHC bite angles of 86.2(2)° (**216a**) and 85.83(15)° (**216b**), with the remainder of bond distances and angles comparable.

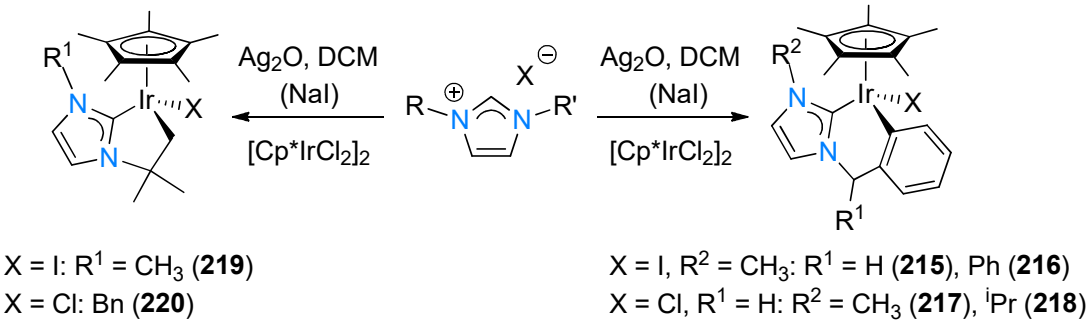

Scheme 46. Aliphatic *versus* aromatic C-H activation in complexes **215-220**.

The authors reacted 1-*tert*-butyl-3-methylimidazolium iodide with silver oxide in DCM, with transmetallation onto $[Cp^*IrCl_2]_2$ to afford complex **219**. ^{1}H NMR spectroscopy revealed resonances of the non-equivalent geminal protons of the cyclometallated CH_2 group (3.08 and 2.49 ppm ($^2J_{HH}$ = 9.9 Hz)). The ^{13}C NMR spectrum showed the carbene carbon signal at 161.8 ppm and the cyclometallated methylene carbon at 27.5 ppm. To investigate which of the cyclometallation processes (aliphatic or aromatic) is the most favourable, the precursor ligand 1-benzyl-3-*tert*-butylimidazolium chloride was employed. The coordination to $[Cp^*IrCl_2]_2$ could lead to a mixture of complexes where cyclometallation occurred in an aliphatic and/or aromatic fashion. Instead, complex **220** was isolated as the sole product *via* aliphatic C-H activation due to the formation of the more stable five-membered metallacycle [135].

4.3 Cyclometallated carbene complexes with arene-based tethers

Complexes with an NHC-tether of type **C** (Figure 1) are discussed in this section, where the synthetic and reactivity routes of each of the complexes are described. Iridium-based monocarbene complexes with aryl-based tethers are hugely popular, with a rather large body of work dedicated to these complexes. The most common series is the mononuclear mono- and biscarbene complexes that will be covered later in this section. The examples have been grouped according to the number of carbon-tethered NHC ligands present on an iridium centre.

4.3.1 Monocarbene complexes

One of the first examples reported in this category is by the group of Crabtree [36,43]. They found that treatment of the bis-phenyl imidazolium salt with $[Cp^*IrCl_2]_2$ in the presence of KO^{t}Bu forms yellow complex **221**, featuring one of the phenyl substituents directly bound to

the iridium centre (Scheme 47). The group of Choudhury [137] used Cs_2CO_3 and NaOAc with $[Cp^*IrCl_2]_2$ a range of imidazolium salts to produce a range of cyclometallated complexes **222-231**.Other groups, including those of Liu [138], Xiao [42], Cross [85], and Macchioni [44] have since diversified the series to include a number of different cyclometallated aryl groups. While the groups of Liu and Macchioni made use of the traditional Ag_2O transmetallation strategy, the other groups made use of NaOAc as mild base in order to access compounds **232-238**. Collectively, the ^{13}C NMR spectra of these complexes showed resonances for the carbene carbon and cyclometallated arene carbon at 157-165 and 142-147 ppm, respectively. These values indicate a relatively small electronic effect of the different substituents present on the arene ring, the linker, as well as the NHC backbone in each example on the ^{13}C carbene and cyclometallated carbon resonances.

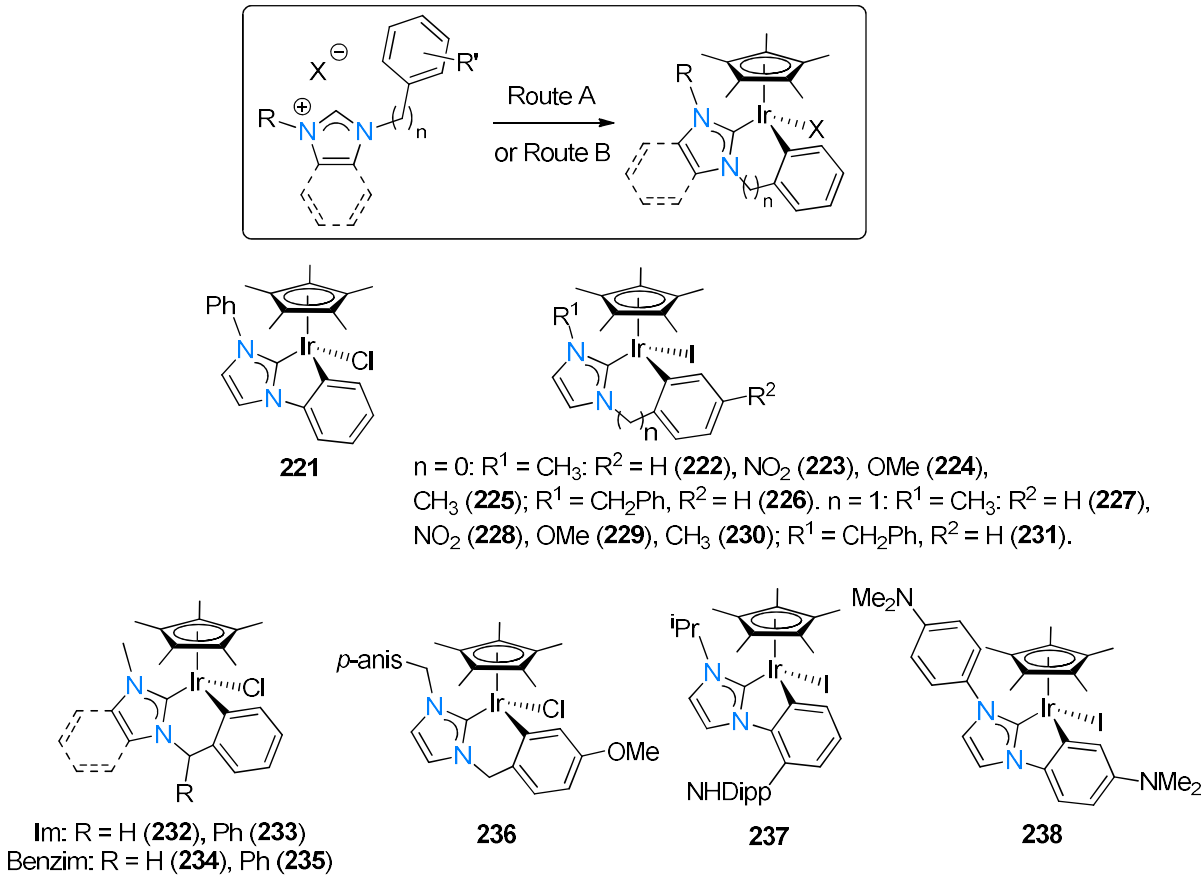

Scheme 47. Arene-cyclometallated complexes **221-238**. Route A: Transmetallation using Ag_2O. Route B: NaOAc (KO^tBu for **221**) or KI (for iodido complexes).

By using a Ag_2O transmetallation strategy for $[IrCl(cod)]_2$, the group of Morris [33] isolated an Ir(III)-hydride complex, **239**, featuring a chiral tridentate NHC ligand in 84% yield (Scheme

48). The hydride signal in the ^{1}H NMR spectrum of **239** appeared at -15.49 ppm. The unique structure of **239** was confirmed using SCXRD (Figure 7).

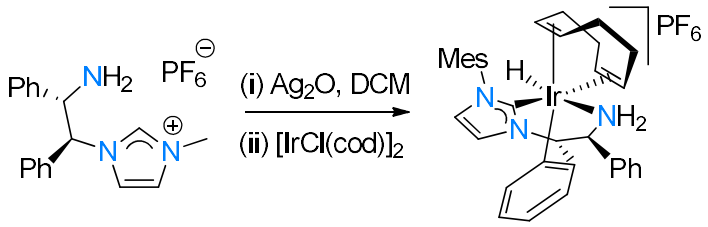

239

Scheme 48. Tridentate chiral Ir(III)-NHC complex **239**.

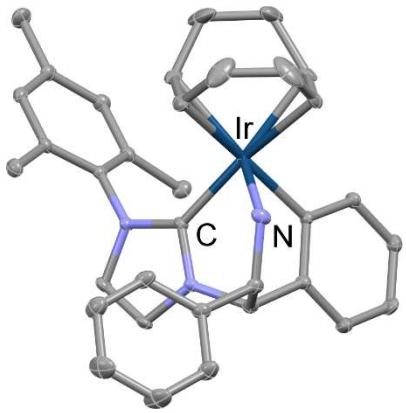

Figure 7. ORTEP plot of **239**. Thermal ellipsoids are drawn at 50% level. For clarity, pentane and DCM solvent molecules, a noncoordinating PF_6 anion, and hydrogen atoms have been omitted.

Several research groups including those of Peris [92], Choudhury [38,139,140], and Grotjahn [141] also included carbon-coordinated pyridyl groups appended to the NHC ligand framework (Scheme 49). By either making use of a mild base such Cs_2CO_3 (Peris and Choudhury), or the standard Ag_2O transmetallation strategy (Choudhury and Grotjahn), pyridyl-containing cyclometallated Ir-NHC complexes **240-246** were isolated. Peris found that treatment of the imidazolium salt with Cs_2CO_3 cleanly reacted with $[Cp^*IrCl_2]_2$ to give complex **240** (75% yield), which features the pyridylidene coordinated to the metal through the *para*-carbon atom. Upon employing the *para*-substituted pyridyl-imidazolium salt, the expected cyclometallated

complex **241** was formed (58% yield) as well as a dimetallic species in which ring-opening of the NHC ligand occurred (15% yield).

The occurance of remote C-H activation of the pyridyl group to cyclometallate to the iridium centre to form five-membered iridacyles seem to be the driving force in the formation of complexes **242** and **243**, as found by the group of Choudhury [139]. The nitrogen atom of the pyridyl group is thus free to coordinate to a second [Cp*$IrCl_2$]-fragment to form dinuclear complexes **242** and **243**. The persistent C-H activation of the pyridyl group is interesting in the case of **243**, since an available N-phenyl group as alternative moiety that may also be susceptible to C-H activation. However, by incorporating a methylene linker between the NHC ring and pyridyl tether, C-H activation of the N-phenyl substituent becomes favoured over the pyridyl ring to yield complex **244** (Scheme 49). In the case of complex **244**, the free pyridyl moiety again coordinates to a second [Cp*$IrCl_2$] fragment to form a dinuclear complex. Grotjahn found that reaction of the more bulky N-6-^{t}Bu-pyrid-2-yl imidazolium salt with Ag_2O, followed by addition of [Cp*$IrCl_2$]$_2$ favoured coordination to the C-3 position of the pyridyl group instead of the N atom. Cyclometallated orange-red complex **245** formed as a cationic Ir(III) complex with a protonated pyridyl fragment, which, upon treatment with Amberjet OH resin, deprotonates the charged pyridyl group, and forms the deep-red neutral Ir(III) complex **246**. The geometries and ligand connectivities were confirmed using NMR spectroscopy and SCXRD (**246** only).

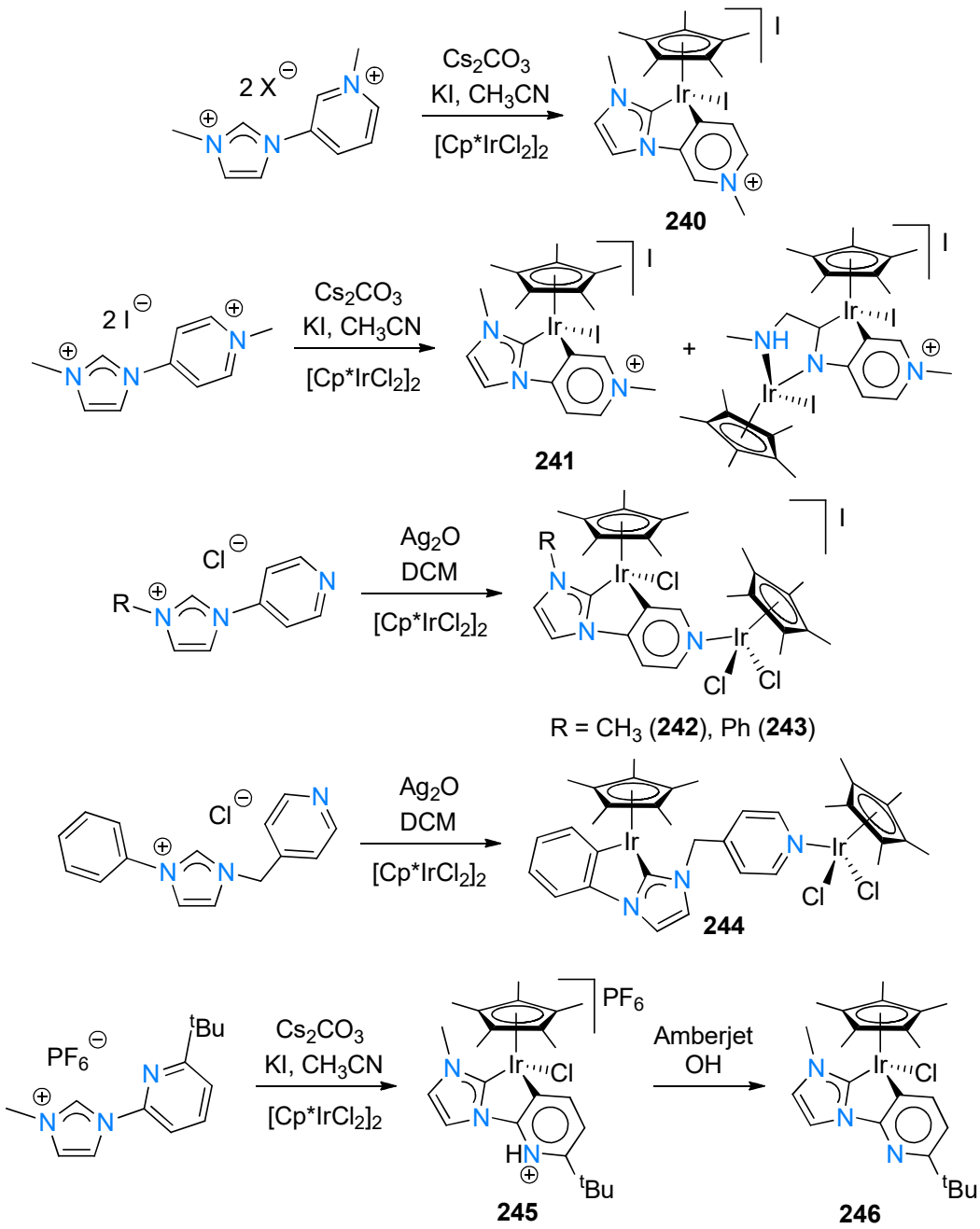

Scheme 49. Synthesis of pyridyl-containing cyclometallated Ir-NHC complexes **240**-**246**.

Choudhury [140] observed *ortho*metallation of the phenyl ring from an NHC ligand featuring a terpyridine pendant group. Complex **247** was obtained in 85% yield by treatment of the imidazolium salt precursor with Cs_2CO_3, followed by $[Cp^*IrCl_2]_2$ (Scheme 50). Subsequent treatment of **247** with 0.5 equivalents of $Zn(OAc)_2$ in the presence of NH_4PF_6, formed the trinuclear cationic complex **248** in 65% yield. The central Zn cation coordinated to two molecules of **248** *via* the terpyridine pendant frameworks.

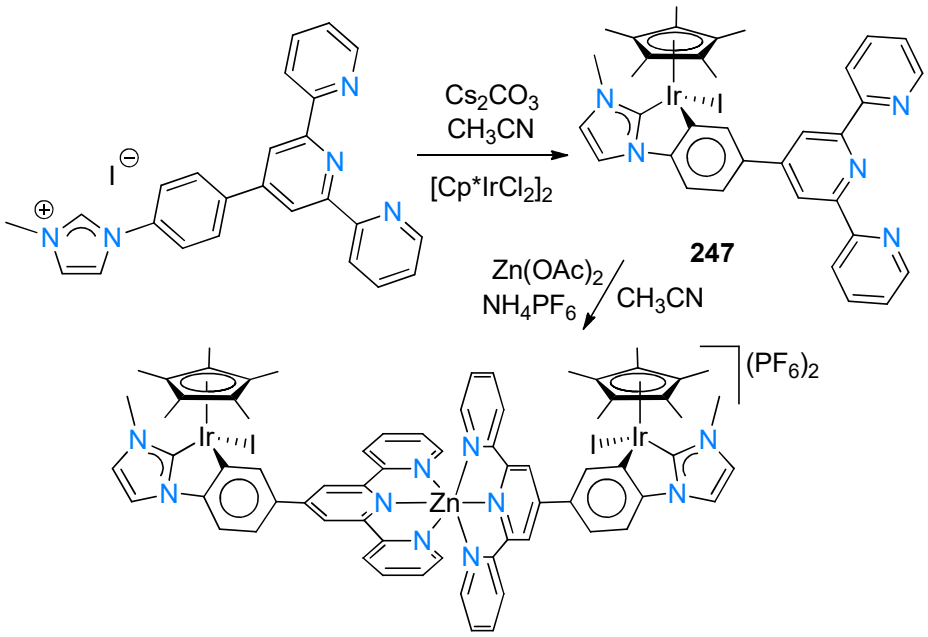

Scheme 50. Synthesis of mono- and trinuclear terpyridine Ir-NHC complexes **247** and **248**.

The groups of Hahn [94,95,102,142-146] and Maity [147] investigated similar larger architecures of NHC ligands featuring imidazolium pendant groups that in turn are metallated to form bis- and triscarbene complexes. Hahn [142] reported that the tris-imidazolium tribromide salt reacts with NaOAc, $[Cp^*IrCl_2]_2$ and $Pd(OAc)_2$ in CH_3CN to form the dinuclear triscarbene complex **249** in 40% yield (Scheme 51). The site-selective metallation stems from the tendency of Pd(II) to form *cis*-dicarbene chelate complexes in the presence of bis-NHC ligand frameworks, whereas Ir(III)-centres tend to bear only one NHC and rather orthometallates the adjacent phenyl group (if present).

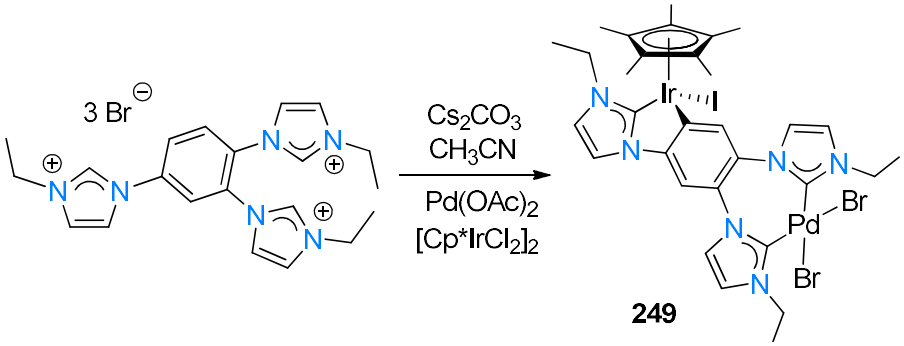

Scheme 51. Synthesis of heterometallic Ir/Pd triscarbene complex **249**.

Similarly, Hahn [95,143] found that the phenyl-bridged bis-imidazolium salts react with Cs_2CO_3, NaOAc, and $[Cp^*IrCl_2]_2$ in CH_3CN to form the cationic Cp*IrCl(NHC)-imidazolium appended complexes **250** and **252** in 83% and 65% yield, respectively (Scheme 52). The tendency to form the monometallated complex for both **250** and **252** holds even upon employing one or more equivalents of the iridium dimer. However, reaction of **252** with $[Cp^*RhCl_2]_2$ forms the dinuclear Ir/Rh-NHC complex **253** in 54% yield, an observation which was ascribed to differences in the reactivity of the two metals. In the case of **250**, exposure to Ag_2O, followed by the addition of [AuCl(tht)] and KI, formed the biscarbene **251** in 34% yield. Molecular structures of **251** and **252** were confirmed by SCXRD. Moving from the 1,4-phenyl bridged bis-NHC ligands to the 1,3-phenyl bridged bis-NHC ligands, this group [94,95] followed a similar method whereby the bis-imidazolium salt reacts with Cs_2CO_3, NaOAc, KI, $[Cp^*IrCl_2]_2$ in CH_3CN to give the imidazolium-pendant Ir(III)-NHC complex **254** (88% yield), which in turn reacts with Ag_2O followed by [AuCl(tht)] and KI to give the corresponding Ir/Au biscarbene complex **255** (56% yield) (Scheme 53). Complex **254** was found to react with Ag_2O and $PdCl(dmba)_2$ to form the heterodimetallic Ir/Pd bis-NHC complex **256** in good yield (78%). The NMR spectra of **256** revealed double signal sets for all resonances, suggesting the formation of two atropisomers in the ratio 52:48.

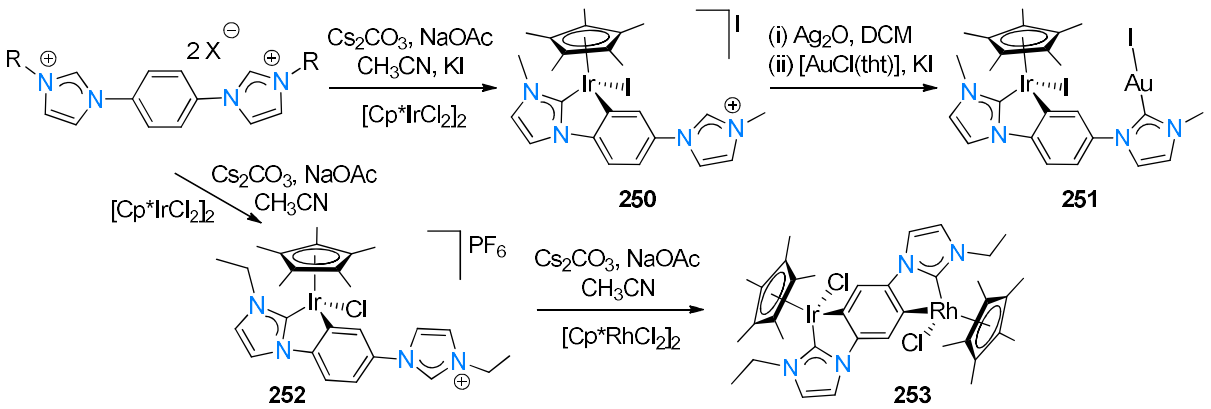

Scheme 52. Synthesis of cyclometallated (bis)carbene complexes **250-253**.

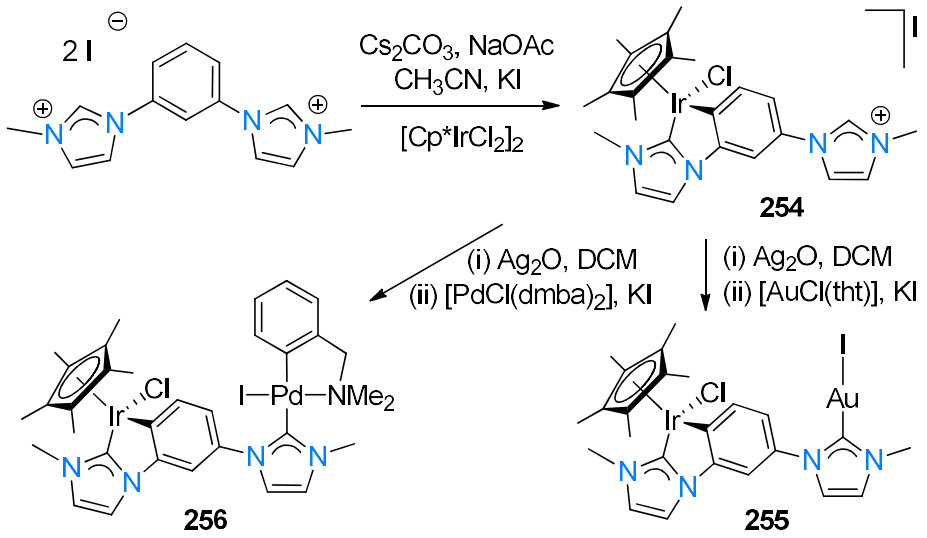

Scheme 53. Synthesis of cyclometallated (bis)carbene complexes **254-256**.

In a similar series of reactions, the group of Maity [147] made use of a 1,4-diphenyl bis-NHC ligand framework and reacted it with K_2CO_3/NaOAc, KI, and $[Cp^*IrCl_2]_2$ in CH_3CN to give the expected mono-metallated complex **257** (65% yield), which is a molecular analogue of complex **250** (Scheme 54). Complex **257** in turn reacts with $PdCl_2$ in pyridine in the presence of K_2CO_3 and KI to give the heterodinuclear complex **258** (73% yield). The mononuclear analogue of **257** featuring the cyclometallated Ir-NHC functionality was also synthesised by Maity, where treatment of the imidazolium salt with K_2CO_3/NaOAc, KI, and $[Cp^*IrCl_2]_2$ in CH_3CN yielded complex **259** (Scheme 55).

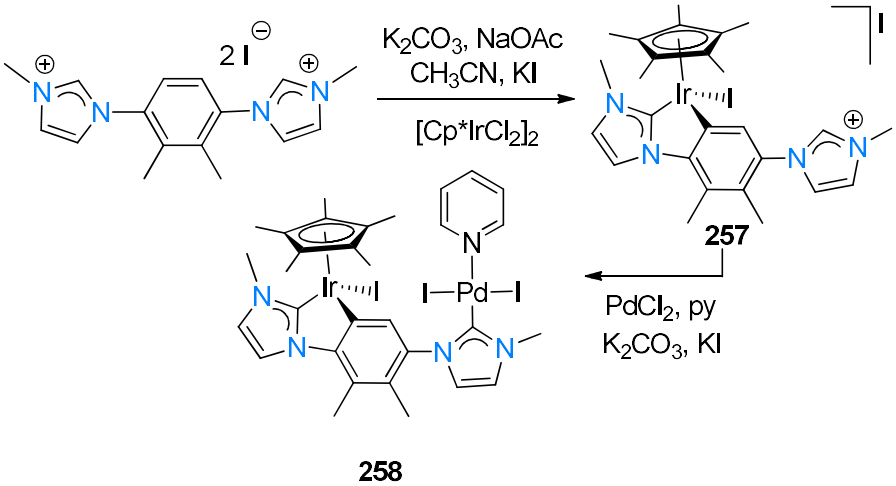

Scheme 54. Synthesis of cyclometallated (bis)carbene complexes **257** and **258**.

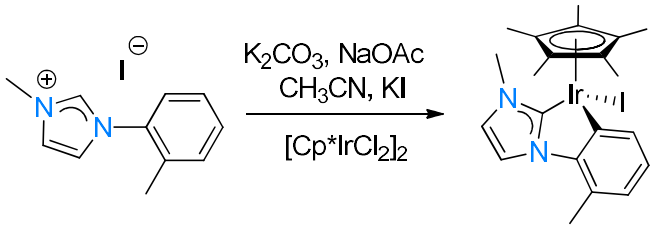

259

Scheme 55. Synthesis of complex **259**.

The group of Hahn [102,144-146] investigated the use of other pendant N-heterocycles in their ligand design, which featured imidazole, theophylline, and adenine moieties. All of the complexes **260-263** were obtained *via* the reaction of the imidazolium salt, NaOAc and $[Cp^*IrCl_2]_2$ (Scheme 56). As part of the formation of the cyclometallated complexes, it is assumed that deprotonation of the imidazolium fragment occurs initially, generating the free carbene that subsequently coordinates to the iridium centre. A second equivalent of NaOAc then deprotonates the pendant N-heterocycle to give the corresponding anionic fragment that subsequently coordinates to the iridium centre, forming the metallacycle. All complexes were obtained in moderate to excellent yields (56-96%), each of which exhibited ^{13}C NMR signals for the carbene (NHC) carbon atom and cyclometallated N-heterocycle at 153-159 and 143-159 ppm, respectively. Chiral iridium centres based on a distorted piano-stool geometry were observed for the molecular structures (SCXRD) of complexes **261** and **262**. Subsequent treatment of complexes **260** and **261** with alkyl dihalides served as a convenient strategy to form biscarbene complexes of Ir(III), whereafter conjugation of a second equivalent of either **260** or **261** to the alkyl halide end of the newly formed biscarbene complexes gave the corresponding tetracarbene complexes.

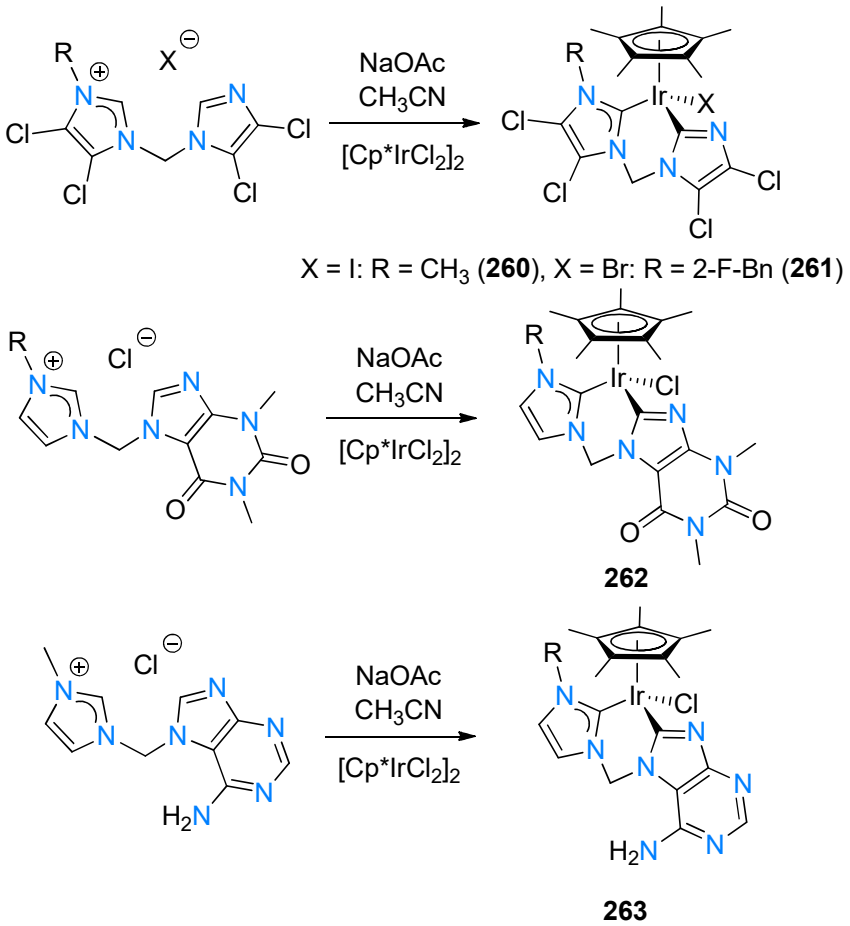

Scheme 56. Synthesis of Ir-NHC complexes (**260-263**) featuring cyclometallated N-heterocycle-appended NHC ligands.

The group of Chi [148] focussed on a tridentate mono-NHC ligand framework and ligated it to Ir(III) in six examples. The synthesis of complexes **264-269** involved a two-step process where the imidazolium ligand was first treated with NaOAc and $[Ir(cod)Cl]_2$ in refluxing acetonitrile (Scheme 57). After heating for 12 hours, the solvent was replaced by decalin, along with the addition of a second (albeit unique) tridentate ligand. The resulting mixure was heated overnight at 200 °C after which the yellow complex was isolated in low yields (23-35%, respectively) (following purification by column chromatography). Interestingly, the isoquinolinyl prochelate gave complex **269** containing a bidentate fragment; if the reaction was done in a "one-pot" method in refluxing xylene, complex **269** was formed instead. Complex **269** could also be obtained upon heating **269** in decalin at high temperatures. The authors thus concluded that complex **269** was possibly an intermediate to the formation of every bis-tridentate product. X-ray diffraction studies revealed the structures of complexes **264** and **269** which showed the coexistence of two tridentate chelates arranged in an orthogonal fashion.

Notably geometrical constraint was observed due to the central metal-ligand bond length being shorter than those at the peripheral of the donors.

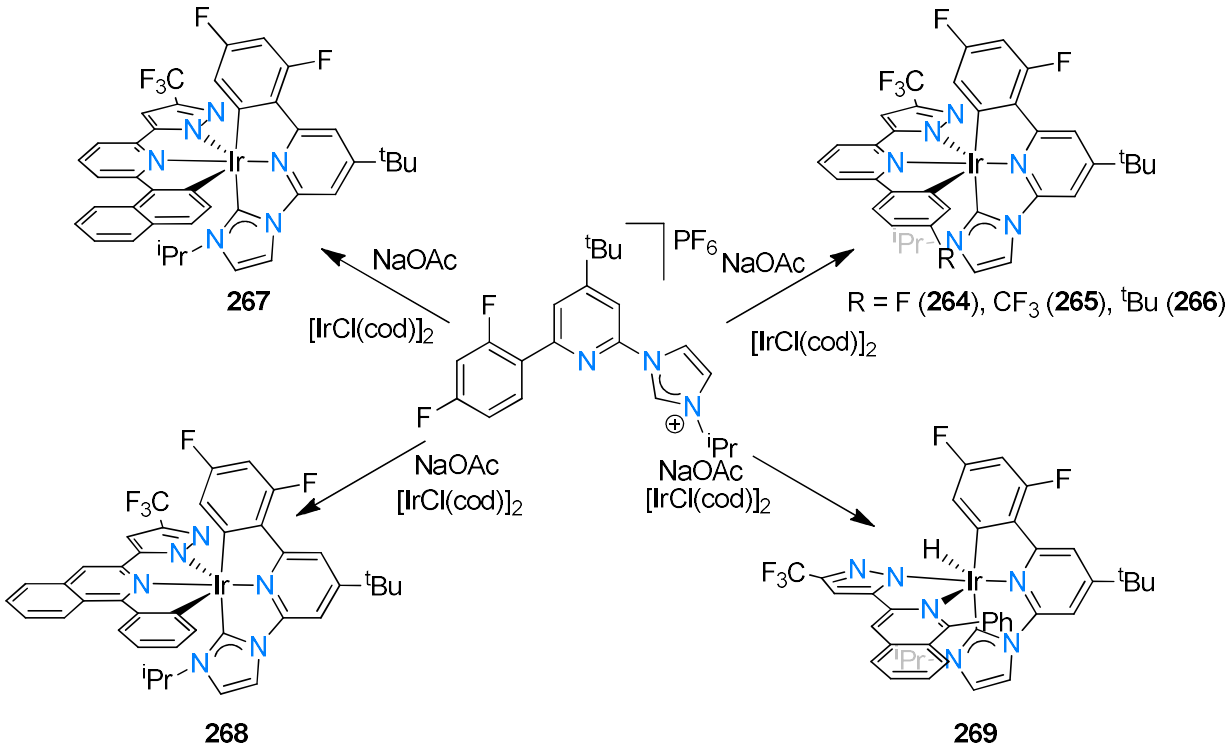

Scheme 57. Synthesis of octahedral cyclometallated Ir(III)-NHC complexes **264-269**.

The group of Willans [37] included carboranes as chelating wingtips in their NHC ligand design. They firstly synthesised the iridium monocarbene complex [Cp*$IrCl_2$(NHC)] from the imidazolium salt and Ag_2O in dichloromethane. Upon addition of a second equvalent of Ag_2O in acetonitrile to the latter complex, cyclometallion occurs to form a mixture of corresponding C- and boron-metallated Ir-NHC complexes in 53% yield (Scheme 58). The C-metallated complex (**270**) could also be obtained as the major product directly from the reaction of the imidazolium salt, ^{n}BuLi, and [Cp*$IrCl_2$]$_2$ (73% yield). If a N-^{t}Bu group-containing carborane NHC ligand is used instead, spontaneous C-H activation of the ^{t}Bu group occurs instead to form complex **271**. Complex **271** also reacts with a second equivalent of Ag_2O, forming the corresponding boron-metallated complex **272** as the only product.

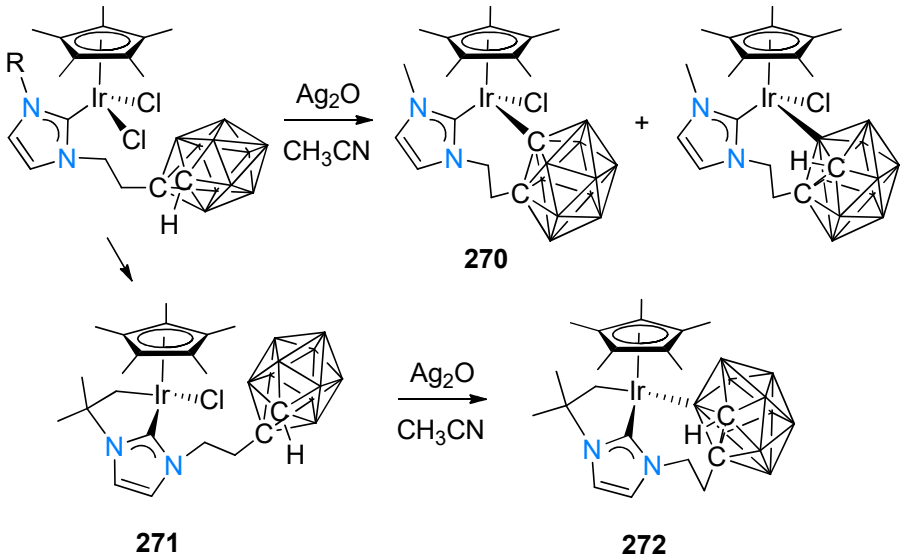

Scheme 58. Synthesis of cyclometallated carborane-NHC complexes **270-272** In the carborane, carbon atoms are highlighted as C with the rest being boron atoms.

Several groups, including those of Crassous [149], Choudhoury [150], Nazeeruddin [151], Zheng [152], Sun [153,154], Wong [155], and Hogan [5] focussed on the synthesis and application of tris-cyclometallated monocarbene complexes of Ir(III) (Scheme 59). As part of the synthetic route, imidazolium salt precursors were treated with the dimeric iridium precursors in the presence of either Cs_2CO_3 (Choudhury) or Ag_2O (all other groups) to form corresponding cyclometallated complexes **273-317**. The group of Crassous (complexes **273** and **274**) was the only group to have mentioned the formation of pairs of isomers in the isolation of the cyclometallated complexes. In addition, complex **274** was obtained as a 63:37 ratio of diastereomers, as determined by ^{1}H NMR spectroscopy and HPLC, which suggests that the cyclometallation process is diastereoselective. SCXRD helped to elucidate the structure of a pure diastereoisomer of **274** with space group $I4_1/a$ and revealed a distorted octahedral geometry of the iridium centre as well as a *trans* arrangement of the pyridyl rings of the bidentate pyridylarene ligands. The molecular structures (SCXRD) of the other complexes determined revealed both the *trans* (**276**, **278-281**, **284**, **287-290**, **302**, **307**, **309**, **312**) and *cis* (**273**, **275**) arrangement of the pyridyl moieties, along with other comparable structural features. In terms of ^{13}C NMR spectra of complexes **273-317**, data is surprisingly scarce, with only a few reports [5,149,150] having conducted ^{13}C NMR spectroscopy experiments. In terms of ^{13}C NMR signals reported, comparable signals for the carbene carbon (NHC) were observed in the range 175-187 ppm.

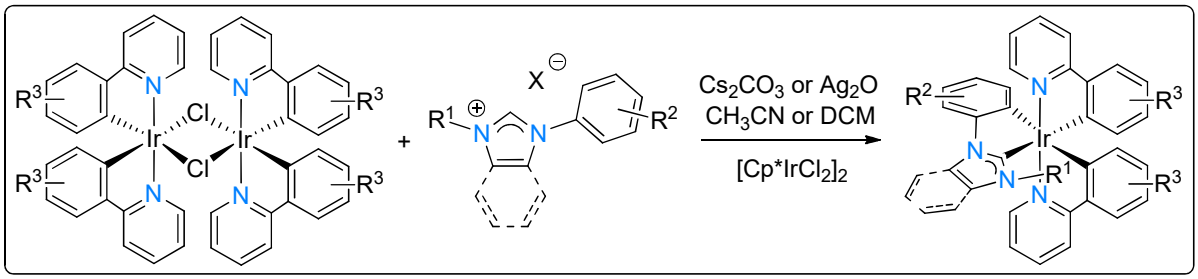

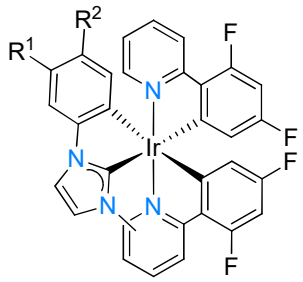

R^1 = H: R^2 = H (**260**), terpy (**262**), F (**267**), CF_3 (**268**). R^1+ R^2 = C_4H_4 (**269**). R^1 = CF_3: R^2 = H (**270**)

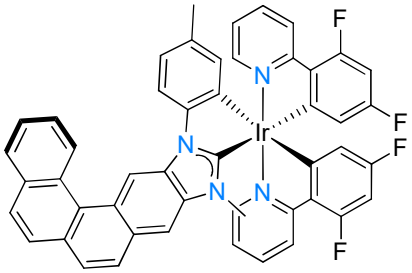

261

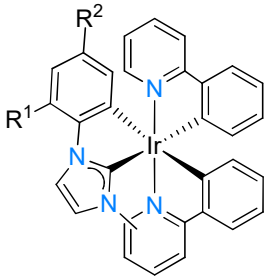

R^1 = H: R^2 = terpy (**263**), H (**290**). R^1, R^2 = CH_3 (**291**), OCH_3 (**292**), Cl (**293**), F (**294**)

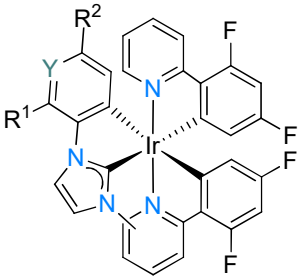

Y = CH: R^1, R^2 = OCH_3 (**264**) Y = N: R^1, R^2 = OCH_3 (**265**); R^1 = CH_3, R^2 = OCH_3 (**266**); R^1, R^2 = H (**271**)

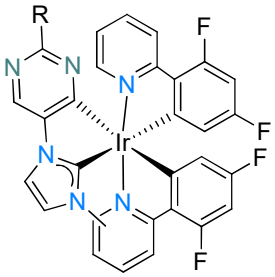

R = H (**272**), CF_3 (**273**)

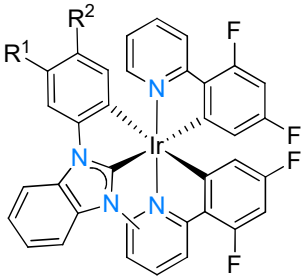

R^1 = H: R^2 = H (**274**), F (**275**), CF_3 (**276**). R^1 = CF_3: R^2 = H (**277**). R^1 + R^2 = C_4H_4 (**278**)

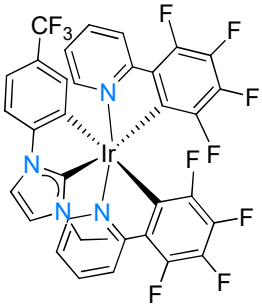

289

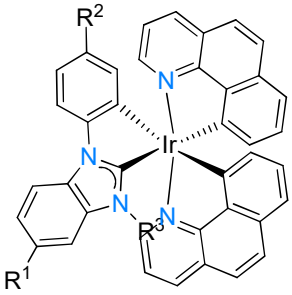

R^3 = CH_3, R^1 = H: R^2 = H (**282**), CN (**283**), NO_2 (**284**), OCH_3 (**285**), NMe_2 (**286**), Bod (**295**), CCBod (**296**); R^2 = H: R^1 = NO_2 (**287**), NMe_2 (**288**), CCBod (**297**). R^3 = $C_7H_{15}O_3$: R^1 = CCBod, R^2 = H (**298**); R^1 = H, R^2 = CCBod (**299**)

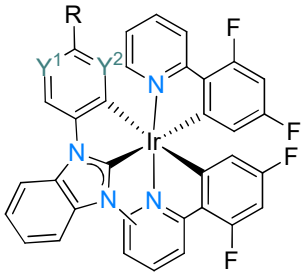

Y^1 = H, Y^2 = N: R = H (**279**). Y^1, Y^2 = N: R = H (**280**), CF_3 (**281**)

Scheme 59. Synthesis of tris-cyclometallated Ir(III)-NHC complexes **273-317**. Bod = boron dipyrromethene (BODIPY); CCBod = ethynyl boron dipyrromethene.

The group of Esteruelas [156] reported on the preparation of tris-heteroleptic Ir(III) complexes with a cyclometallated phenyl-NHC ligand. The synthesis of these complexes involved the synthesis and employment of the Ir(I)-NHC precursor, [IrCl(cod)(NHC)] (NHC = N-methyl-N-phenylimidazole), which was accessed using a silver transmetallation strategy of the silver carbene and $[IrCl(cod)]_2$. Reaction of the Ir(I)-NHC complex with the respective aryl N-heterocycles gave the corresponding dimeric Ir(III)-NHC complexes **318-320** (Scheme 60). High yields (70-81%) of the pale-yellow to orange complexes **318-320** were obtained due to the long reaction times (3-5 days) under reflux in methanol. The NMR spectra of the complexes suggested that they exist as a mixture of isomers (NHC *trans* to pyridyl, or NHC *trans* to Cl), in dynamic equilibrium at room temperature. The authors hypothesised that the isomerisation possibly takes place *via* five-coordinate mononuclear IrCl intermediates, as a result from the breaking of the chloride bridges. The X-ray structure for complex **320a** revealed a distorted octahedron around iridium with the imidazolylidene and isoquinolyl groups mutually *trans*. The authors formed the mononuclear acac derivatives (**321-323**) by cleaving the chloride bridges through the reaction with potassium acetylacetonate. After the addition of K(acac) in THF at 60 °C for 90 minutes complexes, **321-323** (Scheme 61) are obtained in another mixture of isomers (NHC *trans* to pyridyl, or NHC *trans* to oxygen on acac). Interestingly, when the reaction of **320** with K(acac) was done in a mixture of THF and MeOH (2:1), complex **323a** was obtained exclusively in 66% yield.

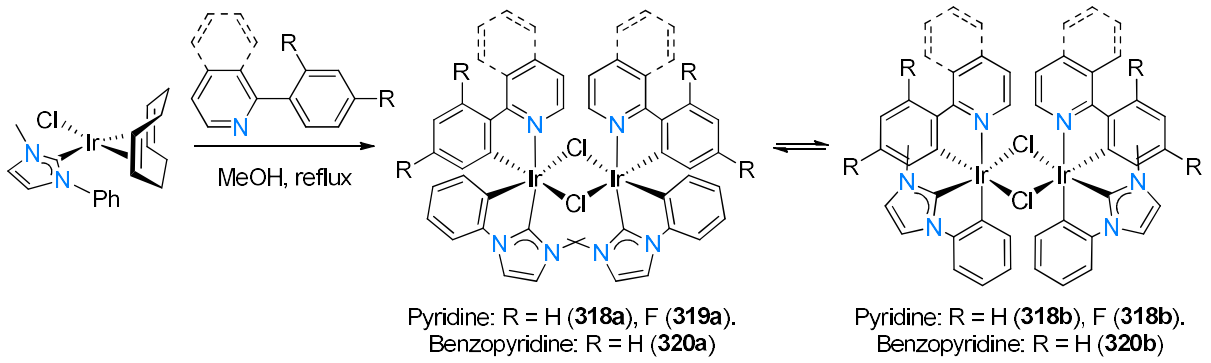

Scheme 60. Synthesis of Ir(III) dimers **318a-320a** and their enantiomers **318b-320b**.

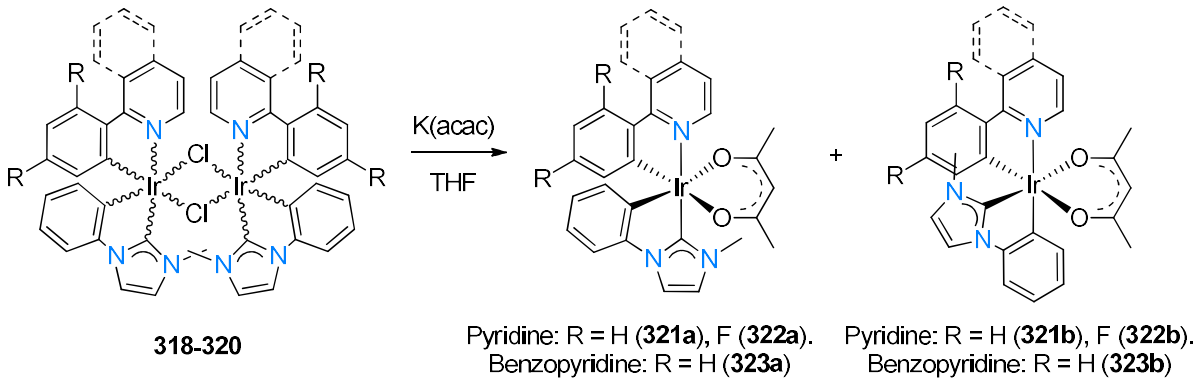

Scheme 61. Formation of bis-cyclometallated Ir(III)-NHC complexes **321a-323b** and **321b-323b**.

The authors also evaluated the possibility to replace the acac ligand with a cyclometallated 2-phenyl-5-methylpyridine ligand. As a first step, complex **323a** was treated with either HBF_4 or HOTf in acetone and H_2O to yield the respective bis(aqua)-Ir(III)-NHC complexes **324** and **325** (Scheme 62). Complexes **324** and **325** were then treated with pinacolboryl to transfer the cyclometallating N,C ligands to the Ir metal fragment. However, due to the asymmetry of the metal precursor, a mixture of isomers was obtained once again. Treatment of **324** with 2-2-pinacolborylphenyl)-5-methylpyridine in the presence of K_3PO_4 for 24h at room temperature gave a mixture of isomers **326a** and **326b**. The authors noted that the amount of isomer **326a** increased with increasing amounts of K_3PO_4 added, with **326a** being formed exclusively when the K_3PO_4:iridium molar ratios were higher than 40:1.

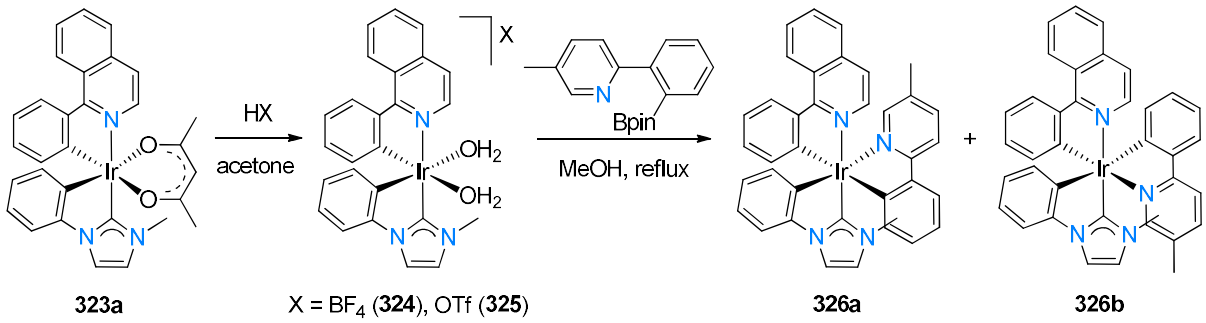

Scheme 62. Synthesis of bis- and tris-cyclometallated Ir(III)-NHC complexes **324-326**.

4.3.2 Biscarbene complexes

The groups of Cheng [157], Zhou [158], and Teets [159,160] have been successful in isolating cyclometallated biscarbene complexes of iridium featuring functionalised pyridyl and isocyanide ancillary ligands. Zhou isolated Ir(III)-NHC dimers **327-329**, **335-336**, **340-341** and

348-349 from the reactions of $[IrCl(cod)]_2$ and the respective imidazolium iodide salts in the presence of NaOMe. Each of the complexes **327-329** react with 5-methoxy picolinic acid to yield the corresponding neutral Ir(III) biscarbene complexes **330-332** (Scheme 63). In contrast, complexes **327-329** react with 2,2'-bipyridine to yield the corresponding cationic biscarbene complexes **333** and **334**. Teets made use of related Ir(III) dimers **335** and **336** and reacted them with aryl isocyanides in the presence of $AgPF_6$ to give the corresponding cationic complexes **337-339** in low (**319**, 27%) to high (**321**, 93%) yield. Reaction of dimers **327**, **340** and **341** with 4-trifluoromethylphenyl isocyanide forms mononuclear complexes **332-334**, which is then subsequently treated with propylamine to form the complexes **345-347**. Complexes **345-347** are formed *via* a cascade reaction whereby metal-mediated nucleophilic addition of the amine to the isocyanide occurs, followed by cyclometallation assisted by the addition of base (K_2CO_3). The biscarbene complexes **350-354** were synthesised *via* the dimers **327**, **348** and **349** by reacting them with the 2-(1*H*-pyrazol-5-yl)pyridine (Hpypz), 2-(1*H*-imidazol-2-yl)pyridine (Hpyim), or 2-(3-trifluoromethyl)-1*H*-pyrazol-5-yl)pyridine (Htfpypz), respectively.

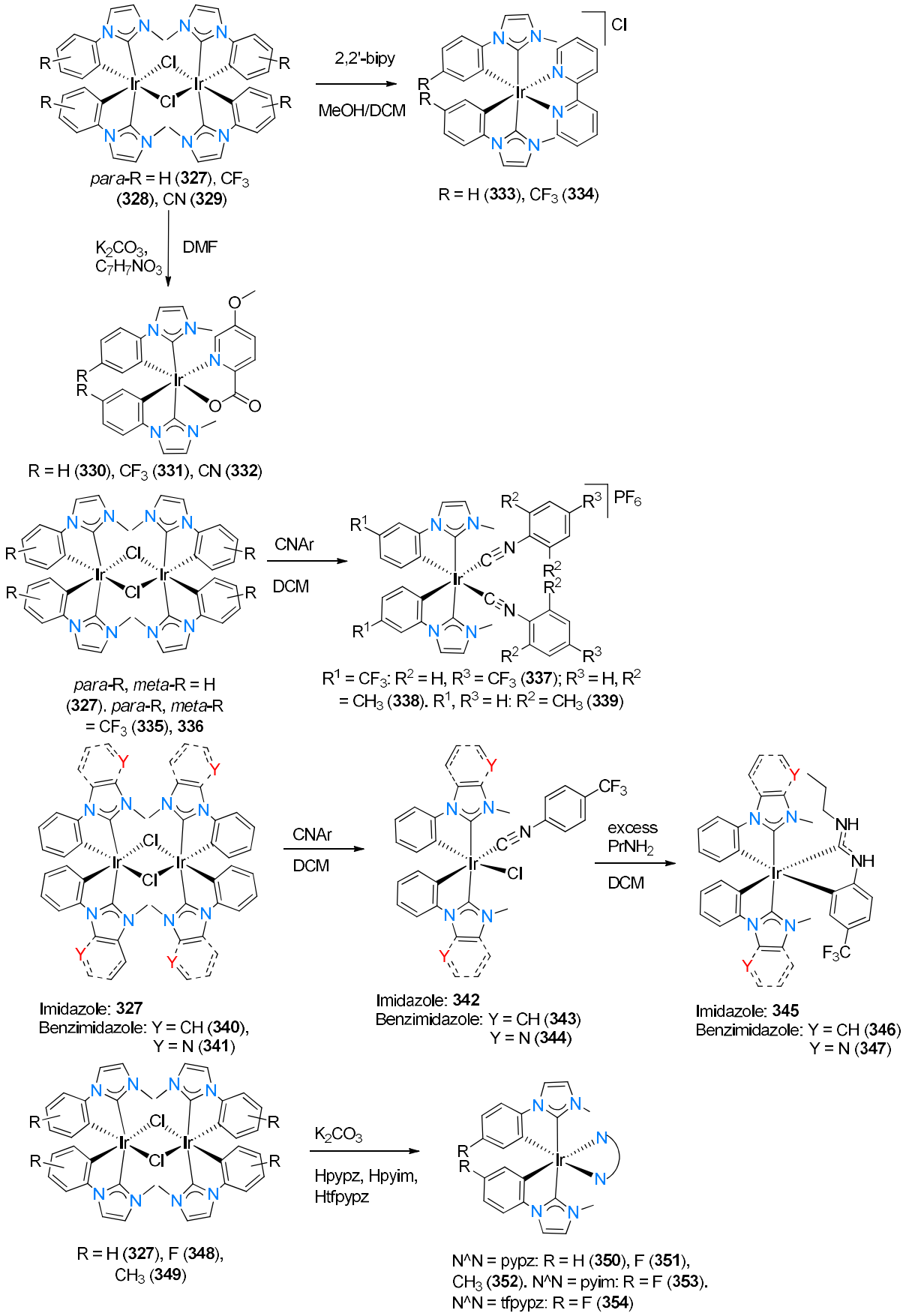

Scheme 63. Synthesis of biscarbene complexes **330-354**

A series of cyclometallated NHC pincer ligand systems have been developed and coordinated to iridium by several groups, including those of Braunstein [161-166], Chianese [16,167,168], Heinekey [169], Wong [170], Chaplin [171], Chi [172], and Esteruelas [173,174]. The group of Braunstein [166] found that treatment of the dimer $[IrCl(cod)]_2$ with the bis-imidazolium salt in the presence of NEt_3 as base, with the addition of KI produced the dimeric Ir(III)-NHC complexes **355** and **356**, each featuring two slightly distorted octahedral iridium centres bridged by two iodido ligands. The bridging iodido bonds in complexes **355** and **356** were found to be cleaved upon heating or ultrasonic activation in the presence of coordinating solvents (CH_3CN or DMSO) to form complexes **357-359** (Scheme 64). Similar reactions described in later reports by these groups [161,174] gave a range of analogous octahedral Ir(III) complexes, each featuring the CCC_{NHC} ligand framework. In general, reaction of the bis-imidazolium salt with the dimeric $[IrCl(cod)]_2$ in the presence of a mild base such as NEt_3, Cs_2CO_3 or CsF gave the octahedral halo/hydrido Ir(III)-CCC complexes (**360-392**, **396**) as the main products (Scheme 65). The sets of complexes **357** and **361**, and complexes **360** with **362** were formed as the main products in the reactions employing the respective imidazolium iodide salts [161]. Other reactions proceeded more selectively to form the corresponding octahedral diiodido Ir(III)-CCC complexes as the sole products (**364**, **365**, **367-376**).

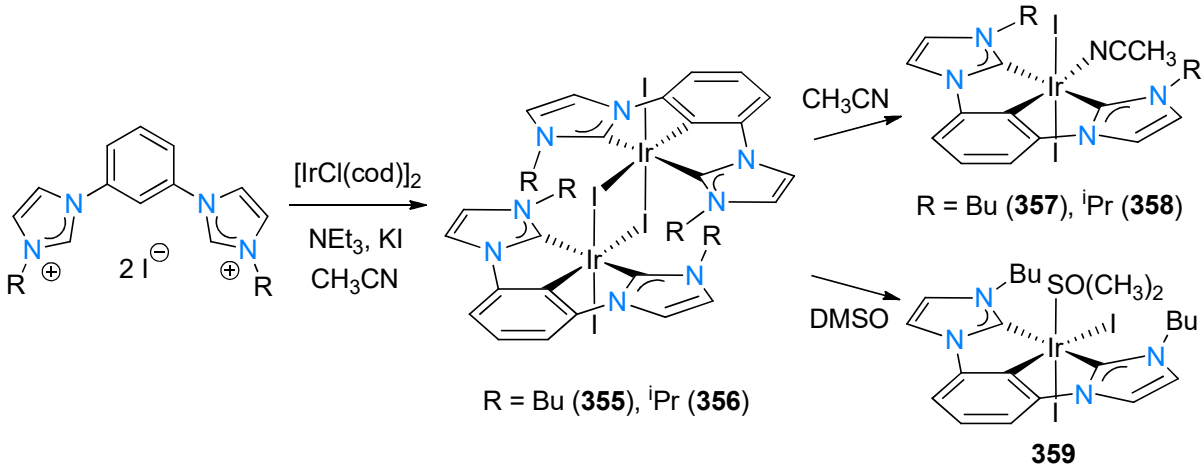

Scheme 64. Synthesis of complexes **355-359** featuring CCC pincer ligands.

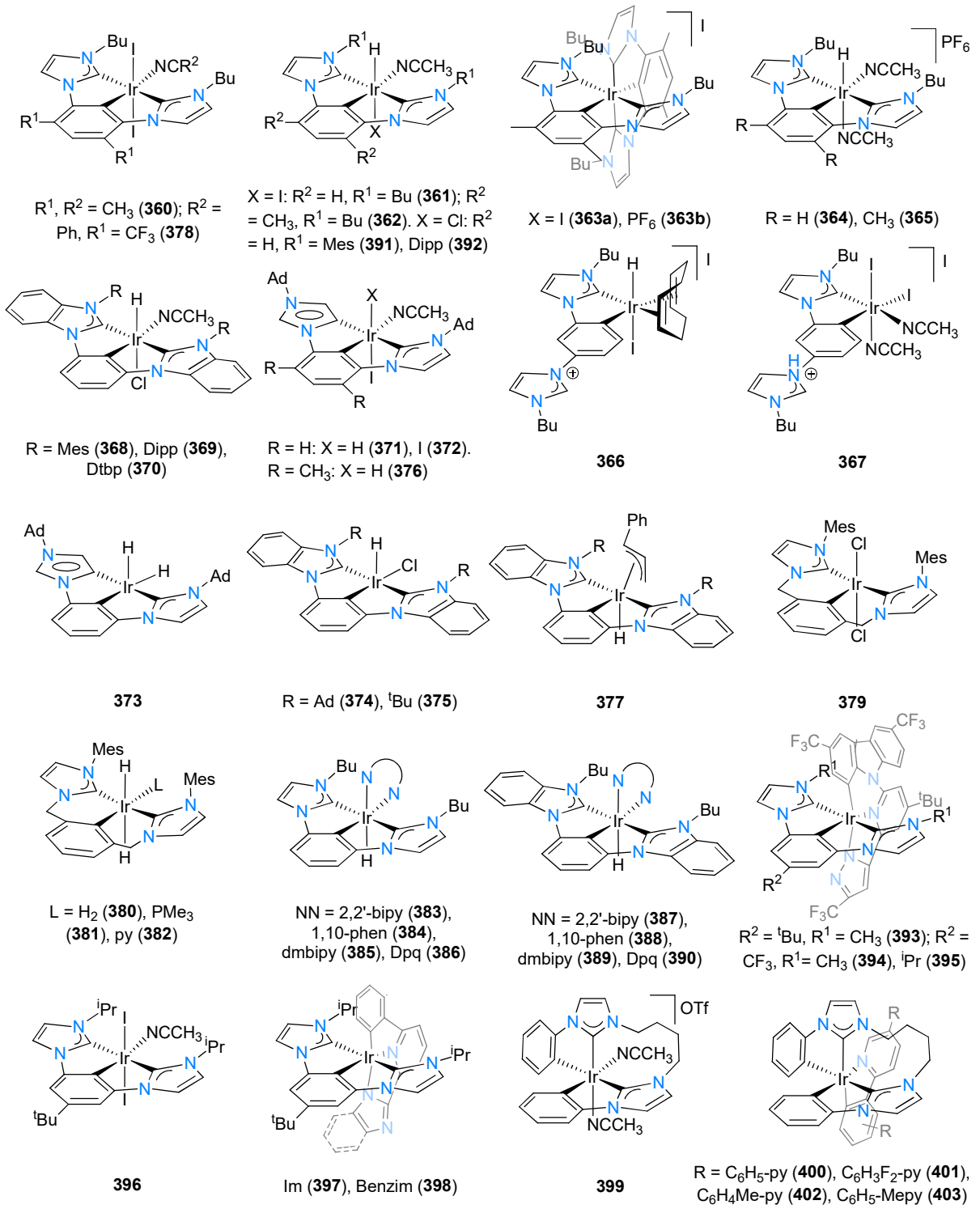

Scheme 65. Cyclometallated Ir(III)-NHC complexes **360-403**. Dtbp = di(tertiarybutyl)phenyl; dmbipy = 4,4'-dimethyl-2,2'-bipyridine; Dpq = dipyrido-[3,2-f:2',3'-h]-quinoxaline.

Upon employing two equivalents of the imidazolium precursor salt of complexes **360** and **362**, in the presence of NEt_3 and KI in refluxing CH_3CN, gives the cationic complex **363a** (66% yield, **363b** after anion metathesis with NH_4PF_6), whereas in the case of the precursor salt of

complexes **357** and **361** (in the absence of KI) the cationic complex **366** formed instead (76% yield) (Scheme 65) [161,175]. Repeating the latter reaction in the presence of KI gave the diiodido cationic complex **367** (86% yield). Reaction of **363a** with excess base formed complex **361**, which led the authors [161] to conclude that complexes **363a** and **366** are intermediates to the corresponding neutral complexes. The cationic derivatives of **361** and **362** were formed *via* reaction with $TlPF_6$ to yield corresponding complexes **364** and **365** [161]. The red, five-coordinate dihydride complex **373** was prepared by Braunstein [163] using H_2 (1 atm.). The ^1H NMR spectrum revealed a high upfield hydride signal at -34.9 ppm. In a similar way, colourless complex **380** was prepared from purple complex **379** in the presence of H_2 (1 atm.) and revealed an upfield hydride signal at -9.04 ppm [169]. The steric demand of the CCC_{NHC} ligand also seems to play a role in the resulting geometry of the Ir complex: for the bulky, yet relatively planar Mes, Dipp and Dtbp substituents on the CCC ligand, six-coordinate complexes (**368-370**) with coordinated acetonitrile is formed (Scheme 65) [16]. However, if the more (spherically) bulky substituents of adamantyl and ^tBu are employed, five-coordinate complexes (**374** and **375**, without coordinated acetonitrile), is formed. Complex **368** was also reactive towards allylbenzene to form complex **377** in the presence of excess NaOMe, and proved that complex **368** catalyses alkene isomerisation *via* an irdium allyl hydride intermediate (**377**) [168]. Despite the vast range of different functional groups present on the CCC_{NHC} ligands, as well as the different ancillary ligand coordinated to iridium in complexes **360-403**, the ^{13}C NMR signal for the carbene carbon(s) of the CCC_{NHC} ligands appeared in the average range of 165-185 ppm, whereas the carbon signal for the cyclometallated carbon atom(s) appeared in the range of 140-146 ppm.

A few dinuclear cyclometallated Ir-NHC complexes are also relevant under this section, and have been prepared by the groups of Danopoulos [176], Baratta [39], and Esteruelas [174,177]. Danopoulos found that treatment of the free carbene CNC ligand with $[IrCl(cod)]_2$ in THF at low temperature (-78 to -30 °C) formed the dinuclear cyclometallated complex **404**, which decomposes at temperatures above -30 °C (Scheme 66). The molecular structure (SCXRD) of **404** could be obtained, although the data quality was only sufficient to show the connectivity of the non-hydrogen atoms. The reaction of the analogous $CN^{Me}C$ free carbene with $[IrCl(coe)_2]_2$ at room temperature however, produced the expected [IrCl(CNC)] complex, along with small amounts of an orange by-product, which after anion exchange with KPF_6 has been identified as the dinuclear complex **405**, featuring an Ir(III) centre coordinated to one CNC ligand, one chlorido, and one η^3-allyl group (from an adjacent Dipp group). The Ir(I) centre exhibits one CNC ligand featuring one normal NHC and one abnormal NHC, along with one

chlorido and one η^2-alkene type bond from the backbone of an NHC bound to the Ir(III) centre. The molecular structure of **405** featuring an unprecedented NHC bonding mode has been elucidated using SCXRD (Figure 8).

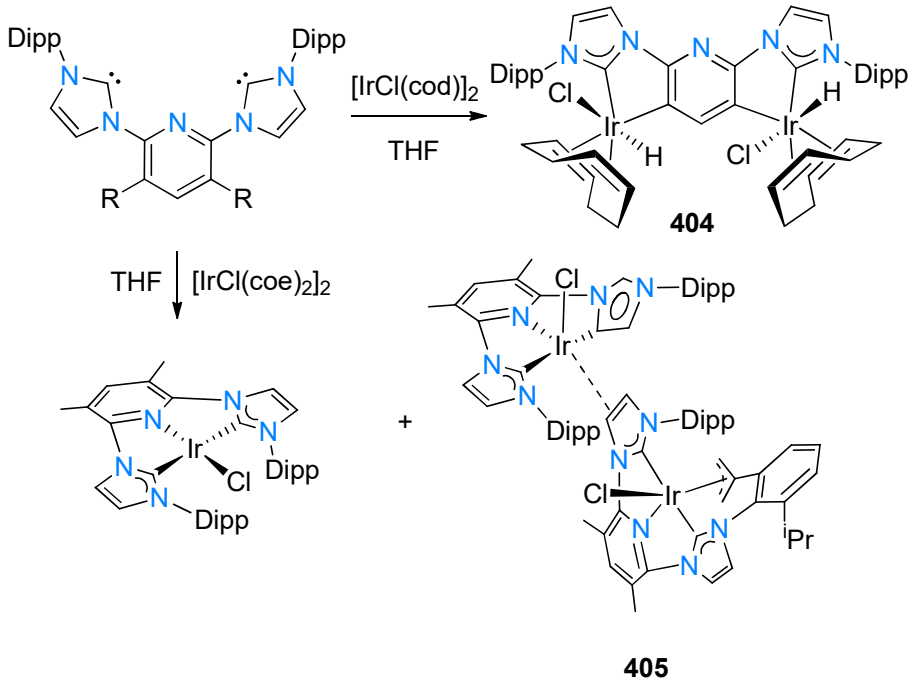

Scheme 66. Synthesis of dinuclear Ir-NHC complexes **404** and **405**.

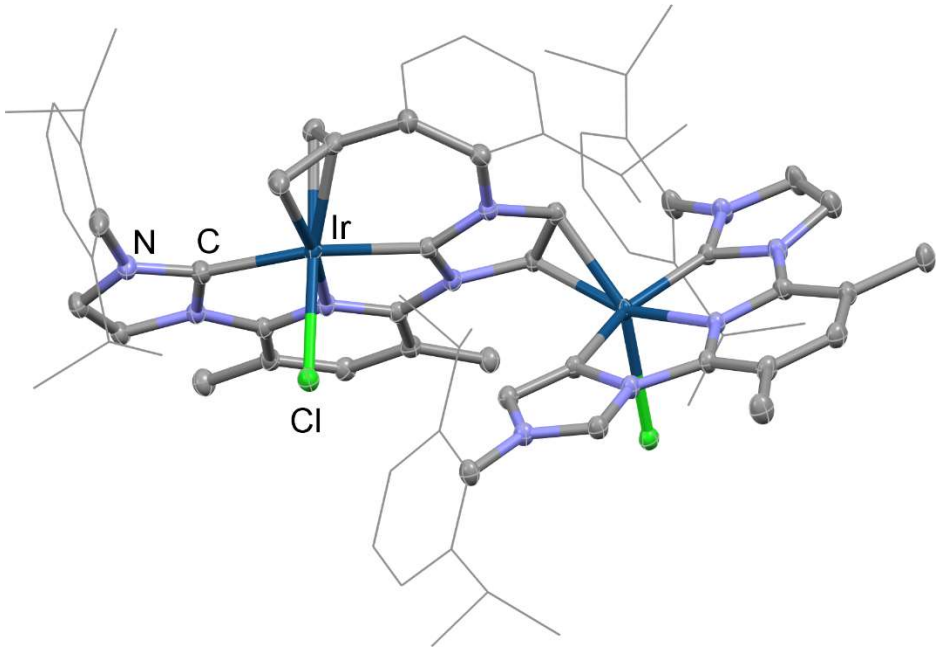

Figure 8. ORTEP plot of **405**. Thermal ellipsoids are drawn at 50% level. For clarity, the diisopropylphenyl (dipp) moieties are shown as wireframe presentations, and acetone solvent molecules, a noncoordinating PF_6 anion, and hydrogen atoms are omitted.

Baratta and co-workers [39] observed the bis-cyclometallation of a 1,4-phenyl-bridged bis-imidazolylidene silver carbene when reacted with $[Cp^*IrCl_2]_2$ *via* transfer metallation to iridium to form complex **406** (64% yield; Scheme 67). The centrosymmetric crystal structure of **406** featuring its three-legged piano stool geomtery was elucidated using SCXRD. Esteruelas *et al.* [177] observed similar reaction outcomes: Reaction of $[IrH_5(P^iPr_3)_2]$ with the 1,3-disubstituted phenyl bis-imidazolium salt formed the corresponding white 4,5-dicyclometallated bis-NHC Ir(III) complex **407** in almost quantitative yield, of which the solid state molecular structure was elicudated. Similarly, they found that the reaction of $[IrH_5(P^iPr_3)_2]$ with either the ethylene-, propylene-, or butylene-bridged bis-imidazolium salts formed the corresponding white dicyclometallated bis-NHC Ir(III) complexes **408-410** in moderate (40-50%) yields. Interestingly, upon employing the methylene-bridged bis-benzimidazolium dibromide salt with $[IrH_5(P^iPr_3)_2]$ C-N bond cleavage was observed, and a 1:1 mixture of the N-coordinated N-phenyl benzimidazole was formed, as well as the white cyclometallated phenyl benzimidazolylidene Ir complex **411**, both of which the molecular structures (SCXRD) were determined. Similar to the rhodium analogue discussed in section 3.3, the group of Hahn [96] observed the double cyclometallation in the formation of the biscarbene complex **412** from the tris-imidazolium salt when treated with Cs_2CO_3 and $[Cp^*IrCl_2]_2$. Both the C_{NHC} and C_{aryl} signals in the ^{13}C NMR spectra of complexes **406-412** were all comparable to related mononuclear Ir-NHC complexes.

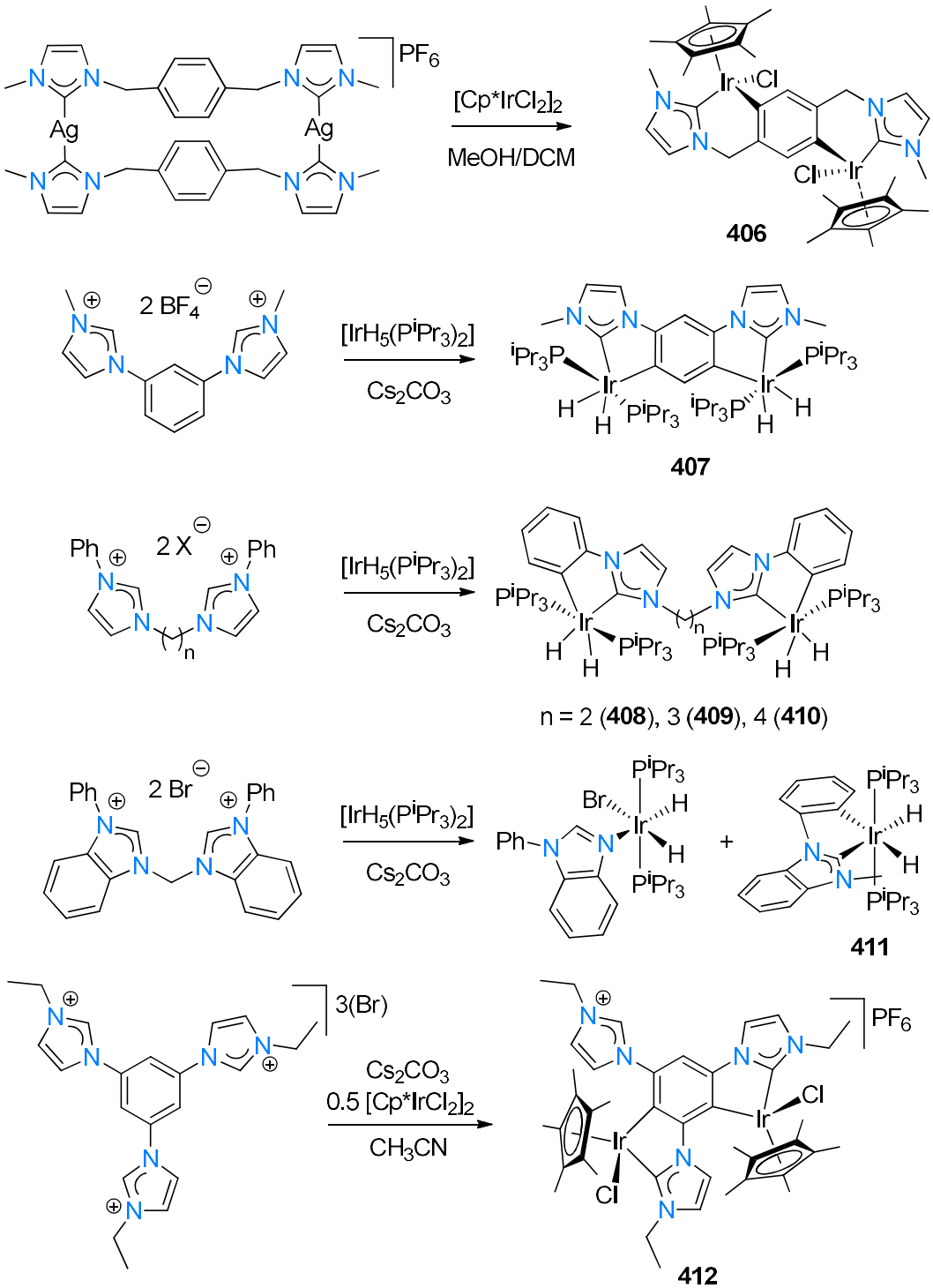

Scheme 67. Synthesis of cyclometallated Ir-NHC complexes **406-412**.

4.3.3 Triscarbene complexes

In this section the groups of Lappert [178], Thompson [179,180], Wong [181], Kang [182], Zysman-Colman [183], and Jin [184] contributed to the field by providing examples of neutral tris-imidazolylidene-containing Ir(III) complexes featuring tris-cyclometallated moieties. Lappert [178] was the first group to report examples of Ir(III)-NHC complexes in 1982. They

showed that $[IrCl(cod)]_2$ reacts with an excess of the dimeric carbene precursors to afford the ortho-cyclometallated tridentate $[Ir(NHC)_3]$ complexes **413** and **414** (Scheme 68).

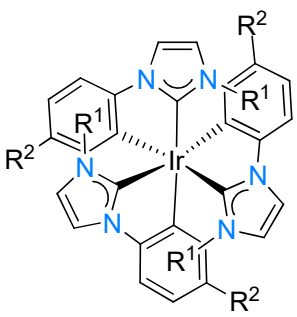

R^1 = tol, R^2 = CH_3 (**413**), R^1 = *p*-OCH_3Ph, R^2 = OCH_3 (**414**)

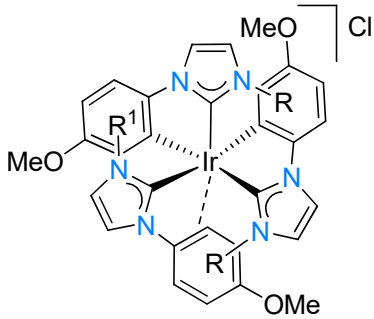

R = *p*-OCH_3Ph (**415**)

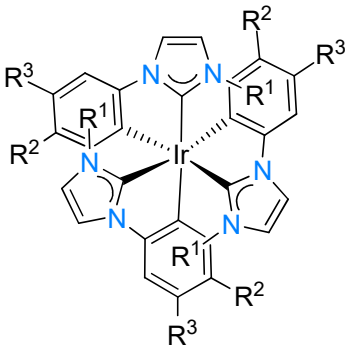

R^3, R^2 = H: R^1 = CH_3 (**316**). R^3 = H, R^2 = CF_3: R^1 = Et (**423**), CH_3 (**425**). R^3 = CF_3, R^2 = H: R^1 = CH_3 (**426**). R^3 = H, R1 = CH_3: R^2 = $POPh_2$ (**427**)

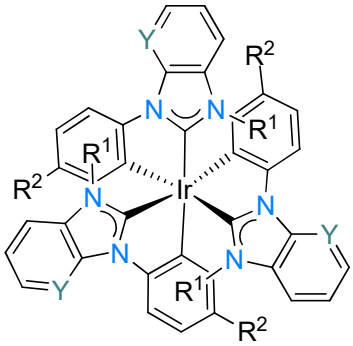

Y = CH: R^1 = CH_3, R^2 = H (**417**). Y = N: R^1 = Et: R^2 = H (**418**), F (**419**), CH_3 (**420**), ^{t}Bu (**421**); R^1 = CH_3: R^2 = H (**422**), $POPh_2$ (**428**), F (**429**)

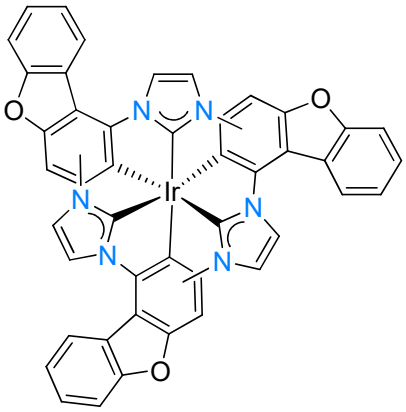

424

Scheme 68. Tris-cyclometallated complexes **413**-**429**.

Complex **414** was shown to react with HCl to give the dicyclometallated derivative **415**, which was proposed as an intermediate to complex **414**. Molecular structures (SCXRD) of both **414** and **415** were elucidated. The structure of **415** revealed a close-contact Ir-$C_{o\text{-}Ar}$ (2.52(1) Å) involving the non-cyclometallated NHC coordinated to the iridium centre, as compared to the cyclometallated Ir-C_{Ar} distances of 2.07(3)-2.09(3) Å. As a modern synthetic strategy, all other groups made use of the silver transmetallation route employing Ag_2O and the respective imidazolium salts. In 2005 Thompson [179,180] reported the N-phenyl imidazolylidene and benzimidazolylidene derivatives **416** and **417** which were isolated as mixtures of *fac* and *mer*

isomers in low yield (< 10%). The *fac* and *mer* isomers could be separated using either column chromatography or selective crystallisation. This was also sthe case with the synthesis and isolation of complexes **418-429**, where mixtures of the *mer* and *fac* isomers were obtained. The kinetically favourable meridional isomer was usually present as the major isomer and could be separated from the *fac* isomer using column chromatography.

4.4 Carbene complexes with cyclopentadienyl-based tethers

This limited section contains examples of Ir-NHC complexes of the type **D** (Figure 1). The groups led by Peris and Royo [18,45,111,112] reported on the preparation of Cp*-functionalised Ir-NHC (and Rh-NHC) complexes, with the main application of catalysis in mind. The preparation of the first Cp*-functionalised complex (**430**) was reported to occur from the reaction of the Cp*-functionalised imidazolium salt, Cs_2CO_3, and $[IrCl(cod)]_2$, followed by addition of KI, and was isolated as a racemic mixture of enantiomers in 70% yield (Scheme 69). Related complexes **431** and **432** occurred *via* the silver transmetallation strategy using the metal precursors ($[MCl(cod)]_2$ with M = Rh, Ir). In the reaction forming **431**, the formed monodentate carbene intermediate was reacted with acetic acid, which facilitates the C-H activation of the cyclopentadienyl to allow it to coordinate in a η^5-fashion. During this reaction, a metal-mediated isomerisation of the double bond in the linker chain must occur to form the final cyclopentadienyl fragment of the coordinated ligand. Further reaction of the Ir(III) complex **399** with LiOAc in methanol leads to the *ortho*-cyclometallation of the phenyl ring in the linker to form doubly cyclometallated complex **433**. This type of C-H activation is not uncommon for Ir complexes as seen in the previous section (4.3). However, examples of the formation of this rigid tridentate coordination featuring two iridacyles within one molecule remains rare (Figure 9).

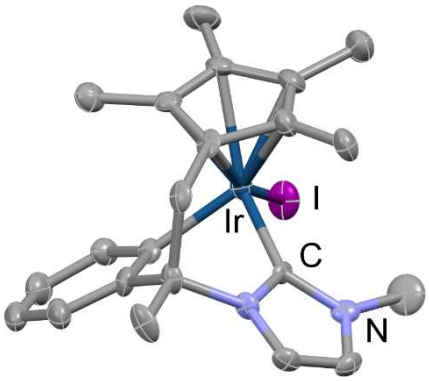

Figure 9. ORTEP plot of **433**. Thermal ellipsoids are drawn at 50% level. For clarity, hydrogen atoms have been omitted.

Danopoulos and Cole-Hamilton [113], as previously mentioned in the rhodium section, reported on indenyl- and fluorenyl-functionalised NHC complexes of rhodium and iridium. The authors attempted to apply their work on forming rhodium complexes (**111-113**) to iridium by reacting the same imidazolium salts with $[Ir(cod)Cl]_2$. However, most reactions gave a large mixture of products that were difficult to separate. The authors did, however, note that reacting a potassium salt of an indenyl-based NHC with $[Ir(cod)Cl]_2$ under CO atmosphere, resulted in the formation of complex **434** (Scheme 69). From the molecular structure of **434** the C_{NHC}-Ir bond length was found to be a typical 2.083(7) Å, while the $C_{indenyl}$-Ir bond length was longer (2.220(7) Å). The two Ir-C_{co} bond lengths were similar (1.871(8) and 1.889(8) Å); however, the longer one was bonded *trans* to the NHC. Enantiomerically pure complex **435** was obtained by Royo [111] in a relatively poor yield (35%), and this was explained by the concomitant formation of a dinuclear species (**436**). X-ray structural analysis of **436** revealed that the molecule contains two Ir(I) centres with different coordination spheres: one of the iridium atoms is coordinated to 1,5-cyclooctadiene, iodido and an NHC ligand, while the other iridium centre is coordinated to a η^5-cyclopentadienyl ring in addition to 1,5-cyclooctadiene. In general, the ^{13}C NMR signals of the carbene (NHC) carbon atoms correlated well for complexes **430-436**, appearing in the range 138-148 ppm.

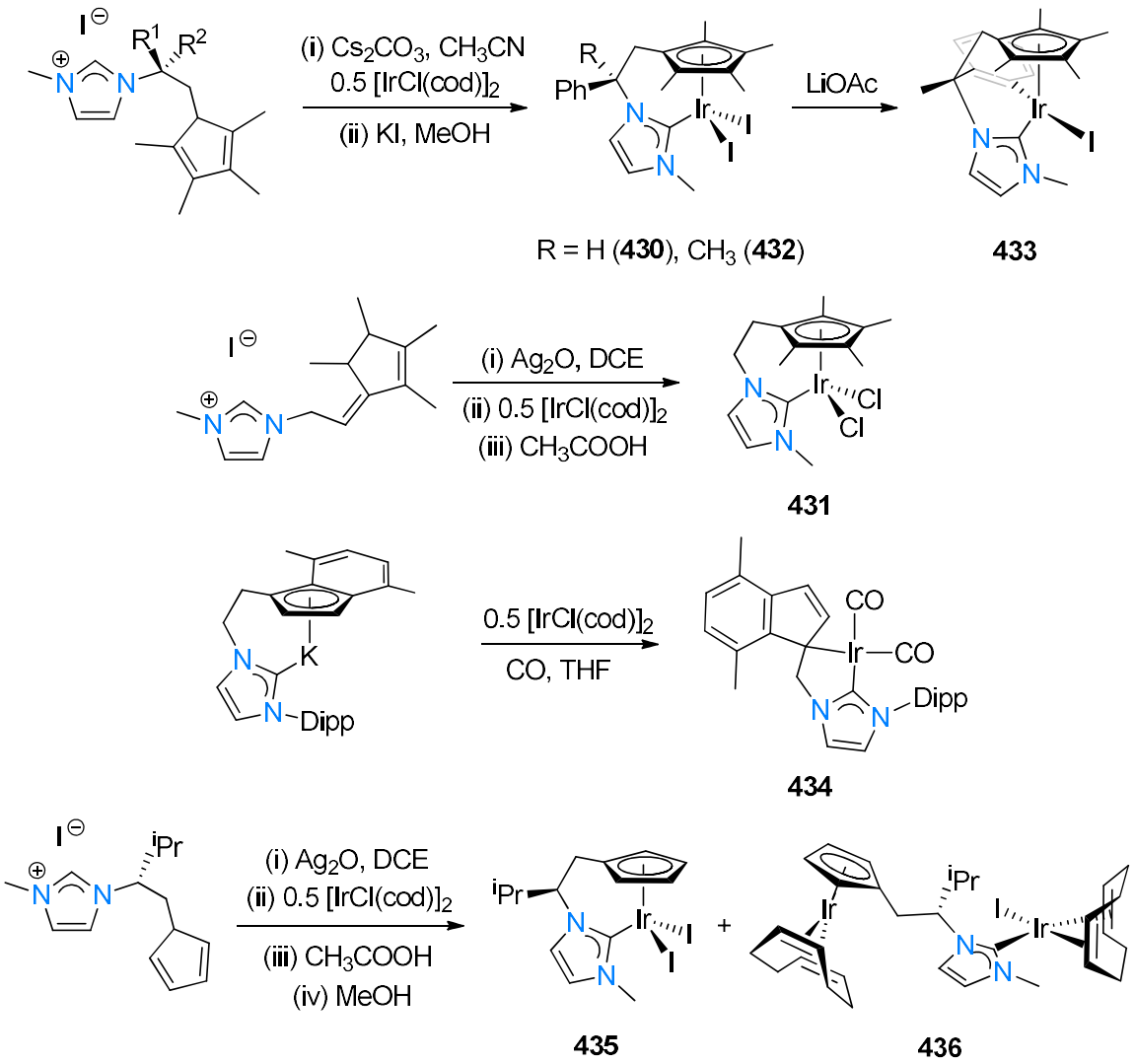

Scheme 69. Synthesis of cyclopentadienyl-based Ir-NHC complexes **430-436**.

5. Applications

The incorporation of carbon-donor tethers as part of NHC ligand frameworks has led to many function-specific applications, which result from the structural and electronic versatility of the ligands and corresponding metal complexes. The applications listed below stem directly from the complexes reviewed in this study and the unique complex numbers assigned will be referred to. The most common application for the complexes is homogeneous catalysis. This topic will be discussed first, followed by the less studied photophysical and biological applications (*vide infra*).

5.1 Homogeneous catalysis

This application, as the most common and popular application, has been sectioned according to the type of organic transformation reaction that is achieved using the complexes of this study as catalysts. Representative and specific catalytic reactions with optimised conditions, as well as substrate screening results (where relevant), have been included. Although the first NHC complex relevant to this review had been reported in 1982 (complexes **413** and **414** by Lappert and co-workers [178]), it was only two decades later, in 2002, when the first catalytic application for compounds of this class was reported. Since then, an expansion on the various types of catalytic reactions investigated resulted in a plethora of unique organic transformations. However, considering the scope of this review, only selected reactions are listed below.

5.1.1 Hydrosilylation

From the group IX triad of metals, rhodium has proven to be the metal of choice for the C-H activation involving sp^2 and sp-hybridised carbon bonds. Redox-active complexes **108** and **109** of Labande and co-workers [110] showed activity in the hydrosilylation reaction of acetophenone and four derivatives (Scheme 70). At a catalyst concentation of 1 mol% (**108** or **108**), THF solutions containing the carbonyl substrates and Ph_2SiH_2 were left to convert at room temperature over the course of 17 hours, to give conversions of 43-54% (**108**) and 78-90% (**109**). In the case of trifluoroacetophenone, conversions of more than 99% were achieved using either **108** or **109**. The Rh(III) complex **109** was notably more active than Rh(I) complex **108**, showing an initial catalytic activity of **109** to be 20 times greater than that of **108**.

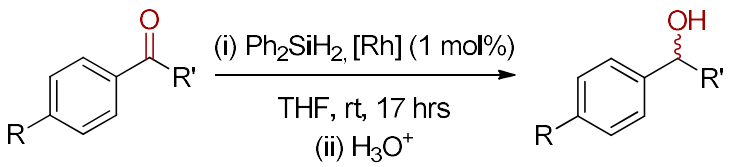

Scheme 70. Catalytic hydrosilylation of carbonyl compounds.

The groups of Li [75], Fout [185], Deng [64], and Nishiyama [106] investigated the use of cobalt and rhodium-based catalysts in the catalytic hydrosilylation of alkenes, while the group of Hollis [104] evaluated the catalytic use of rhodium catalysts in the same reaction employing alkynes (Scheme 71). Li [75] employed the Rh-based complex **36** (0.1 mol%) for which high

activity was observed over a period of two hours (89% conversion, TON = 911, Table 1). Compared to related monodentate NHCs in the same study, complex **36** showed similar activity and selectivity to the β-adduct (87%, no by-products). The disappearance of the coordinated alkene in **36** was observed and the corresponding monodentate β-silyl-substituted NHC complex was formed during the catalytic reaction. The group of Fout [185] developed a highly chemoselective cobalt catalyst (**20**) for the hydrosilylation of alkenes, which showed a broad functional group tolerance with tertiary silanes. Using 5 mol% of complex **20** and one equivalent of $HSiPhMe_2$, alkenes featuring hydroxyl, amino, ester, epoxide, ketone, aldehyde, and nitrile groups were selectively converted to the corresponding β-silane adducts in high yields over time (1-24 hours, Table 1). In the model reaction employing 1-octene, a variety of secondary and tertiary silanes were useded, with $HSiPh_3$ and $HSiEt_3$ being the least efficiently converted (<5 and <35%, respectively). During their substrate screening study, the authors found that the less hindered alkene in substrates having more than one alkene is selectively hydrosilylated, whereas the silyl-adducts of cyclic alkene substrates were not observed. Some limits in terms of chemoselectivity was observed in the reaction using 10-undecenal, where a ratio of 1.4:1 of the aldehyde-silated *versus* alkene-silated products were found after one hour.

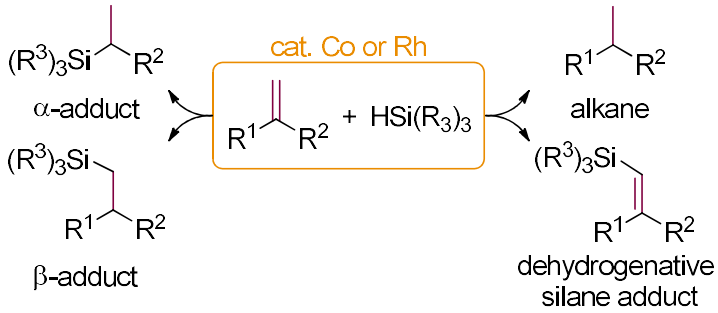

Scheme 71. Selectivity in the catalytic hydrosilylation of alkenes. R = alkyl, alkoxy, aryl.

The group of Deng [64] found that the same reaction utilising 1-octene, H_3SiPh, and their cyclometallated cobalt complexes **12-14** as catalysts (0.1 mol%), took place without solvent at room temperatures to give conversions of 55-94% within 5 minutes (Table 1). In addition to impressive initial rates of reactions (TOF values up to 11280 h^{-1}), high regioselectivity was observed, with the β-hydrosilated product obtained as the main product (> 88%). The authors also confirmed that decreased activity of the catalysts in the later stages of the reactions was not as a result of catalyst decomposition, as further addition of 1-octene and H_3SiPh to the mixture showed continued conversion, albeit with slightly lower rates.

Table 1. Catalytic hydrosilylation of unsaturated hydrocarbon compounds.

Substrate	Silane	Conv. (%)	Metal	Catalysts	Activity (TON (hr))[a]	Selectivity (%)[b]			Ref
						β	α	other	
	$HSi(OEt)_3$	89	Rh	**36**	911(2) (**36**)	87	13	-	[75]
	$HSiPhMe_2$	94	Co	**20**	19(7) (**20**)	100	-	-	[185]
H_2N	$HSiPhMe_2$	62	Co	**20**	12(26) (**20**)	100	-	-	[185]
H_3CO	$HSiPhMe_2$	98	Co	**20**	20(7) (**20**)	100	-	-	[185]
N	$HSiPhMe_2$	97	Co	**20**	19(9) (**20**)	100	-	-	[185]
O	$HSiPhMe_2$	94	Co	**20**	19(3) (**20**)	100	-	-	[185]
O	$HSiPhMe_2$	99	Co	**20**	20(2) (**20**)	100	-	-	[185]
C_6H_{13}	$HSiPhMe_2$	50-94	Co	**12-14**, **20**	940(0.1) (**12**)	88	7	5	[64,185]
HO	$HSiPhMe_2$	75	Co	**20**	15(3) (**20**)	100	-	-	[185]
HO	$HSiPhMe_2$	95	Co	**20**	19(4) (**20**)	100	-	-	[185]
NC	$HSiPhMe_2$	70	Co	**20**	14(6) (**20**)	100	-	-	[185]
	$HSiPhMe_2$	75	Co	**20**	15(17) (**20**)	100	-	-	[185]
O	$HSiPhMe_2$	81	Co	**20**	16(2) (**20**)	100	-	-	[185]
O	$HSiPhMe_2$	97	Co	**20**	19(2) (**20**)	100	-	-	[185]
O $(CH_2)_7$	$HSiPhMe_2$	~90	Co	**20**	18(1) (**20**)	40	-	60	[185]
O	$HSiPhMe_2$	87	Co	**20**	17(5) (**20**)	100	-	-	[185]

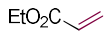	$HSiPhMe_2$	95	Co	**20**	19(3) (**20**)	100	-	-	[185]
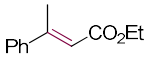	$HSi(OEt)_2Me$	23-91	Rh	**103**	91(1) (**101**)	-	-	100	[106]
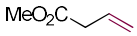	$HSiPhMe_2$	92	Co	**20**	18(2) (**20**)	100	-	-	[185]

[a] The turnover number (TON) reported after a specified amount of hours. [b] Corresponding data of the same study noted under the Activity column.

Nishiyama [106] reported that the conversion of an internal alkene featuring an ester group took place selectively to yield the corresponding chiral alkane (Table 1). Complex **102** was less active (23% conversion) than **103** (91% conversion) after one hour, with both catalysts lacking enantioselectivity (21-49% *ee*). The group of Hollis [104] found that the rhodium complex **99** (2-3.5 mol%) is an active catalyst in the conversion of internal and terminal alkynes using $HSiPhMe_2$, with conversions of 57-100% (Scheme 72). Terminal alkynes were converted to predominantly β-*Z*-silane adducts, whereas the β-*E*-silane adducts were obtained as major products from internal alkynes in chloroform or benzene. In their study, a limited temperature effect on the activity of the catalyst was noted. For example, using phenylacetylene as substrate achieved a conversion of 87% at room temperature after two hours while 100% conversion was obtained at 80 °C after twelve hours. For both of these reactions, the selectivity towards the β-*Z*-silane adduct was 95%, with TONs of up to 50 being recorded.

The group of Mata [116] used alkenyl-functionalised iridium carbene complexes (**123-126**) for of the catalytic hydrosilylation of terminal (phenylacetylene) and internal alkynes (1-hexyne) and found the best conversions (68%-92%) for complexes **123** and **126**. The complexes were most active for phenylacetylene. Interestingly the NHC ligands with 4,5-substituted backbones (**124** and **125**) showed a lower activity than the unsubstituted complex (**123**). It was theorised that steric influences played a role in the reactions outcome, outweighing the electronic benefits of having a substituted backbone. The complexes were highly selective for the Z isomer, which was the only product in some cases. None of the experiments yielded the α-adduct in the case of the terminal alkyne. The reactions were performed at room temperature as well as 60 °C; the increase in temperature resulted in higher conversions, although a slight decrease in

selectity for the Z-isomer was observed. Catalyst loadings as low as 0.1 and 0.01 mol% were also found to produce high activities at 60 °C, however with slower kinetics.

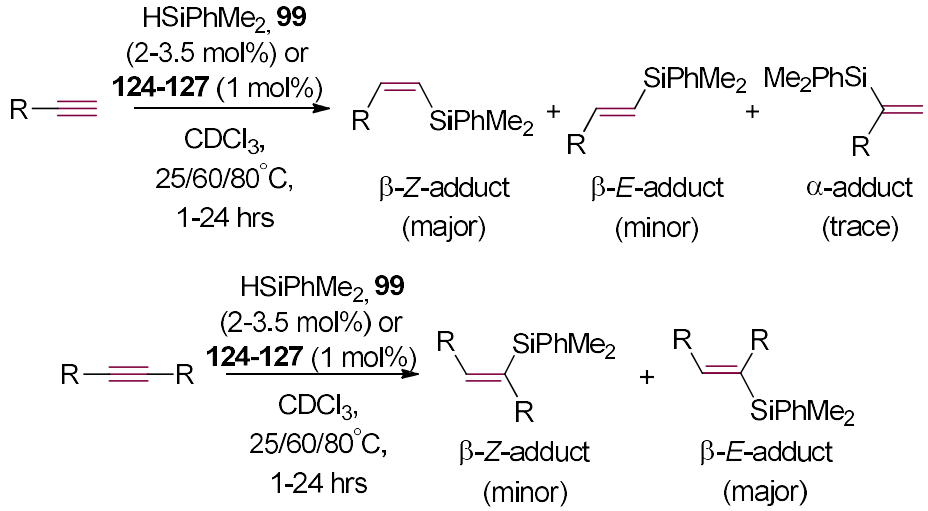

Scheme 72. Catalytic hydrosilylation of terminal and internal alkynes.

5.1.2 Annulation

Two decades after the first example of an iridium NHC complex was reported in 1982 by Lappert [178], the groups of Bergman and Ellman [73] investigated the use of Rh-NHC complex **35** as a catalyst in the annulation reaction of functionalised benzimidazoles (Scheme 73). During a catalytic cyclisation (5-10 mol% catalyst loading) involving an N-alkenyl benzimidazole substrate, complex **35** in d_8-toluene at 135 °C cleanly converted the substrate (up to 75%) after ~5.5 hours.

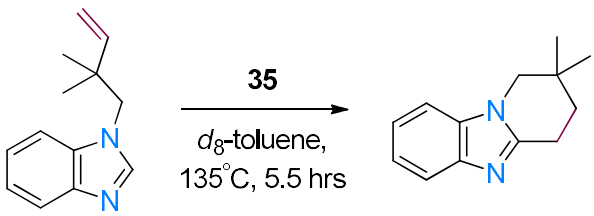

Scheme 73. Annulation of an N-alkenyl benzimidazole.

In a later study [74] it was shown that a variety of N-heterocycles may be converted into the corresponding cyclised adducts, utilising $RhCl(PPh_3)_3$ or $[RhCl(coe)_2]_2$ as catalysts. The groups of Wang [91] and in particular Choudhury [86-90] investigated the use of Rh-NHC complexes (and their precursor, $[Cp^*RhCl_2]_2$) as active catalysts in the cascade C-H

activation/annulation reactions involving (benz)imidazolium salts and internal alkynes (Scheme 74). By making use of $[Cp^*RhCl_2]_2$, a base, an oxidant, a (benz)imidazolium salt, and an internal alkyne, selective mono- and/or double C-H activation could be mediated to form corresponding di- or tri-heterocyclic salts.

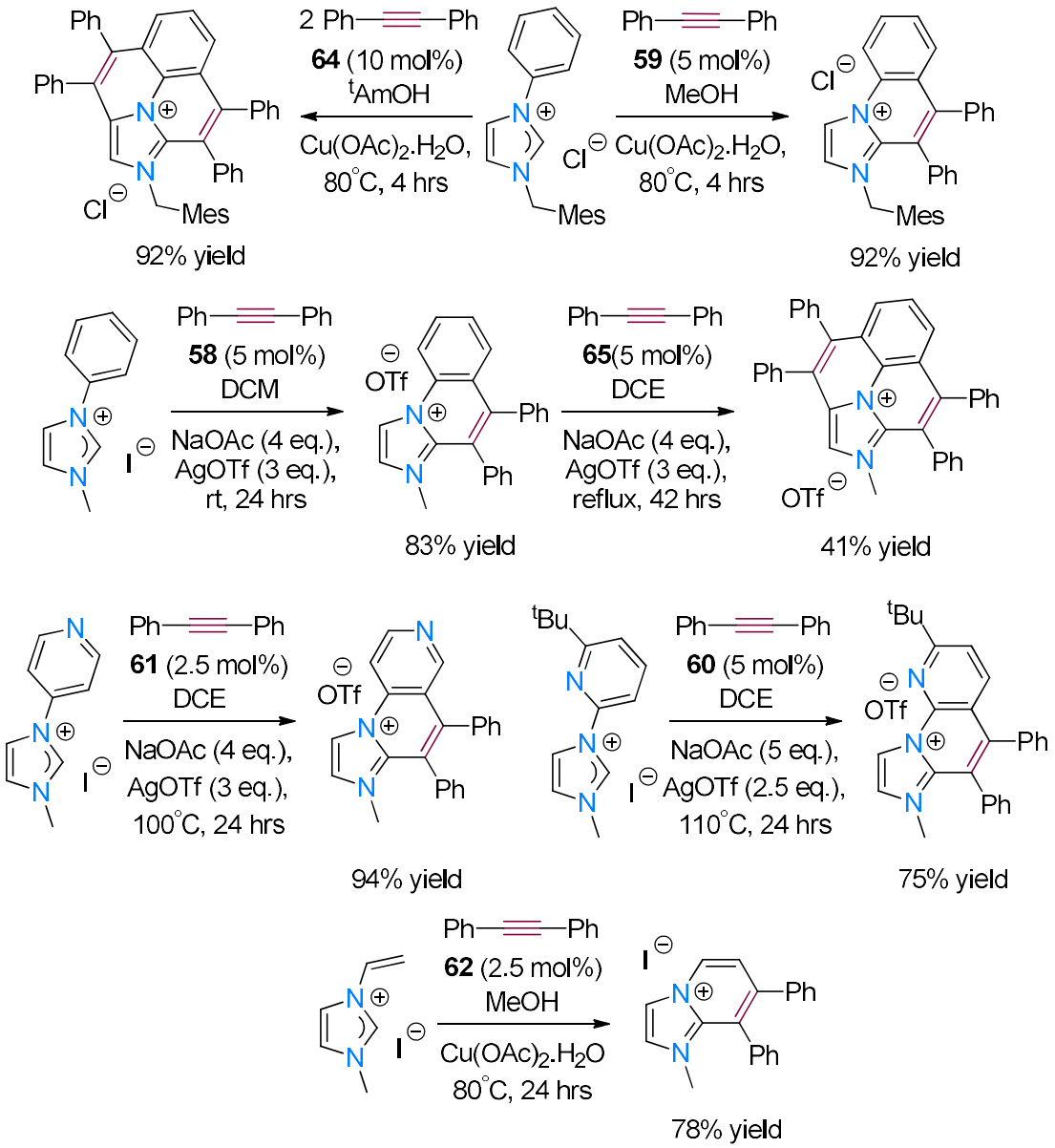

Scheme 74. Annulation reactions of imidazolium salts with diphenylacetylene.

As a means to identify the catalytic intermediates, the cyclometallated Cp*Rh-NHC complexes (**58-62**, **64**, and **65**) were isolated and used in turn as catalysts in the annulation reactions of imidazolium salts and internal alkynes. In a typical reaction, the Cp*Rh-NHC complex (5 mol% per Rh centre), imidazolium salt (0.1 mmol), diphenylacetylene (0.1 mmol), NaOAc (4 eq.),

and AgOTf (3 eq.) in either DCM or DCE is heated to 80-100 °C for 4-24 hours, after which the resulting cyclised imidazolium salts are isolated (41-97% yield). During these studies, several mechanistic studies assisted in underpinning the directing role of the NHC ligand during the C-H activation process and helped to identfiy catalytically active Rh(III) intermediates in the annulation process.

Hollis and co-workers [186] tested complexes **101** and **355** as catalysts for hydroamination/cyclisation (Scheme 75) of secondary amines in the presence of air and water with 2.5 mol% catalyst loading at 110 °C overnight. The results showed that the five-membered pyrrolidine ring was formed almost exclusively without the formation of the six-memembered piperidine ring. In some cases in the ^{1}H NMR spectra, new resonances appeared in the olefin region, indicating that isomerisation of the terminal alkene to the internal alkene occurred usually at trace amounts. The alkyl groups R^1 and R^2 was varied throughout their experiments and in most cases majority of the cyclised product was formed 90-98%. Isomerisation occurred in trace amounts except when the R^1 = H, when no cyclisation occurred and isomerisation was found to be 50% (complex **101**) and 75% (complex **355**). In general, the Rh complex **101** had a higher activity than the Ir analogue (**355**). However, the Ir analogue **355** was found to have better activity towards catalysing derivatives with diphenyl substituted backbone (R^2 = Ph, Scheme 75).

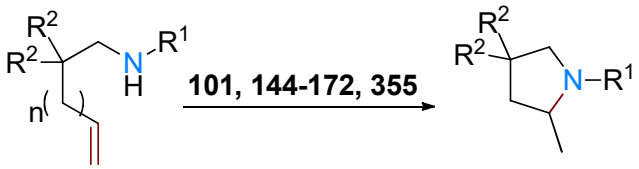

Scheme 75. Catalytic hydroamination/cyclisation of secondary amines.

Dorta [120-124] tested their entire range of complexes for hydroamination/cyclisation of amino alkenes, starting with complexes **144-146** [122]. Initially, a catalyst loading of 0.5 mol% at room temperature showed good activity, with **146** performing exceptionally. Complex **146** obtained full conversion within approximately 3.5 min (TOF of *ca.* 3500 h^{-1}). Due to the excellent performance of **146**, a variety of secondary amines were screened. With catalyst loadings of 2 mol%, complexes **146-148** gave good conversion of *N*-benzyl-2-phenyl-pent-4-en-1-amine to its cyclised product (>99, 65 and >99% respectively). The lower activity of **147** was attributed to the complex being prone to decomposition, thus reducing catalyst longevity and activity. Complex **146** showed high activity (77-96% conversion) and a high functional group tolerance. However, when an internal alkene was used rather than a terminal alkene, the

conversion obtained was negligible. Complexes **149-151** were tested on an extensive range of twenty-two different secondary amines. For the initial test, a simple secondary amine (R^1 = Bn, R^2 = Ph, Scheme 75) was used. All three catalysts showed excellent activities with full conversion achieved within 1h at room temperature with catalyst loading of 1 mol%. The enantioselectivity of the catalyst depended on the counter anion that was used, with [NTf_2^-] providing the highest *ee* (99.5%). The complexes showed to be insensitive to variations of the nitrogen substituent, high functional group tolerance and high activity (conversion values of 81-99%) with catalyst loadings of 1-7 mol%. When n = 2 the six membered ring product that formed showed a reduction in selectivity, with 62% *ee*. When R^2 = H, cyclisation would not occur at room temperature, yet still occurred at 80 °C with 5 mol% catalyst loading. The authors evaluated the asymmetric intramolecular hydroamination reaction using complex **171** (5 mol% loading) at 70 °C in DCM for 24 hours. High activity and high selectivity were observed with conversions of 81-95% and 87-98% *ee*. In a later study [123], the activity of complexes **152-160,** with modified diene ligands, were compared to that of complexes **145** and **146** tested previously. Complex **154**, containing the benzobarrelene ligand, showed comparable catalytic activity with >99% conversion using only 0.25 mol% catalyst loading. Therefore **154** is a more active catalyst than its cod analogue (**145**). However, the electron poor TFB-and TCB-containing complexes (**152**, **153**, **155**, **156**, **158** and **159**) were unable to cyclise effectively, with mostly poor conversion 7-24% when using 2 mol% catalyst loading. Finally, complexes **160-172** were tested not only for intramolecular hydroamination but also for a ring opening reaction. In the intramolecular hydroamination reaction, similar activity was observed compared to the activity of complexes **144-159**. The catalysts that incorporate cod and BB as diene ligands (**149-152**, **155**, **158**, **162**, **165**, **168**, **171-173**) show high activity and selectivity (88-95% conversion and 82->99% *ee*). Those with electron-poor TFB and TCB as the diene ligands (**153-157**, **160**, **163**, **166**, **167**, **170**) are only able to provide trace amount of conversion under the standard reaction conditions (2 mol% catalyst, ^{t}BuOH, 60 °C). However, the complexes with cyclooctane groups on the naphthalene substituents showed a lower activity even with the more electron rich dienes (26% conversion for **172** and 11% conversion for **168**). Dorta [123] then went on to test the catalyst activity of **160-172** for ring-opening amination of oxabicycles (Scheme 76) with the screening done on a single set of substrates (R^1 = H, R^2 = Me). They kept catalyst loadings at 2 mol% to keep the conditions identical. Interestingly, all the complexes (**160-172**) showed good activity with conversions from 52-93% and good selectivity (54-75% *ee*). This is in contrast to what was observed for the hydroamination reaction, where the complexes containing electron poor TFB and TCB showed poor activity

with only trace amounts of product formation. Overall complex **172** showed some of the highest activity and enantioselectivity, even providing a conversion of 67% at room temperature, which increased to 91% at 50 °C in CH_3CN. Complex **172** was tested with a variety of substrates and was shown to be highly active and selective for all substrates with good functional group tolerance (91-94% conversion and 86-92% *ee*). The *syn*-analogue of **171**, complex **173**, proved to be more active and selective, with excellent conversion (94% yield) and high optical purity of 96% *ee* at room temperature.

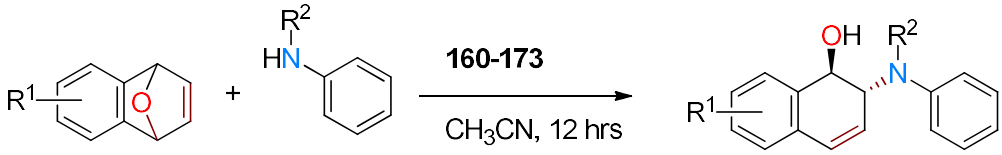

Scheme 76. Ring opening reaction

5.1.3 Addition

The group of Hollis [187] looked at the use of Rh-NHC complex **101** as an active catalyst for the 1,4-addition of aryl boronic acids to α,β-unsaturated ketones using environmentally friendly alcohol/water as solvents (Scheme 77). As part of their optimisation of conditions study, the authors found that a 1:1 $MeOH/H_2O$ solvent mixture, a catalyst loading of 2 mol%, and 80 °C collectively gave the highest yields of the addition products. While good catalytic activity for the conversion of a range of cyclic enones as well as α,β-unsaturated carbonyl compounds were observed at 50 °C (⩾ 77% yield), and even at room temperature (using cyclohexanone: 99% yield after 24 hours), 80 °C was chosen as the optimised temperature to give consistently high yields for all the substrates investigated, with minimal formation of unwanted by-products such as biphenyl. In general, high yields of products were obtained for boronic acids featuring electron rich substituents (> 97% in 1 hour), while the boronic acids featuring moderately withdrawing substituents were slightly more reactive (> 99% in 1 hour). The boronic acids with strong electron withdrawing substituents were less reactive, requiring longer reaction times to obtain moderate to high yields (46-99% after 7-72 hours) and in some cases no reaction was observed at all (e.g. 1,3-dibromophenyl boronic acid).

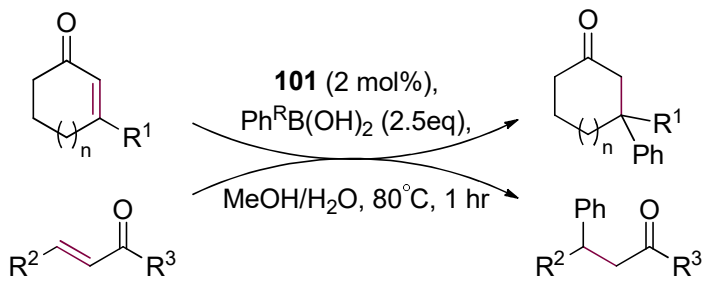

Scheme 77. Michael addition of aryl boronic acids to alkenes. R = H, 4-Me, 2-Me, 4-^{t}Bu, 2,4,6-$(Me)_3$, napht, 3-Br, 3,5-$(Br)_2$, 4-NO_2, 2-OMe, 4-CO_2Me. R^1 = H, Me. R^2 = Ph, C_5H_{11}. R^3 = H, Me, Ph.

5.1.4 Isomerisation

The group of Kunz [59,76] investigated the catalytic transformation of epoxide isomerisation using Co (**2**), Rh (**37**), and Ir (**135**) complexes, featuring CNC pincer NHC ligands with chelating alkene tethers, as catalysts (Scheme 78). As part of the first report, the group found that the rhodium complex **37** was highly catalytically active for the rearrangement of terminal epoxides into methyl ketones at room temperature. When using toluene-d_8 or C_6D_6 as solvent, full regioselectivity and quantitative yields of the methyl ketones were obtained in short reaction times (2-3 hours). A thorough substrate screening study was conducted, which showed good functional group tolerance, as well as high regio- and chemoselectivity, to obtain the corresponding products in good to excellent yields. Applying the cobalt and iridium analogues in the same reaction under the same conditions, no conversion was observed even after six days. After increasing the temperature to 80 °C with 5 mol% of the catalyst and 10 mol% of additive (LiBr) in C_6D_6, reactions using either complex **2** or **135** were surprisingly sluggish (six days) and resulted in low (32% conversion, 18% yield, **2**) to high (100% conversion, 92% yield, **2**) substrate conversions. The relatively low activity of the cobalt and iridium catalysts as compared to the rhodium catalyst was reasoned to be due to the higher stability of the coordinated N-allyl groups, one of which needs to dissociate to generate a vacant site on the resultant nucleophilic species. Employment of H_2 gas (1 bar) in the catalytic reactions succeeded to hydrogenate the N-allyl groups of **2** and **135**, with an initial enhanced activity over the course of 24 hours (5-52% yields). After 24 hours the reactions were found to halt, produce by-products from side-reactions (2-phenylethanol, polymerisation products) with no additional main products obtained even upon extending reaction time.

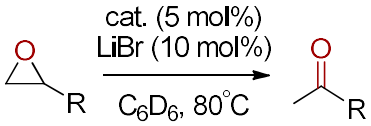

Scheme 78. Catalytic isomerisation of terminal epoxides.

The group of Chianese [16] discovered the capablity of complex **368** in isomerisation (Scheme 79, Table 2) of 1-hexene in *n*-octane at 150 °C while attempting transfer-dehydrogenation of *n*-octane with 1-hexene as the hydrogen acceptor. The authors noted that isomerisation of 1-hexene takes place more rapidly than the expected dehydrogenation reaction. The isomerisation of 1-hexene interestingly yielded a mixture of 2-hexene isomers much faster than the conversion to 3-hexene isomers, with a trace amount of the 3-isomers being formed.

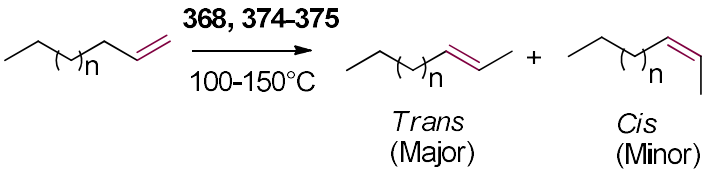

Scheme 79. Catalytic isomerisation of terminal alkenes

Table 2. Catalytic isomerisation of unsaturated hydrocarbon compounds.

Substrate	Additive NaO^{t}Bu (mM)	Conv. (%)	Catalysts	Activity (TON, h)[a]	Selectivity (%)[b]			Ref.
					trans	*cis*	other	
1-Hexene	2	42	**368**	420(0.25)	67	29	4	[16]
1-Hexene	2	73	**368**	720(1)	65	26	8	[16]
1-Hexene	0	28	**368**	280(1)	58	38	4	[16]
1-Octene	25	97	**368**	484(24)	75	22	3	[16]
1-Octene	0	4	**368**	24(24)	-	-	-	[16]
1-Octene	25	97	**375**	487(24)	47	15	38	[16]
1-Octene	0	3	**375**	15(24)	-	-	-	[16]
1-Octene	25	97	**374**	488(24)	46	13	41	[16]
1-Octene	0	3	**374**	16(24)	-	-	-	[16]

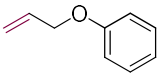	20	40	**374**		16	84	-	[162]
	20	10	**368**		42	58	-	[162]
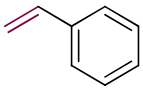	20	71	**374**		-	-	-	[162]
	20	92	**368**		-	-	-	[162]
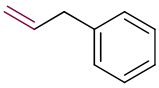	20	>99	**375**	267(0.25)	95	5	-	[162]
	20	>99	**368**	149(0.25)	95	5	-	[162]

[a] The turnover number (TON) reported after a specified amount of hours.[b] *Trans*: % of *trans*-2-hexene or *trans*-2-octene. *Cis*: % of *cis*-2-hexene or *cis*-2-octene. Other: Internal isomers (3-hexenes or 3-octenes and 4-octenes). Not determined in experiments with no base additive and 1-octene as substrate.

Additionally, the isomerisation of 1-octene in toluene at 100 °C was tested. In the absence of a base, all three complexes (**368, 374** and **375**) were minimally active for the isomerisation reaction. However, the addition of 10 equivalents of sodium *tert*-butoxide relative to the complex yielded a large increase in activity in all cases. The authors concluded that the higher production of 3- and 4-octene isomers by **374** and **3375** implies that they are more active for isomerisation of alkenes than **368**. To test this theory the reaction was monitored over time; complex **368** (2 mol%) at 100 °C consumed the 1-octene over a course of a few hours. Within the first 4 hours the ratio of *trans*-2-octene to *cis*-2-octene was found to be constant at 4:1, while the formation of 3- and 4-octene isomers was negligible even after 24 hours. In the same reaction, using **374** (2 mol%) at 60 °C, 1-octene was fully converted to *cis*- and *trans*-2-octene isomers after 30 minutes. However, an increasing fraction of 3- and 4-octene isomers were observed over the 24 hours of the experiment. To determine the effect of functional groups and substrate sizes the authors [168] tested complexes **368** and **374** in the alkene isomerisation of an allyl alcohol, vinylcyclohexane, allyl phenyl ether and allylbenzene. The authors noted that with the alcohol almost no conversion was found and therefore it was not pursued any further. Conversely, the complexes where active for the other alkene substrates. For the isomerisation of allyl phenyl ether (Table 2), the reactions were slower and required a higher temperature (120 °C). The authors theorised that the oxygen of the ether moiety coordinates to the catalyst during isomerisation, which introduces competitive coordination of the ether over the alkene. This could contribute to the decreased activity of the complexes towards allyl phenyl ether. Vinylcyclohexane readily isomerised to ethylidenecyclohexane with both complexes with no futher conversion to 1-ethyl-1-cyclohexene or other cyclohexene isomers. Complex **368** performed more efficient when using vinylcyclohexane as substrate, most likely due to the reduced steric repulsion between the coordinated alkene and the N substitutens on **368** (mesityl

groups) *vs* **374** (adenyl groups). Both complexes yielded complete conversion of allylbenzene in 24 h at 100 °C, with **374** giving a faster conversion (TON of 267) in the first 15 minutes compared to **368** (TON of 149 after 15 minutes). Both complexes gave a high selectivity for the *E* isomer *vs* the *Z* isomer (95:1).

5.1.5 Alkylation

By using the cyclopentadienyl-functionalised complexes **430** and **431**, synthesised by the groups of Peris and Royo [112], the catalytic alkylation of secondary alcohols and primary alcohols, as well as primary alcohols and primary amines was achieved (Scheme 80). High catalytic activity and excellent selectivity were observed notably for both catalysts, where for example 93% of product was obtained (> 99% conversion) with a catalyst concentration of 0.7 mol% (**431**) for the reaction between benzyl alcohol and aniline. In the catalytic β-alkylation reactions of secondary alcohols, both **430** and **431** compared well with high conversions (80% (**431**) after 24 hours and 90% (**430**) after 6 hours).

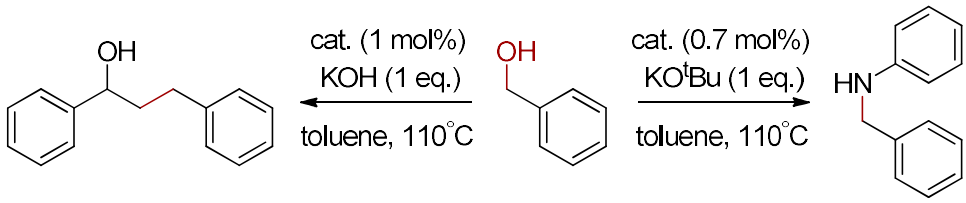

Scheme 80. Alkylation of primary alcohols with primary amines and secondary alcohols.

Maity and co-workers [147] used **258** (5 mol%) in α-arylation of oxindole with phenylbromide and 2-methylphenylbromide. Using complex **258** resulted in a relatively low yield without the use of an additive (32-53%); however, with the use of 5 mol% PPh_3 the activity of **258** increased to 65% conversion. Additionally, **258** (0.5 mol%) was tested for application in the Suzuki-Miyuara cross coupling reaction, showing high conversion (99%) with both arylboronic acids($PhB(OH)_2$ and $4\text{-}Me(Ph)B(OH)_2$.

Hahn and co-workers [94] tested complexes **58**, **84** and **256** in a Suzuki-Miyaura coupling in *n*-butyl alcohol. With a catalyst loading of 2 mol% all complexes achieved excellent conversion 99% but had poor selectivity, with a wide range of side products being formed.

5.1.6 Hydrogenation

Several groups, including those of Fout [30,31], Tamm [77], and Labande [109] investigated the use of cobalt (Fout), rhodium (Labande), and iridium (Tamm) NHC complexes as active

catalysts in the hydrogenation of alkene, nitrile, and carbonyl substrates. Fout made use of well-defined Co(I)-NHC complexes **22** and **23** in the hydrogenation of alkenes. Studies employing the better-performing **22** showed that during the catalytic reaction, **22** is converted to **24** under the conditions employed (4 atm. H_2 gas). This has been observed at the end of the reaction (2 hours), confirming the H_2-adduct (**24**) to be the resting state of the catalytic cycle. Complex **22** was shown to be useful in converting styrene into ethylbenzene at room temperature in quantitative yield within two hours. An expanded substrate scope was included in the study, which showed a wide functional group tolerance, all being converted quantitatively in relatively short reaction times (2-22 hours). Fout also showed that cobalt-NHC complexes **16**, **28**, and **29** were catalytically active in the hydrogenation of nitriles (Scheme 81). At cobalt catalyst loadings of 2 mol%, H_2 (4 atm.), KO^tBu (6 mol%), $NHBEt_3$ (4 mol%) in toluene at 115 °C, a variety of alkyl and aryl nitrile substrates were converted into the corresponding primary amines (78-99% yield, except for CH_3CN (39%)) after eight hours. The low yield of ethylamine hydrochloride (39%) from acetonitrile was ascribed to product loss due to the volatility of ethylamine (bp = 16-20 °C).

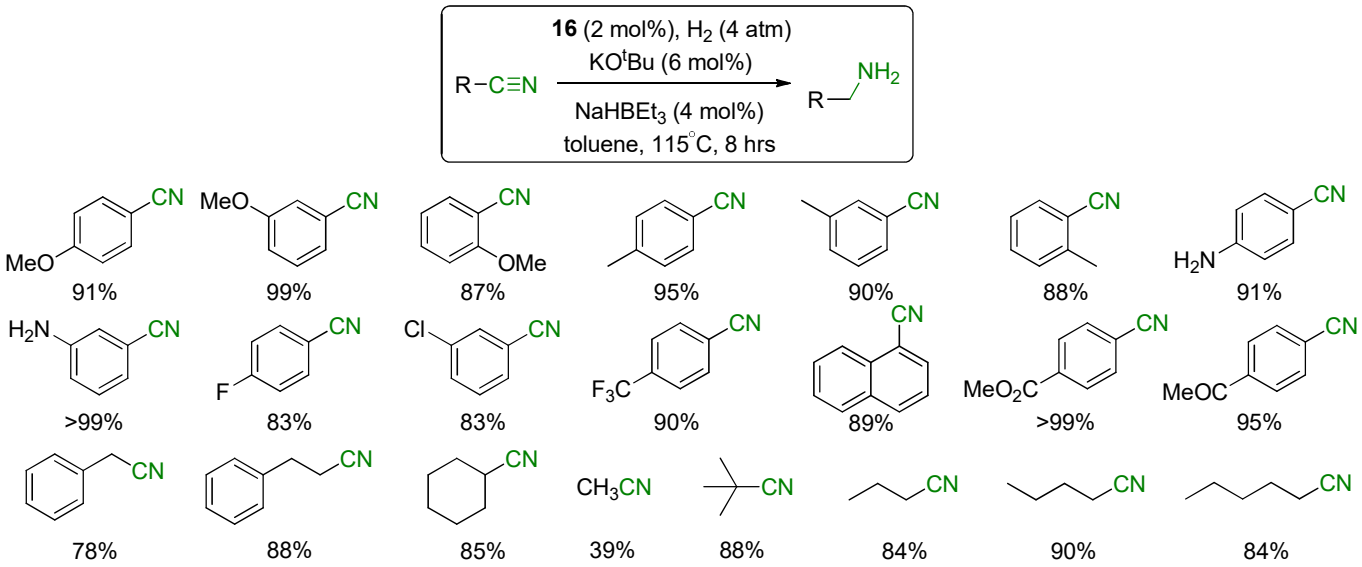

Scheme 81. Catalytic nitrile hydrogenation (% conversion).

The group of Tamm looked at the hydrogenation of alkenes in non-polar media using the iridium-NHC complexes **139-141**. As a benchmark study, complexes **139-142** (0.1 mol%) were added to dichloromethane solutions containing 1-methylcyclohexene at room temperature and H_2 (1 atm.), with the resulting mixtures left to stir for five hours. The highest initial activity was exhibited by complex **141** (TOF_{max} = 532 h^{-1}), but this complex gradually deactivated

within 80 minutes due to a lack of stability, that led to an overall conversion of 58%. Complexes **139** and **142** exhibited very low activity (13% and 6% final conversions, respectively) under the same experimental conditions. Complex **140** was the only catalyst capable of achieving a high conversion (95%) within five hours (TOF_{max} = 510 h^{-1}). Using **140**, a variety of cyclic and acyclic substrates were converted in a few hours (0.5-2 hours) with typical catalyst loadings of 0.01-0.1 mol%. The reactions were found to be active with catalyst concentrations as low as 0.001 mol% to give quantitative conversions, albeit over longer time periods (12 hours). Labande [109] found in a preliminary catalytic study that their rhodium catalyst **108** was active in the Grignard-type arylation of 4-nitrobenzaldehyde *via* C-H activation of 2-phenylpyridine to yield the corresponding alcohol (Scheme 82). Under unoptimised conditions, complex **108** was capable of achieving 33% conversion at 65 °C in THF after 24 hours.

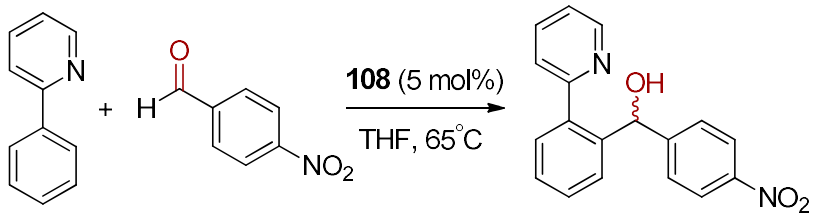

Scheme 82. Grignard-type arylation.

Chianese and co-workers [16] initially tested their complexes **368-370** and **374-375** on transfer-dehydrogenation of *n*-octane at 150 °C with NaO^{t}Bu as additive and norbornene as hydrogen acceptor. The mesityl complex **378** and di-*tert*-butylphenyl complex **380** showed medium activity with 12% and 10% conversions, respectively. The complexes **374**, **375**, and **380** showed no activity for transfer-dehydrogenation of *n*-octane. The authors theorised that the steric bulk of the hydrogen acceptor and transition metal complex played an important role in the low activity reported. Norborene and *tert*-butylethylene, both commonly employed hydrogen acceptors, are bulky compounds which possibly inhibited the reaction. Transfer-dehydrogenation with 1-hexene as hydrogen acceptor was attempted, which then led to isomerisation of 1-hexene as discussed in section 5.1.4 previously.

The group of Crabtree [36] tested complex **221** for transfer hydrogenation of acetophenone using 1 mol% catalyst loading in refluxing isopropyl alcohol (82 °C) for 3 hours. Without the use of an additive, the complex showed negligble conversion; however with the addition of 2 mol% $AgBF_4$ the conversion was found to be about 9%. The best conversion (15%) was

achieved *via* the use of 10 mol% KOH as additive. The authors noted that even the metal precursor $[Cp^*IrCl_2]_2$ outperformed the complex **221** as catalyst.

Willans and co-workers [37] tested chelating NHC carboranes of Ir in transfer hydrogenation reactions of acetophenone to 1-phenylethanol. The mixture of C-cyclometallated complex **270** along with its boron-cyclometallated counterpart, showed high conversions with loadings of both 1 mol% and 0.5 mol% (>99% and 91% conversion, respectively). However, it was noted that without the addition of KO^{t}Bu , no conversion was observed. C-cyclometallated complex **270** on its own provided a conversion of 75% with a catalyst loading of 1 mol% in addition to 10 mol% of KO^{t}Bu. Non-carborane containing cyclometallated complex **232** (1 mol%) was also tested and showed a much lower conversion percentage at 39%. The authors theorised that the higher activity upon cyclometallation of a carborane *vs* phenyl substitutent is likely due to metal-ligand bifunctional catalysis, where the carborane anion becomes involved in the catalysis reaction. Additionally Choudhury and co-workers [137] investigated the hydrogenation of acetophenone using **222-231**. It was found that the six-membered metallacycles (**227-231**) were catalytically more active (80% yield) than their five-membered analogues (**222-226**) with yields of 40%.

Groups led by Hahn and Oro [17] tested **128** and **129** in transferhydrogenation of cyclohexanone to cyclo-hexanol with 2-propanol as hydrogen source and KOH as an additive. The complexes **128** and **129** showed a relatively low turnover frequency (approximately 70 and 50 h^{-1}, respectively). The authors theorised that the η^2-allyl coordination reduces the availability of a vacant coordination site for subtrate coordination and activation.

Morris and co-workers [33] investigated the ketone hydrogenation activity of chiral tri-dentate complex **239** using twenty-five different ketone substrates with an array of steric and electronic properties. They used the catalyst **239** (0.2 mol%) with KO^{t}Bu as additive (1.6 mol%) in 25 bar of H_2 gas at 50 °C, allowing it to react for 2 hours. Overall, complex **239** showed good conversion values (30-99%) with a higher stereoselectivity than another non-chelating complex tested. The authors theorised that this could be due to the more rigid structure of the tri-dentate complex. The group also tested complex **239** for the hydrogenation of benzylidene acetone, to observe the selectivity between olefin and ketone (Scheme 83). They found that complex **239** was, as expected, more active towarfds alkene hydrogenation. However, trace amounts of allyl alcohol and saturated alcohol were observed as well.

Groups led by Peris [40], Baratta [39], and Choudhury [38] tested their complexes for catalytic transfer hydrogenation of ketones (Table 3) and imines. Baratta and co-workers [39] completed their reactions under refluxing conditions with NaO^{i}Pr as base and solvent, whereas the Peris

group [40] used ^{i}PrOH/KOH at refluxing conditions. Choudhury [38] used KOH as additive and heated the 2-propanol to 100 °C.

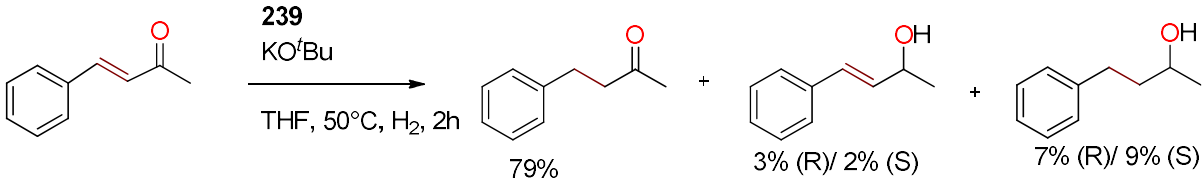

Scheme 83. Hydrogenation of benzylidene acetone

Table 3. Catalytic transfer hydrogenation of ketones and imine.

Substrate	Conv. (%)	Catalysts	[Catalyst] (mol%)	Time (h)	Ref.
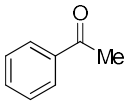	>99	**120**	1	3	[40]
	70	**120**	0.1	19	[40]
	58	**243**	1	1	[38]
	84	**244**	1	1	[38]
	66	**243**	1	1.5	[38]
	96	**244**	1	1.5	[38]
	57	**406**	0.5	14	[39]
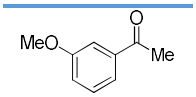	86	**406**	0.5	5	[39]
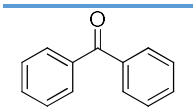	>99	**120**	1	5	[40]
	99	**406**	0.5	16	[39]
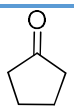	99	**406**	0.5	8	[39]
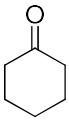	99	**406**	0.5	4	[39]
	>99	**117**	1	0.5	[40]
	>99	**118**	1	0.5	[40]
	90	**118**	1	0.5	[40]

	>99	**120**	1	0.5	[40]
	>99	**120**	0.1	5	[40]
	91	**121**	1	0.5	[40]
	85	**117**	1	5	[40]
	56	**118**	1	5	[40]
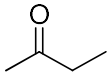	36	**119**	1	5	[40]
	>99	**120**	1	5	[40]
	89	**121**	1	5	[40]
	22	**406**	0.5	12	[39]
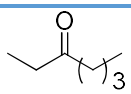	5	**406**	0.5	8	[39]
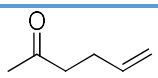	86	**406**	0.5	10	[39]
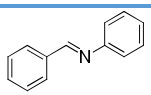	>99	**120**	1	9	[40]

The Maity group [147] used the heterobimetallic complex **258** in a tandem Suzuki-Miyaura coupling/transfer hydrogenation reaction (Scheme 84).

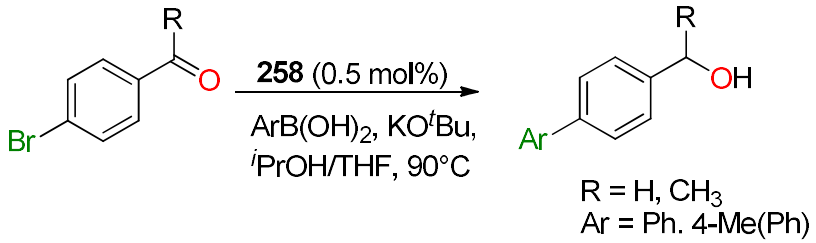

Scheme 84. Suzuki-Miyaura coupling/transfer hydrogenation reaction

Complex **258** delivered 85% yield of 4-biphenylmethanol in 2 hours, which was much higher than the mononuclear Pd(II) and Ir(III) counterparts (38-41% conversion). Additionally, **259** showed good yields (65-76%) of the respective products when 4-bromoacetophenone and phenylboronic acid derivatives were used. The increased activity of this heterobimetallic complex is ascribed to the dual action of Pd(II) and Ir(III) centres during the reaction.

Peris and co-workers [94] used Rh- and Ir-based heterobimetallic NHC complexes for tandem Suzuki-Miyaura coupling/transfer hydrogenation of *p*-bromoacetophenone (Table 4).

Table 4. Suzuki-Miyaura coupling/transfer hydrogenation of *p*-bromoacetophenone.[a]

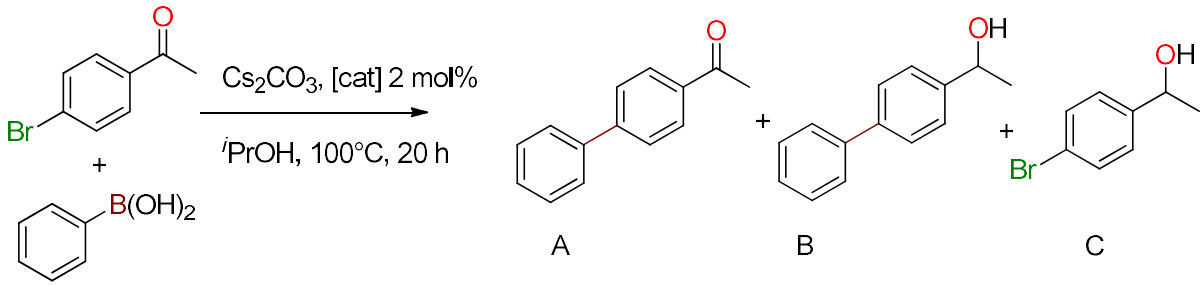

Metal	Catalysts	Additive	Conv. (%)	Time	Yield (%)[b]			Ref
					A	B	C	
Rh	**58**	Pd-NHC	98	20	36	62	-	[86]
Rh	**58**	Pd-NHC	99	20	15	84	-	[86]
Ir	**222**	Pd-NHC	98	20	25	73	-	[137]
Rh, Pd	**76**	None	99	20	46	53	-	[94]
Rh, Pd	**84**	None	99	20	17	82	-	[94]
Ir, Pd	**256**	None	99	20	15	84	-	[94]
None	None	None	70	20	-	-	54	[94]

[a]Reaction conditions: 0.36 mmol of *p*-bromoacetophenone, 0.54 mmol of phenylboronic acid, 1.08 mmol of Cs_2CO_3, 2 mL of 2-propanol, 2 mol% catalyst loading, 100 °C, 20 h.

The groups of Chaplin [171] and Braunstein [163] used complexes **373**, **391** and **392** in transfer dehydrogenation reactions of cyclooctane with *tert*-butylethylene as hydrogen acceptor. However, even under exteme conditions (24 h, 150 °C for Chaplin [171] and 10 h, 200 °C for Braunstein [163]), none of the complexes showed significant conversion (*ca.* 2-3.6 TONs). Braunstein used 0.1 mol% of complex **373** without the use of an additive (3.6 TON), whereas Chaplin used 0.5 mol% of **391-392** with the use of 1 mol% of KO^{t}Bu (*ca.* 2 TON).

5.1.7 Hydroformylation

Complex **113** was tested by Danopoulos and Cole-Hamilton [113] for its catalytic activity in the hydroformylation of 1-octene (Scheme 85), as well as for the carbonylation of methanol reactions. Complex **113** was active for the hydroformylation of 1-octene, albeit with slow conversion over the period of eight hours. However, the reaction experienced competitive isomerisation of terminal to internal alkynes, which were also formylated to form a mixture of different branched and linear products (overall linear to branched ratio of 1:1.25).

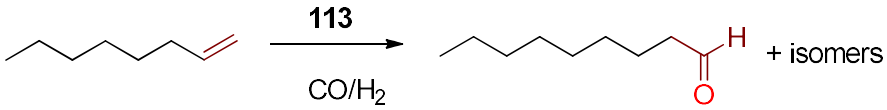

Scheme 85. Hydroformylation of 1-octene to form a mixture of products

Higher activity was observed in the carbonylation of methanol reaction using **113**, where the catalyst was stable under the conditions employed. The activity of **113** compared well with well-known Monsanto-based catalysts for this reaction: 1.5 mol.dm^{-3}.h^{-1} ([**113**] = 5 mmol.dm^{-3}, 150 °C) *vs* 1.7 mol.dm^{-3}.h^{-1} ([$(RhI_2(CO)_2)^-$] = 5 mmol.dm^{-3}, 150 °C) and 1.7 mol.dm^{-3}.h^{-1} ([$(RhCp^{Me4}$-$PEt_2(CO))$] = 5 mmol.dm^{-3}, 150 °C).

5.1.8 Hydroboration

The group of Hollis [69,105] was successful in applying complexes **34**, **99**, and **100** as active catalysts in the hydroboration of alkene and carbonyl-containing compounds. In their pilot study utilising the cobalt complex **34** (0.3 mol%), the hydroboration of styrene at room temperature was investigated. While no activity was observed without a hydride source ($LiBHEt_3$), addition of 1 mol% $LiBHEt_3$ led to quantitative conversion within one hour to give the Markovnikov hydroboration adduct as the major product (20:1). After addition of another 1.1 mmol of styrene and pinacolborane to the reaction mixture, 95% conversion was achieved after an additional hour. The rhodium analogues (**99** and **100**) were then investigated in the room temperature β-boration of acyclic and cyclic substrates. While during the optimisation study iodido complex **99** showed higher activity (72% conversion in one hour) compared to chlorido complex **100** (57% in one hour), the mixture of **99** and **100** provided the highest activity (>99% in one hour). The authors reasoned that the excess $NHMe_2$ present in a freshly prepared mixture of **99**/**100** assists as a base to accelerate the reaction rate. They found that a five month old sample of **99**/**100** (~4 mol%) achieved only 83% conversion of 2-cyclohexenone in one hour. An expanded substrate scope was studied using fresh **99**/**100** (~4 mol%) in either MeOH or EtOH as solvent, which gave conversions of 70-100% (except 3-methylcyclohexenone, 40%) within one hour at room temperature (Scheme 86). No conversions for substrates containing strong electron withdrawing groups (*trans*-β-nitro styrene and 1-(dimethylamino)-2-nitroethylene (both not shown), as well as acrylonitrile were observed, even upon extending reaction time to 24 hours.

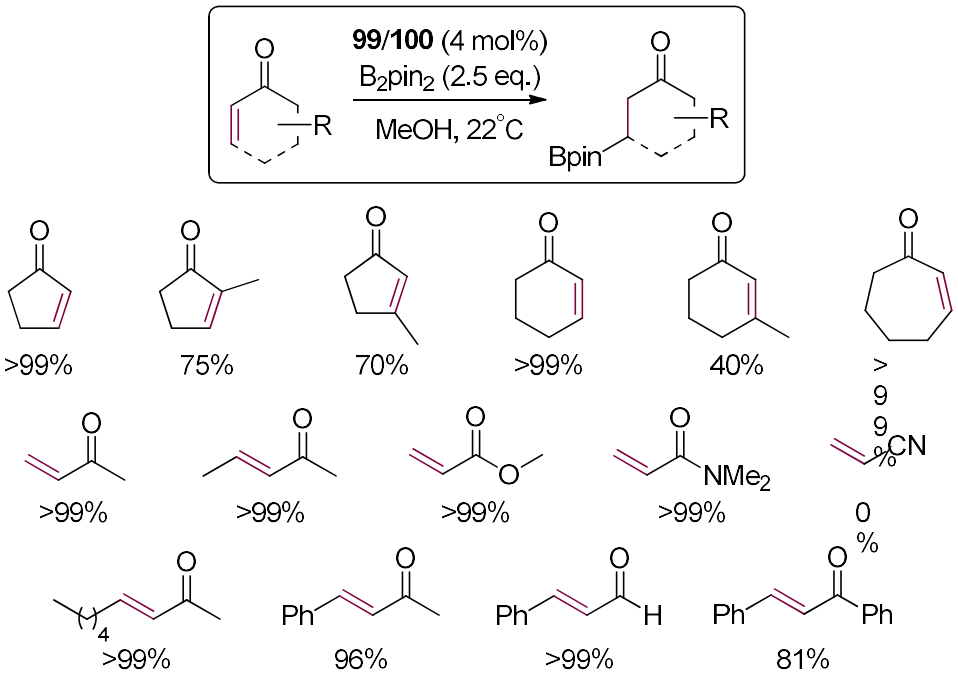

Scheme 86. Catalytic hydroboration of alkenes (% conversion).

Chianese and co-workers [167] first did a catalyst screening with complexes **368-370** for the borylation of *m*-xylene with B_2pin_2 and NaO^{t}Bu as additive. They found complex **368** to be the most active (conversion of 57%). A variety of substrates was converted using **368** as catalyst. The electron-deficient substrate 1,3-bis(trifluoromethyl)benzene was transformed with the most efficiency, giving a yield of 94% even without the addition of NaO^{t}Bu. In general, the borylation occurred at the least sterically hindered arene C-H bond.

5.1.9 Deuteration

Nolan and co-workers [83,128] performed catalyst screening of their complexes **53**, **54**, **184**, **185** and **188** for isotopic exchange of silanes (Scheme 87).

Scheme 87. Deuteration of silanes.

Table 5. Catalytic screening for deuteration of $HSiPh_3$.

Catalysts	Metals	[Catalyst] (mol%)	Time (h)	Conv. (%)
None	None	0	3	0
53	Rh	1	3	87
54	Rh	1	3	64
181	Ir	1	3	91
182	Ir	1	3	93
183	Ir	1	3	87

The Rh-based complexes **53** and **54** showed lower activity (87 and 64% conversions, respectively) compared to their Ir analogues **185** and **186** (93 and 87% conversions, respectively). Unexpectedly, the neutral complex **185** had a higher activity than the $14e^-$ cationic complexes **54** and **186**. Complex **185** showed the best conversion and was thus used to catalyse the deuteration of ten additional silanes. This complex gave good conversions overall, with most silanes giving 90 to 99% conversion. The exception was $HSiCl(^iPr)_2$, which only gave 48% conversion after 3 hours. Sterically unencumbered silanes were easy to deuterated with $HSiEt_3$, being converted almost completely even with a catalyst loading as low as 0.01% after 3 hours. The sterically strained silanes required longer reaction times and higher temperatures (50 °C) to convert fully, with $HSi(SiMe_3)_3$ taking 16 hours to provide a 93% conversion.

Peris and co-workers [136] tested **215** and **217** for their capabilities of deuterating a variety of different organic compounds at 100 °C with catalyst loadings of 2 mol%. Acetone-d_6 as well as methanol-d_4 were tested, and the latter gave superior conversion at lower reaction times. Complexes **215** and **217** were seen as suitable catalysts because the halide ligands were readily removed with the addition of AgOTf which forms the triflate derivative of **215**/**217**. In diethyl ether the complex **215**/**217** preferentially deuterated the internal methylene position with 65% conversion while 45% deuteration of the methyl position could be achieved. For THF **215**/**217** had very low deuteration, however ketones such as ethylmethyl ketone and acetophenone showed quantitative deuteration of the α-positions at reaction times of 6 hours. In terminal olefins the complex **215**/**217** showed high selectivity for the vinylic protons.

5.1.10 Imine Reduction

The catalytic conversion of C=O containing groups is a common transformation found throughout organic synthesis. The reduction of imines, however, is more difficult due to the lower polarisation of the C=N bond.

The group led by Hahn [144] used their complexes **260** and **261** for catalytic reduction of imines in MeOH at 60 °C in the presence of 3 bar H_2(g) with a catalyst loading of 5 mol% (Scheme 88).

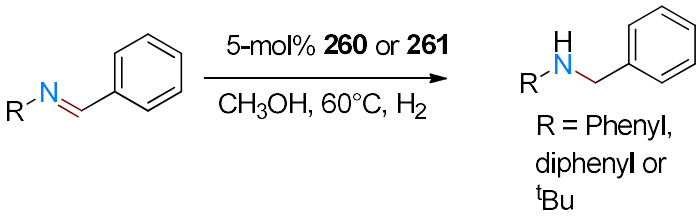

Scheme 88. Catalytic reduction of imines.

After approximately 3 hours of reacting *N*-benzylideneaniline with **260**, 82% conversion was observed, whereas **261** only afforded 75% conversion with the same substrate. In addition, **260** was tested as catalyst for the conversion of both *N*-benzylidene-*tert*-butylamine and *N*-benzyl-1,1-diphenylmethanamine. After 3 hours, 85% conversion of *N*-benzyl-1,1-diphenyl-methanamine was afforded, with only 7% conversion of *N*-benzylidene-*tert*-butylamine; however, after 32 hours conversion of 85% was achieved. The steric bulk of *N*-benzylidene-*tert*-butylamine clearly affected the ease of reduction.

5.1.11 Solvolysis

Catalytic solvolysis is one method used to liberate hydrogen stored in hydrogen-rich ammonia-borane for the use in alternative fuel [188]. Nolan and co-workers [188] reported on the solvolysis of ammonia-borane in a 1:1 mixture of THF and H_2O with catalyst loadings of 500 ppm for complexes **185** and **186** [84]. At 24 °C, complex **185** showed a TOF of 111 500 h^{-1} after 20 min of reaction time. Complex **186** was considerably more active, with a TOF of 173 000 h^{-1} after 300 seconds of reaction time. Reducing the catalyst loading for **186** to 50 ppm, in combination with a slight increase in temperature (40 °C), yielded a release of approximately 3 moles of H_2/mol of ammonia-borane after 20 minutes of reaction time. The authors tested solvolysis of a different hydrogen source, Me_2NHBH_3, using complex **186**. Due to the steric bulk of the substrate, the reaction required a longer reaction time (40 min) and higher

temperature (40 °C), resulting in a release of 3 moles H_2 per mole of substrate. Even though Me_2NHBH_3 only possesses 2 moles of H_2, 3 moles of H_2 gas are still produced. This shows that H_2O is also a source of hydrogen in this reaction. Complex **189** was also tested for catalytic solvolysis and was found to have a very similar activity to that of **186**. These results led the authors to believe that **189** acted as a resting state for the active catalyst.

5.1.12 Oxidation

Xiao [42] tested **223** for oxidation of 1-phenylethanol in trifluoroethanol with NaOAc (2.5 mol%) as additive and catalyst loading of 0.1 mol%. After 20 hours, complex **226** afforded a good conversion of 80%. However, this *ortho*-metallated complex **226** showed lower activity than the non-metallated analogue (100% conversion), which shows that *ortho*-metallation does not necessarily play a significant role in this oxidation reaction.

Choudhury [140] used complexes **234** and **235** for catalytic sp^3 C-H bond oxidation in the presence of $NaIO_4$. The complexes were found to be active towards oxidation of ethyl benzene, cyclooctane and *cis*-decalin in an acetone-H_2O mixture (3:1 v/v) with yields of 39-45% for **247** and 43-47% for **248**. Interestingly, the Zn-containing complex **247** showed slight improvement in activity even though the authors questioned the robustness of the Zn(II)-(terpyridine)$_2$ coordination under oxidative conditions. The complexes were highly selective towards the *cis*-isomer in the case of *cis*-decalin, with the *cis*- and *trans*-isomers forming in a 98:2 ratio.

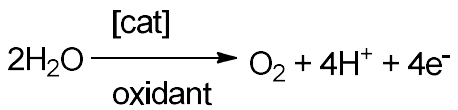

Scheme 89. Water oxidation reaction

Crabtree [43] used complex **221** for water oxidation (Scheme 89) with cerium(IV) ammonium nitrate (CAN) as the primary oxidant in combination with $NaIO_4$. With CAN (78 mM, pH 0.89) complex **221** (4.5 μM) gave 8 turnovers min^{-1}. With the harsh conditions of CAN and a low pH the authors noted a lag phase of oxygen evolution (data obtaned from Clark-type electrode) as well as oxygen consumption upon injection. The authors theorised that it could possibly be due to the oxidation of the Cl^- ligand on the complex to OCl^-. Higher catalyst loadings of **221** led to higher rates of oxygen evolution. This is possibly due to the harsh conditions, resulting in the loss of the NHC ligand forming a $[Cp^*Ir(H_2O)_3]^{2+}$ fragment, which contributes to the

catalysis. Ce(IV) oxidations require low pH, which contribute to deactivation of the catalysts, thus $NaIO_4$ is used as a replacement which can act as oxidant near neutral pH. With complex **221** and 5 mM $NaIO_4$ at a pH of ±5, rate values of 12-16 turnovers.min^{-1} were achieved with a diminished lag phase and no initial oxygen consumption.

Macchioni [44] tested complex **238** for catalytic activity in water oxidation (Scheme 89) with 1.0 mM CAN. The authors monitored the consumption of Ce(IV) using UV-Vis spectroscopy at 340 nm every five seconds to the determine the activity. The concentration of the complex **238** was varied from 1.0 μM to 4.0 μM and a TON of 62-250 was achieved. Interestingly, the catalyst concentration of 1.0 μM yielded the highest TON of 250. However, a relatively consistent TOF of 6.9 min^{-1} was found for the variation of catalyst concentration, indicating relative stability most likely due to the strong π-donating 4-*N*,*N*-dimethylaminophenyl wingtip groups.

Royo [45] prepared complex **430** for use in water oxidation (Scheme 89) in the presence of $NaIO_4$ in an attempt to achieve milder conditions than the standard used CAN. Initially, the use of 70 μM of complex **430** with 125 mM CAN as sacrificial oxidant, yielded a TON of 343±2. Subsequently 10 μM of complex **430** was reacted with 250 mM $NaIO_4$ as sacrificial oxidant, which resulted in TON of >11000. With an increase in $NaIO_4$ concentration to 500 mM, the TON increased to >24000. These results show that catalytic degradation occurs with a powerful oxidant like CAN, whereas with $NaIO_4$ much milder conditions led to higher activity.

5.2 Luminescence and Phosphorescence

From all the complexes covered in this review, iridium-based NHCs are the only ones used for the application of luminescence and phosphorescence [189]. This is mostly due to the high efficiency and chemical stability of iridium(III) complexes. The high efficiency is a result of strong spin orbit coupling of the heavy iridium metal centre, allowing faster energy transfer from singlet to triplet states, resulting in the efficient phosphorescence of these complexes [189]. From literature it is observed that Ir is a very active metal for photochemistry and construction of OLEDs (organic light emitting devices) [190,191].

Chi and co-workers [148] employed their complexes **264-268** in photoluminescence and manufacturing of efficient OLEDs. Quantum yields (Φ) of nearly 100% were found for complexes **264-266** indicating that the bis-tridentate structure of the Ir(III) complexes increases the stability and thus reduces the non-radiative decay processes, which in turn improves the Φ obtained. Interestingly, the lifetime of the excited states decreased with increasing Φ, with the

shortest lifetime being for **266** at 3.01 μs with the highest Φ of approx. 100%. The longest lifetime was observed for **267** with 9.23 μs, but it had the lowest Φ of 25%. Thus can be concluded that the naphthyl group has a detrimental effect on the luminescence compared to the phenyl group it replaces. The authors theorised that the lower Φ observed for **267** and **268** could possibly be due to the higher rigidity of the chelate, where **268** is much more rigid than **267**. This has an influence on the radiative decay rate (k_r), as **268** has a lower k_r than **267** (1.1 x 10^5 s^{-1} for **268** and 2.7 x 10^4 s^{-1} for **267**) while both complexes exhibited similar non-radiative decay. The ligand thus might have a large effect with regards to enhancing the radiative process. The authors chose **265** and **268** as dopants in the fabrication of OLEDs to investigate the applications in electroluminescent devices, with **265** being used for a green OLED and **268** used for a red OLED. Both devices reached their highest values at doping levels of 4 wt% with the maximum EQE (%) reached by the device with **265** as dopant at 18.8%, while the device with **268** as dopant reached 12.5%. In a later study, the group led by Chi [172] used their complexes **393-395** for blue-emitting OLEDs, showing very high Φ values for all the complexes (83.5-100%) with **393** achieving the higest Φ. When all the complexes (**393-395**) were doped (10 wt%) on solid DPEPO (bis[2-(diphenylphosphino)phenyl]ether oxide) matrices, the Φ value for **393** decreased to 80.3%. By contrast, the Φ values for **394** and **395** increased (83.5% to 86.9% for **394** and 82.7% to 95.6% for **395**). OLEDs constructed from the complexes showed impressive EQEs, with the **395-**containing OLED performing the best with an EQE of 21.6% at maximum efficiency.

Crassous [149] showed their complexes **273** and **274** to be active for phosphorescence with both complexes having very high phosphorescence lifetimes and good Φ values (Table 6). Due to the strikingly long lifetimes, the luminescence of both complexes is highly sensitive to oxygen, with the lifetimes decreasing by a factor of >500 when the solvent is aerated.

Choudhury [150] studied their complexes **275** and **276** for dual-emissive ratiometric O_2 probes by having an oxygen sensitive phosphorescent centre at the iridium and an O_2 insensitive fluorescence at the terpyridine moiety (Scheme 90). Both complexes showed two emission bands, 405 nm and 515 nm for **276** and 405 nm as well as 485 nm for **275**, with emission properties displayed in Table 6. The complexes had longer lifetimes for the high energy emission band. Upon introduction of oxygen, the lifetime of the low-energy emission bands decreased, while the lifetime of the high-energy emission band was mostly unaffected. Therefore the high-energy band was assigned as fluorescence and the low-energy band as phosphorescence.

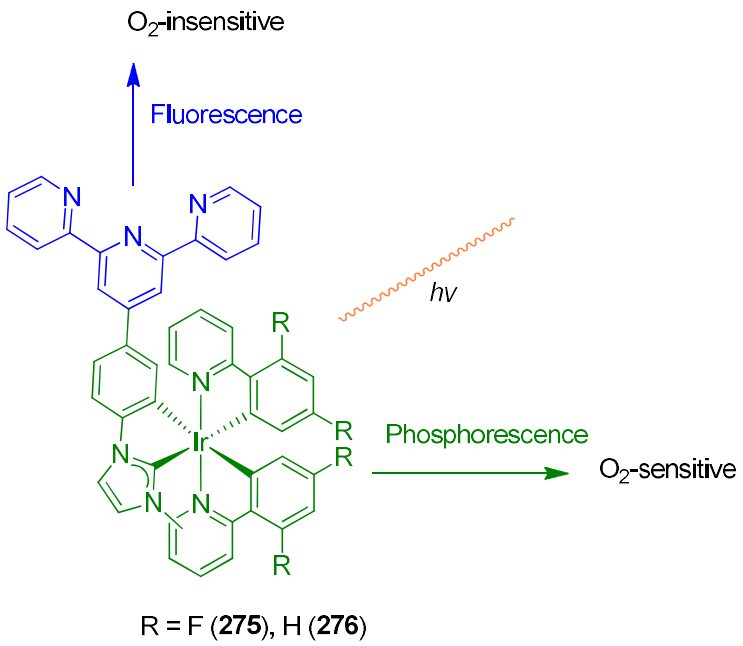

Scheme 90. Dual-emissive ratiometric O_2 probes.

Nazeeruddin [151] tested their complexes **277-279** using steady-state and time-resolved photoluminescence measurements. The Φ_{PL} obtained for the three complexes were relatively high, with complex **278** having the highest quantum yield at 66% with a relatively short luminescence lifetime of 0.45 µs. Complexes **277** and **279** were not as effective, with Φ_{PL} values of 34% and 31% respectively. However, the photoluminescence lifetime of **277** (0.46 µs) was slightly longer than that of **278** and even more so than that of **279** (0.38 µs). The radiative decay (k_r) of **278** was found to be the highest at 1.47 x 10^6 s^{-1} and its non-radiative decay (k_{nr}) was the lowest at 0.75 x 10^6 s^{-1}. Due to **278** and **279** being the most blueshifted emitting complexes, the authors investigated their abilities to perform as OLED emitters. The turn-on voltage of both devices was similar, indicating that charge transport is not significantly affected by the type of emitter used. However, it was observed that the efficacy, power efficiency and external quantum efficiency were higher for device 2 (with **278** as dopant), with values of 8.0 cd A^{-1} (4.2 V), 6.3 lm W^{-1} (3.8 V), and 3.2% (4.2 V), respectively.

Zheng and co-workers [152] tested their large range of complexes **273**, **281-288**, **290-296** and **298-299** for photoluminescent activity (Table 6). With complex **280** being the best performing, however the authors chose second best performing complex **283** to create an OLED with a dopant concentration of 9 wt% (EQE of 10.3%).

Sun [153] tested their complexes **295-301** for high-performance yellow OLEDs (Table 6). All complexes showed long lives (except for **295** and **300**) and oxygen-sensitive bright yellow

luminescence, suggesting that the emission is phosphorescent in nature. Due to the high Φ value of **296**, the authors constructed a PHOLED based on this complex (10 wt%). This device achieved a high EQE of 20.6%.

Wong and co-workers [155] tested their complex **302** for phosphorescent activity as well as for use in a sky-blue PHOLED. The photophysical data for **302** is listed in Table 6. A PHOLED was constructed with a high EQE of 20.6%.

Hogan [5] applied their complexes **303-307** to photoluminescence. Each complex exhibited intense photoluminescence in dilute acetonitrile solutions at room temperature, with Φ ranging from 0.42 to 0.68 with **306** being the most efficient and **304** being the least efficient. The lifetime of photoluminescence was also in a range of 1.59-2.06 μs with **306** having the longest lifetime. The authors suggested that the differences in quantum yield was likely due to the differences in the rate of non-radiative decay, due to k_{nr} being inversely proportional to Φ, with the exception of **307** which had a high k_{nr} of 2.3 x 10^5 s^{-1} but a Φ of 53.1%. Interestingly, the authors noted that the photoluminescence for the cyclometallated iridium complexes were extremely sensitive to the presence of oxygen and thus ensured to maintain anaerobic conditions.

Esteruelas [156] investigated the photochemical properties of their range of complexes **321a-323b** and **326a** (Table 6). The complexes were found to be phosphorescent emitters when excited by a photon in a doped PMMA film at 5 wt% as well as in 2-MeTHF, showing overall good quantum yield values (ranging from 34-93%). Complex **321a** exhibited the best results (Φ of 93%). Therefore the authors constructed an OLED based on **321a** which had a high luminous efficacy (LE) of 13.0 cd/A and a high EQE of 12.9%. In later work, Esteruelas [173,174] obtained the photophysical data for their complexes **397-403** (Table 6). An OLED based on **398** proved to be decent with an EQE of 12.0%. The substituents on the phenylpyridine had some influence on the emission of the complex, where the fluoride disubstituted complex **401** underwent a higher energy shift of ~30 nm. The authors theorised that the high quantum yields of the complexes in solution could be ascribed to the rigidity of the structure that is imposed by the linker between the NHC moieties and that these play a role in the brightness of the emitters.

Teets [159] investigated the photophysical properties of **337-339** (Table 6). Interestingly, the authors noted that these complexes did not emit in solution. However, once doped on solid PMMA support, deep-blue emission was observed. Due to the lack of emission in a solvent, the τ values could not be obtained. In a later study [160], complexes **345-347** were studied for

their photophysical properties (Table 6). Similarly to **337-339** complex **345** did not emit in solution, however once doped on the PMMA support, emission was observed.

Cheng and co-workers [157] reported the photophysical properties of complexes **350-354** (Table 6). The authors observed that the Φ_{PL} values showed a dependence on the type of N^N ligand present. With complexes **350-352** containing the same ligand having similar activities. Where complexes **352-354** contain the same cyclometallated carbene ligand but different N^N ligands, gave an irregular trend. Subsequent OLEDs were constructed using **351**, **352** and **354**, with a range of EQEs of 9.1-15.2%. The OLED constructed with complex **352** as dopant was the most effective with the EQE of 15.2%.

Braunstein [175] tested their complexes **363a** and **363b** for their photophysics in solution and solid state. Both **363a** and **363b** exhibited high Φ_{PL} of 41% and 38%, respectively, in CH_3CN. The excited state lifetimes for each where 8.9 and 9.4 µs. When changing from CH_3CN at room temperature to butyronitrile at 77 K, a hypsochromic shift with longer lifetimes of 15.7 and 15.2 µs for **363a** and **363b**, respectively, were observed. This suggests that the excited states of the frozen complexes are more ligand-centred, due to the lack of solvent stabilisation in the rigid matrix. Some differences were noted in comparing the behaviour of the complexes in solid state to that in solution. Crystals of **363a** exhibited a broad and featureless emission profile with a large decrease in excited-state lifetime and Φ value (12% compared to 41% in solution). Interestingly, **363b** did not show such a significant decrease, with a Φ value of 20% in solid state compared to 38% in solution. Preliminary electroluminescent devices were constructed by spin coating **363a/363b** and PMMA (1:1) in chlorobenzene. The authors used various doping concentrations (from 5-100%). Even though the efficiency of the unoptimised device was low, electroluminescence in the near-UV region was observed (386 and 406 nm). Complex **363b** was the most effective as dopant with a Φ value of 0.40 and a longer excited state lifetime of 9.1 µs compared to **363a** (Φ of 30% and 6.5 µs lifetime). As the doping concentration was increased to 100%, the activity of the devices decreased from quantum yields of 40% for **363b** at 5% concentration to 5% Φ at 100% concentration. The authors theorised that this decrease in activity was due to formation of trapping species.

Wong and co-workers [170] reported the emission data for their range of complexes **383-390** in solution at 298 K with a complex concentration of 3.0×10^{-5} M (Table 6). In general, it was observed that CH_2Cl_2 proved to be a better solvent for emission spectroscopy with higher quantum yields achieved as well has longer lifetimes of the excited states of the complexes. It is clear that complex **384** was the most efficient of the range of complexes due to its Φ and

lifetime in both CH_3CN and CH_2Cl (3.50%, 0.2244 µs in CH_3CN and 11.9%, 0.790 µs in CH_2Cl_2, respectively).

Thompson and co-workers [179] tested their complexes **416-417** for near-UV phosphorescence. Both complexes showed strong emission at 77K in the near-UV spectrum and both luminesced at room temperature in solution. Both facial and meridional isomers of the two compounds were studied. The quantum yields due to photoluminescence (Φ_{PL}) for *fac*-**416** and *mer*-**416** were relatively low (2% and 5%, respectively). There was a greater difference between the Φ_{PL} values of the *fac*- and *mer*-isomers of **417**, with quantum yields of 4% and 0.2% respectively. The emission spectra of both complexes have luminescent lifetimes between 2 and 7 µs with the emission spectra between the two isomers being very similar in appearance. The radiative and non-radiative decay rates of *fac*-**416** ($k_r = 5 \times 10^4$ s^{-1}, $k_{nr} = 2 \times 10^6$ s^{-1}) are similar to those of *fac*-**417** ($k_r = 1.8 \times 10^5$ s^{-1}, $k_r = 4 \times 10^6$ s^{-1}). Interestingly, the *mer*-isomer of **417** has a lower photoluminesence efficiency and a higher nonradiative decay than the *fac*-isomer. Both compounds were found to have low stability at room temperature and the lifetimes of these could be improved by cooling them down to low temperatures or by immobilising the complexes in a rigid matrix. The authors tested this by dispersing complexes **416-417** in polystyrene, which increased the lifetimes by almost an order of magnitude at room temperature. This behaviour means that these complexes act as phosphorescent dopants in applications such as OLEDs.

Table 6. Emission properties of a range of complexes.

Complex	Temperature (K)	Solvent	Quantum yield (Φ) (%)	Lifetime (τ)/µs	Ref.
291	298	CH_2Cl_2	6	1.9	[152]
282	298	CH_2Cl_2	14	2.1	[152]
287	298	CH_2Cl_2	26	1.7	[152]
273	298	CH_2Cl_2	65	1.8	[152]
288	298	CH_2Cl_2	37	1.9	[152]
280	298	CH_2Cl_2	73	1.8	[152]
289	298	CH_2Cl_2	30	1.8	[152]
281	298	CH_2Cl_2	57	1.9	[152]
290	298	CH_2Cl_2	51	1.9	[152]

283	298	CH_2Cl_2	69	1.8	[152]
297	298	CH_2Cl_2	63	1.9	[152]
284	298	CH_2Cl_2	61	1.8	[152]
298	298	CH_2Cl_2	28	1.9	[152]
285	298	CH_2Cl_2	33	1.7	[152]
299	298	CH_2Cl_2	11	1.7	[152]
286	298	CH_2Cl_2	32	1.9	[152]
292	298	CH_2Cl_2	9	2.1	[152]
293	298	CH_2Cl_2	25	1.9	[152]
294	298	CH_2Cl_2	32	1.7	[152]
295	298	CH_2Cl_2	30	1.8	[152]
296	298	CH_2Cl_2	62	2.1	[152]
273	298	CH_2Cl_2	9	350	[149]
274	298	CH_2Cl_2	13.3	280	[149]
275	298	EtOH	26	0.5	[150]
276	298	EtOH	31	0.5	[150]
301	298	Toluene	16	5.3	[153]
300	298	Toluene	15	3.52	[153]
303	298	Toluene	6.4	2.64	[153]
304	298	Toluene	4.6	2.48	[153]
302	298	Toluene	1.6	0.16	[153]
306	298	Toluene	8.8	4.03	[153]
307	77	THF	60	17.6	[155]
315	298	Toluene	0.27	0.045	[153]
345	298	CH_2Cl_2	-	-	[160]
		PMMA	13	6.1	
346	298	CH_2Cl_2	1.3	-	[160]
		PMMA	31	1.8	
347	298	CH_2Cl_2	39	-	[160]
		PMMA	48	0.85	
350	298	PMMA	16.6	1.2	[157]
351	298	PMMA	18.0	1.0	[157]
352	298	PMMA	16.5	1.0	[157]

353	298	PMMA	30.7	6.5	[157]
354	298	PMMA	11.0	1.0	[157]
383	298	CH_3CN	0.453	0.021	[170]
384	298	CH_3CN	3.50	0.244	[170]
385	298	CH_3CN	1.09	0.038	[170]
386	298	CH_3CN	0.797	0.030	[170]
387	298	CH_3CN	0.200	0.010	[170]
388	298	CH_3CN	0.899	0.051	[170]
389	298	CH_3CN	0.418	0.015	[170]
390	298	CH_3CN	0.245	0.011	[170]
383	298	CH_2Cl_2	1.34	0.047	[170]
384	298	CH_2Cl_2	11.9	0.790	[170]
385	298	CH_2Cl_2	3.31	0.091	[170]
386	298	CH_2Cl_2	3.82	0.121	[170]
387	298	CH_2Cl_2	0.603	0.026	[170]
388	298	CH_2Cl_2	4.92	0.181	[170]
389	298	CH_2Cl_2	1.35	0.043	[170]
390	298	CH_2Cl_2	1.16	0.051	[170]
321a	298	PMMA	70	1.3	[156]
		2-MeTHF	93	1.8	
321b	298	PMMA	71	1.3	[156]
		2-MeTHF	78	1.8	
322a	298	PMMA	86	1.5	[156]
		2-MeTHF	67	1.4	
322b	298	PMMA	77	1.3	[156]
		2-MeTHF	90	1.1	
323a	298	PMMA	87	1.1	[156]
		2-MeTHF	56	0.2	
323b	298	PMMA	72	1.0	[156]
		2-MeTHF	74	0.6	
326a	298	PMMA	34	0.2	[156]
		2-MeTHF	40	0.9	
337	298	PMMA	13	-	[159]

338	298	PMMA	14	-	[159]
339	298	PMMA	14	-	[159]
397	298	PMMA	73	2.1	[173]
		MeTHF	60	1.2	
398	298	PMMA	49	4.1	[173]
			56	4.1	
400	298	2-MeTHF	~100	3.9	[174]
401	298	PMMA	87	1.3	[174]
401	298	2-MeTHF	73	1.6	[174]
402	298	PMMA	93	1.7	[174]
402	298	2-MeTHF	~100	3.1	[174]
403	298	PMMA	96	1.8	[174]
403	298	2-MeTHF	~100	2.4	[174]
***Fac*-424**	298	CH_2Cl_2	68	11.2	[182]
***Mer*-424**	298	CH_2Cl_2	53	11.0	[182]
425	298	CH_2Cl_2	72	0.28, 18.12	[183]
426	298	CH_2Cl_2	25	0.698, 18.20	[183]
429	298	2-MeTHF	95	0.116	[184]

Thompson [180] investigated the phosphorescent capabilities of the *fac*- and *mer*-isomers of complex **422** in de-aerated 2-MeTHF. The *fac*- and *mer*-isomers showed Φ of 76 ± 5% and 78 ± 5%, respectively, at 295 K. The quantum yields were greatly improved at a lower temperature for both isomers (Φ = 95 ± 5% at 77K). The excited state lifetime for both isomers also improved from 1.2 µs (*fac*-isomer) and 0.8 µs (*mer*-isomer) at 295 K to 3.9 and 1.0 µs, respectively, at 77 K. A shorter lifetime for the *mer*-isomer results in a higher $k_r = 1.0 \pm 0.2 \times 10^6\ s^{-1}$ *vs* the *fac*-isomer which had a $k_r = 6.4 \pm 1.3 \times 10^5\ s^{-1}$. Meanwhile the non-radiative decay of both isomers were found to be similar (approximately 2.0-2.7 x $10^5\ s^{-1}$). PHOLEDs (phosphorescent organic light-emitting devices) were constructed using both the *mer*- and *fac*-isomers. The *mer*-isomer constructed device had a higher external quantum effeciency (EQE) at 14.4 ± 0.4% *vs* 10.1 ± 0.2% for the *fac*-isomer at low luminance. The EQE decreased slightly (9.0 and 13.3% respectively) at L = 1000 cd.m^{-2} and it decreased by 50% at L = 7800 cd.m^{-2}. Interestingly, the EQE difference of the *fac*-isomer *vs* the *mer*-isomer was found to be

consistent with the trend found in solid-state photoluminescence quantum yields of the isomers doped in TSPO1 (diphenyl-4-triphenylsilylphenylphosphine oxide).

Wong and co-workers [181] reported that the five *mer*-isomer triscarbene complexes **418-423** all exhibited strong blue emissions at 420-450 nm with high Φ values at low temperatures. It was noted that complex **421** obtained a lower Φ (75%) compared to **418-420** and **422** most likely due to the stronger rotation of the *tert*-butyl substituent, which may quench the excited state of **421** in solution. Complexes **418**, **419**, **420**, and **422** had Φ values of 85%, 97.5%, 99%, and 78% respectively. Subsequent PHOLEDs fabricated with complexes **418**, **420** and **421** showed an EQE range of 7.6-19.0% at maximum efficiency.

Kang [182] reported that the two isomers of complex **424**, the *fac*- and *mer*-isomers, were studied for their photophysical properties (Table 6). As with many complexes in this section, the excited state lifetime was longer at the lower temperature of 77 K (20.7 and 23.7 μs for the *fac*- and *mer*-isomers, respectively). PHOLEDs constructed from the two isomers were evaluated as well, with their activity being very similar. The *fac*-isomer of **391** had a slightly better EQE of 18.5% compared to 18.2% for the mer-isomer at maximum efficency.

Zysman-Colman and co-workers [183] described highly efficient blue OLEDs based on complexes **425-426**. Complex **425** was found to be the most efficient with a high Φ (72%) in de-aerated DCM. Both complexes showed biexponential excited state lifetimes (τ) with longer τ values at 77 K. The Φ values of the complexes when doped, showed a similar trend where Φ for **425** is 46.6% and 13.7% for **426**. The authors continued to manufacture OLEDs based on **425** with a variety of different architectures, achieving a range of EQE from 7.2-13.4%. The use of **426** in the electron blocking layer (EBL) of the devices gave better performance (12.3-13.4%).

Jin [184] applied their complexes **427-429** in blue PHOLEDs. Complexes **427-428** were insoluble in 2-MeTHF thus they did not calculate the Φ values for eitherwhile complex **429** was found to have Φ of 95%. The photoluminescence intensity for **429** increased as the viscosity/rigidity of the medium increased, i.e. luminescence intensities were higher in DMSO than in DCM and higher for solid state than for solution. In solution the τ values were low (0.116-0.159 μs). However, they increased drastically when doped (10 wt%) on a PMMA film (2.48-6.2 μs). Complex **429** showed the highest Φ but had the lowest τ, while **427** had the longest lifetimes. The authors created pure blue PHOLEDs from the complexes by doping 20% on TSPO1, with complex **427** giving the highest EQE at 8.6% but relatively low values for complexes **428** (3.8%) and **429** (7.1%).

In summary, the complexes with the highest quantum yields (≥95%) were found to be **266**, **393**, **395**, **402**, **403**, **419**, **420** and **429**. However many of these high performing luminescent complexes had short excited state life-times (<10 μs). The complexes with the longest excited state life-times were found to be **273** and **274** (350 and 280 μs, respectively) although their performances were poor, with low Φ values (9 and 13.3%, respectively). The best performing OLED was found to be the **395**-containing OLED with an EQE of 21.6%, while the best performing PHOLEDs were devices constructed from **296** and **302**, where both achieved an EQE of 20.6%

5.3 Biological

Despite the extensive applications for the complexes mentioned in this review, literature reports that focus on biological applications are limited. Only the iridium complexes of this study have been studied for biological application, with the first article published only recently (2013). The lack in literature for this application shows that this field offers vast novel research opportunities.

Liu [138] applied their half-sandwich Ir(III) NHC complexes (**222-225**) to antitumor and other biological applications. The complexes were tested against A549 lung cancer cells using the MTT (3-(4,5-dimethyl-2-thiazolyl)-2,5-diphenyltetrazolium bromide) assay after 24 hours. The IC_{50} values obtained showed better activity than the widely used anti-cancer agent *cis*-platin (IC_{50} of 21.3 ± 1.7 μM), with the IC_{50} values ranging from 3.9 to 11.8 μM. Complex **225** showed the best activity with the lowest IC_{50} value, which the authors theorised is most likely due to the added lipophilicity of **225** with additional phenyl rings. The authors also reported the lipophilicity (log $P_{o/w}$) of each complex, a value indicating how well a complex is able to permeate through the cell membranes, which is essential for cell imaging. The log $P_{o/w}$ of complexes **222** and **225** were -1.12 and -0.57, respectively. This shows that fusion of a benzene ring to the backbone of the NHC ligand in combination with phenyl moieties on the substituents, effectively increased the lipid solubility of **225**.

Sun [154] tested their complexes **308-312** for photodynamic therapy and antimicrobial activity (Scheme 91). For photodynamic therapy highly photoluminescent complexes are required, hence the photophysical properties of the complexes were determined, and Φ values ranging from 1% to 6.3% with relatively long excited state lifetimes of 3.12-4.96 μs were found. The ability of each complexes to produce singlet oxygen was assessed in CH_3CN. Complex **310** was found to be the most effective at generating singlet oxygen at all wavelengths with a

quantum yield of close to 37%. Complexes **310** and **312** were tested for cytotoxicity and photocytotoxicity towards human melanoma cell line SKMEL28 by exposing the cancer cells to 1nM – 300 µM solutions of the complexes. Complex **310** was non-toxic towards SKMEL28 with half maximal effective concentration (EC_{50}) of >300 µM, while **312** was cytotoxic with an EC_{50} value of 20 µM. Both complexes were observed to be photocytotoxic (with visible light) with **312** exhibiting EC_{50} of 150 nM and **310** an EC_{50} of 10 µM. Using red light, both complexes showed a decreased phytocytotoxic activity but the EC_{50} were still lower than observed without light. The complexes were also tested for activity against *Staphylococcus aureus*. Despite **310** being active against SKMEL28 cells, it was inactive against *S. aureus* in both light and dark conditions. However, **312** was non-toxic in the dark but very phototoxic in visible light with EC_{50} of 6.67 µM.

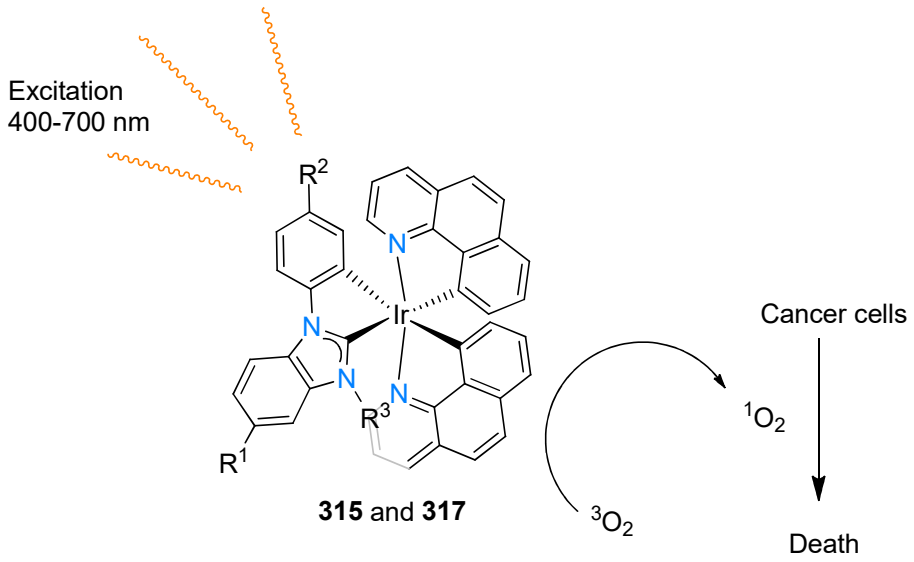

Scheme 91. Photocytotoxicity of complexes **315** and **317**.

Zhou [158] tested complexes **330-334** as living cell imaging reagents. Linking with what was covered in the previous section, the luminescent complexes were first tested for their cytotoxicity towards HeLa and A549 cell lines using the MTT assay. The half maximal inhibitory concentration values (IC_{50} values) were shown to be in a range of 49.80->200 µM towards the HeLa cell line and a range of 62.57->200 µM towards A549 cell line. Both complexes with $–CF_3$ moieties, **331** and **334**, exhibited the highest cytotoxicity. The log $P_{o/w}$ values were in a range of 0.56 to 1.57, with the neutral complexes (**330-332**) having higher values than the cationic complexes (**333-334**). To determine cell imaging capabilities, HeLa

cells were incubated with complexes **330-334** (20 μM) at 37 °C for 2 hours. Intense intracellular luminescence was observed in the living HeLa cells The authors performed the same tests at 4 °C and no luminescence was observed, thus suggesting there is an energy dependent process for the cellular uptake of the complexes.

6. Conclusion and outlook

Multidentate NHC complexes of group IX metals featuring carbon-based tethers show an impressive variety in structure and application. The range of carbon-based N-tether groups that exhibit a variety of hybridization states add to the versatility of the resulting multidentate NHC ligands to be tailored to the electronic requirements of the metal and its subsequent applications. The atom-specific tether derivatives that have been developed underpins their versatility and adaptiveness to unique chemical environments to provide stability and function to their corresponding metal complexes, more so than the corresponding pnictogen and chalcogen tether groups. The pre- and post-coordination functionalisation of the carbon-tethered NHC ligands to group IX metals presents a unique opportunity for the isolation and application of reactive, catalytically active, and mostly stable complexes. Examples reviewed showed unique reactivity pathways of the metal complexes, and includes small molecule activation, C-H activation of sp^2- and the more difficult to activate sp^3-hydrocarbon groups, unusual migratory insertion reactions, facile interconversion between metal oxidation states, as well as an impressive array of homogeneous catalytic transformation reactions. The ever-expanding development of group IX carbon-tethered NHC complexes continues to highlight the usefulness of incorporation of functionalised NHC ligands into transition metal complexes for more than just complex stabilisation. Ongoing efforts in ligand development will hopefully see the expansion of Co-NHC complex chemistry and its applications as part of a global research trend to apply (photo/redox-)active and multi-functional ligand frameworks to earth-abundant transition metals.

Declaration of Competing Interest

The authors declare that they have no known competing financial interests or personal relationships that could have appeared to influence the work reported in this paper.

Acknowledgements

This work has received support from the South African National Research Foundation (ML Grant No. 120840, FPM Grant No. 117995) and the University of Pretoria (ML, FPM).

References

[1] K. Riener, S. Haslinger, A. Raba, M.P. Högerl, M. Cokoja, W.A. Herrmann, F.E. Kühn, Chem. Rev., 114 (2014) 5215-5272. https://doi.org/10.1021/cr4006439.
[2] M.G. Gardiner, C.C. Ho, Coord. Chem. Rev., 375 (2018) 373-388. https://doi.org/10.1016/j.ccr.2018.02.003.
[3] A.D. Ibrahim, K. Tokmic, M.R. Brennan, D. Kim, E.M. Matson, M.J. Nilges, J.A. Bertke, A.R. Fout, Dalton Trans., 45 (2016) 9805-9811. https://doi.org/10.1039/C5DT04723D.
[4] M. Iglesias, L.A. Oro, Chem. Soc. Rev., 47 (2018) 2772-2808. https://doi.org/10.1039/C7CS00743D.
[5] B.D. Stringer, L.M. Quan, P.J. Barnard, D.J.D. Wilson, C.F. Hogan, Organometallics, 33 (2014) 4860-4872. https://doi.org/10.1021/om500076w.
[6] Y. Chi, T.-K. Chang, P. Ganesan, P. Rajakannu, Coord. Chem. Rev., 346 (2017) 91-100. https://doi.org/10.1016/j.ccr.2016.11.016.
[7] R. Visbal, M.C. Gimeno, Chem. Soc. Rev., 43 (2014) 3551-3574. https://doi.org/10.1039/C3CS60466G.
[8] C.A. Smith, M.R. Narouz, P.A. Lummis, I. Singh, A. Nazemi, C.-H. Li, C.M. Crudden, Chem. Rev., 119 (2019) 4986-5056. https://doi.org/10.1021/acs.chemrev.8b00514.
[9] L. Oehninger, R. Rubbiani, I. Ott, Dalton Trans., 42 (2013) 3269-3284. https://doi.org/10.1039/C2DT32617E.
[10] M. Soleilhavoup, G. Bertrand, Acc. Chem. Res., 48 (2015) 256-266. https://doi.org/10.1021/ar5003494.
[11] P.A. Guńka, W. Buchowicz, Dalton Trans., 45 (2016) 8688-8692. https://doi.org/10.1039/C5DT04663G.
[12] S. Hameury, P. de Frémont, P. Braunstein, Chem. Soc. Rev., 46 (2017) 632-733. https://doi.org/10.1039/C6CS00499G.
[13] A. Vivancos, C. Segarra, M. Albrecht, Chem. Rev., 118 (2018) 9493-9586. https://doi.org/10.1021/acs.chemrev.8b00148.
[14] J.B. Waters, J.M. Goicoechea, Coord. Chem. Rev., 293 (2015) 80-94. https://doi.org/10.1016/j.ccr.2014.09.020.
[15] S. Gründemann, A. Kovacevic, M. Albrecht, J.W. Faller, R.H. Crabtree, J. Am. Chem. Soc., 124 (2002) 10473-10481. 10.1021/ja026735g.
[16] A.R. Chianese, S.E. Shaner, J.A. Tendler, D.M. Pudalov, D.Y. Shopov, D. Kim, S.L. Rogers, A. Mo, Organometallics, 31 (2012) 7359-7367. https://doi.org/10.1021/om300468d.
[17] F.E. Hahn, C. Holtgrewe, T. Pape, M. Martin, E. Sola, L.A. Oro, Organometallics, 24 (2005) 2203-2209. https://doi.org/10.1021/om0500873.
[18] A.P. da Costa, M. Viciano, M. Sanaú, S. Merino, J. Tejeda, E. Peris, B. Royo, Organometallics, 27 (2008) 1305-1309. https://doi.org/10.1021/om701186u.
[19] M.-M. Gan, J.-Q. Liu, L. Zhang, Y.-Y. Wang, F.E. Hahn, Y.-F. Han, Chem. Rev., 118 (2018) 9587-9641. https://doi.org/10.1021/acs.chemrev.8b00119.
[20] E. Peris, Chem. Rev., 118 (2017) 9988-10031. https://doi.org/10.1021/acs.chemrev.6b00695.

[21] P. Braunstein, F. Naud, Angew. Chem. Int., 40 (2001) 680-699. 10.1002/1521-3773(20010216)40:4<680::aid-anie6800>3.0.co;2-0.
[22] A. Bader, E. Lindner, Coord. Chem. Rev., 108 (1991) 27-110. https://doi.org/10.1016/0010-8545(91)80013-4.
[23] N.N. Greenwood, A. Earnshaw, Chemistry of the Elements (2nd ed.), Butterworth-Heinemann, Oxford, 1997.
[24] K. Szabo, O. Wendt, Pincer and pincer-type complexes, Wiley Online Library, 2014.
[25] D. Morales-Morales, Pincer Compounds: Chemistry and Applications, Elsevier, 2018.
[26] G. Van Koten, R.A. Gossage, The privileged pincer-metal platform: Coordination chemistry & applications, Springer, 2015.
[27] D. Morales-Morales, C.G. Jensen, The chemistry of pincer compounds, Elsevier, 2011.
[28] J.A. Przyojski, H.D. Arman, Z.J. Tonzetich, Organometallics, 32 (2013) 723-732. 10.1021/om3010756.
[29] M. Asay, D. Morales-Morales, Dalton Trans., 44 (2015) 17432-17447. 10.1039/C5DT02295A.
[30] K. Tokmic, C.R. Markus, L. Zhu, A.R. Fout, J. Am. Chem. Soc., 138 (2016) 11907-11913. 10.1021/jacs.6b07066.
[31] K. Tokmic, B.J. Jackson, A. Salazar, T.J. Woods, A.R. Fout, J. Am. Chem. Soc., 139 (2017) 13554-13561. https://doi.org/10.1021/jacs.7b07368.
[32] E.L. Kolychev, S. Kronig, K. Brandhorst, M. Freytag, P.G. Jones, M. Tamm, J. Am. Chem. Soc., 135 (2013) 12448-12459. https://doi.org/10.1021/ja406529c.
[33] K.Y. Wan, F. Roelfes, A.J. Lough, F.E. Hahn, R.H. Morris, Organometallics, 37 (2018) 491-504. https://doi.org/10.1021/acs.organomet.7b00915.
[34] H. Valdés, M.A. García-Eleno, D. Canseco-Gonzalez, D. Morales-Morales, ChemCatChem, 10 (2018) 3136-3172. 10.1002/cctc.201702019.
[35] A. Azua, J.A. Mata, E. Peris, Organometallics, 30 (2011) 5532-5536. 10.1021/om200796c.
[36] U. Hintermair, J. Campos, T.P. Brewster, L.M. Pratt, N.D. Schley, R.H. Crabtree, ACS Catal., 4 (2014) 99-108. https://doi.org/10.1021/cs400834q.
[37] J. Holmes, C.M. Pask, C.E. Willans, Dalton Trans., 45 (2016) 15818-15827. https://doi.org/10.1039/C6DT02079H.
[38] S. Semwal, D. Ghorai, J. Choudhury, Organometallics, 33 (2014) 7118-7124. https://doi.org/10.1021/om500876k.
[39] A. Volpe, S. Baldino, C. Tubaro, W. Baratta, M. Basato, C. Graiff, Eur. J. Inorg. Chem., (2016) 247-251. https://doi.org/10.1002/ejic.201501027.
[40] R. Corberán, M. Sanaú, E. Peris, Organometallics, 26 (2007) 3492-3498. https://doi.org/10.1021/om070188w.
[41] T. Chen, X.-G. Liu, M. Shi, Tetrahedron, 63 (2007) 4874-4880. https://doi.org/10.1016/j.tet.2007.03.150.
[42] S. Gülcemal, D. Gìlcemal, G.F.S. Whitehead, J. Xiao, Chem. Eur. J., 22 (2016) 10513-10522. https://doi.org/10.1002/chem.201601648.
[43] T.P. Brewster, J.D. Blakemore, N.D. Schley, C.D. Incarvito, N. Hazari, G.W. Brudvig, R.H. Crabtree, Organometallics, 30 (2011) 965-973. https://doi.org/10.1021/om101016s.
[44] A. Savini, A. Bucci, G. Bellachioma, S. Giancola, F. Palomba, L. Rocchigiani, A. Rossi, M. Suriani, C. Zuccaccia, A. Macchioni, J. Organomet. Chem., 771 (2014) 24-32. https://doi.org/10.1016/j.jorganchem.2014.05.029.
[45] Z. Codolà, J.M.S. Cardoso, B. Royo, M. Costas, J. Lloret-Fillol, Chem. Eur. J., 19 (2013) 7203-7213. https://doi.org/10.1002/chem.201204568.
[46] M. Kim, S. Chang, Org. Lett., 12 (2010) 1640-1643. 10.1021/ol100437j.
[47] H. van Rensburg, R.P. Tooze, D.F. Foster, A.M.Z. Slawin, Inorg. Chem., 43 (2004) 2468-2470. 10.1021/ic049917f.

[48] J.M. Praetorius, M.W. Kotyk, J.D. Webb, R. Wang, C.M. Crudden, Organometallics, 26 (2007) 1057-1061. 10.1021/om060942y.
[49] W. Gil, A.M. Trzeciak, J.J. Ziółkowski, Organometallics, 27 (2008) 4131-4138. 10.1021/om800143m.
[50] S. De, A. Udvardy, C.E. Czégéni, F. Joó, Coord. Chem. Rev., 400 (2019) 213038. https://doi.org/10.1016/j.ccr.2019.213038.
[51] M. Poyatos, J.A. Mata, E. Peris, Chem. Rev., 109 (2009) 3677-3707. https://doi.org/10.1021/cr800501s.
[52] N.U.D. Reshi, J.K. Bera, Coord. Chem. Rev., 422 (2020) 213334. https://doi.org/10.1016/j.ccr.2020.213334.
[53] V. Charra, P. de Fremont, P. Braunstein, Coord. Chem. Rev., 341 (2017) 53-176. https://doi.org/10.1016/j.ccr.2017.03.007.
[54] G. Sipos, R. Dorta, Coord. Chem. Rev., 375 (2018) 13-68. https://doi.org/10.1016/j.ccr.2017.10.019.
[55] A.A. Danopoulos, T. Simler, P. Braunstein, Chem. Rev., 119 (2019) 3730-3961. https://doi.org/10.1021/acs.chemrev.8b00505.
[56] W. Gil, A.M. Trzeciak, Coord. Chem. Rev., 255 (2011) 473-483. https://doi.org/10.1016/j.ccr.2010.11.005.
[57] Y.-F. Han, G.-X. Jin, Chem. Soc. Rev., 43 (2014) 2799-2823. https://doi.org/10.1039/C3CS60343A.
[58] M. Albrecht, Chem. Rev., 110 (2010) 576-623. https://doi.org/10.1021/cr900279a.
[59] Y. Tian, T. Maulbetsch, R. Jordan, K.W. Törnroos, D. Kunz, Organometallics, 39 (2020) 1221-1229. https://doi.org/10.1021/acs.organomet.0c00018.
[60] J. Du, L. Wang, M. Xie, L. Deng, Angew. Chem. Int., 54 (2015) 12640-12644. https://doi.org/10.1002/anie.201505937.
[61] Y. Gao, Q. Chen, X. Leng, L. Deng, Dalton Trans., 48 (2019) 9676-9683. https://doi.org/10.1039/C9DT00731H.
[62] J. Sun, L. Luo, Y. Luo, L. Deng, Angew. Chem. Int, 56 (2017) 2720-2724. https://doi.org/10.1002/anie.201611162.
[63] Z. Mo, D. Chen, X. Leng, L. Deng, Organometallics, 31 (2012) 7040-7043. https://doi.org/10.1021/om300804a.
[64] Z. Mo, Y. Liu, L. Deng, Angew. Chem. Int. Ed., 52 (2013) 10845-10849. https://doi.org/10.1002/ange.201304596.
[65] J. Sun, C. Ou, C. Wang, M. Uchiyama, L. Deng, Organometallics, 34 (2015) 1546-1551. https://doi.org/10.1021/acs.organomet.5b00114.
[66] J. Sun, Y. Gao, L. Deng, Inorg. Chem., 56 (2017) 10775-10784. https://doi.org/10.1021/acs.inorgchem.7b01763.
[67] Y. Liu, J. Cheng, L. Deng, Acc. Chem. Res., (2019) 244-254. https://doi.org/10.1021/acs.accounts.9b00492.
[68] A.A. Danopoulos, J.A. Wright, W.B. Motherwell, S. Ellwood, Organometallics, 23 (2004) 4807-4810. https://doi.org/10.1021/om049489l.
[69] S.W. Reilly, C.E. Webster, T.K. Hollis, H.U. Valle, Dalton Trans., 45 (2016) 2823-2828. https://doi.org/10.1039/C5DT04752H.
[70] Z. Xi, B. Liu, C. Lu, W. Chen, Dalton Trans., (2009) 7008-7014. 10.1039/B906242D.
[71] R.P. Yu, J.M. Darmon, C. Milsmann, G.W. Margulieux, S.C.E. Stieber, S. DeBeer, P.J. Chirik, J. Am. Chem. Soc., 135 (2013) 13168-13184. 10.1021/ja406608u.
[72] J.A. Denny, R.W. Lamb, S.W. Reilly, B. Donnadieu, C.E. Webster, T.K. Hollis, Polyhedron, 151 (2018) 568-574. https://doi.org/10.1016/j.poly.2018.05.040.
[73] K.L. Tan, R.G. Bergman, J.A. Ellman, J. Am. Chem. Soc., 124 (2002) 3202-3203. https://doi.org/10.1021/ja017351d.

[74] J.C. Lewis, R.G. Bergman, J.A. Ellman, Acc. Chem. Res., 41 (2008) 1013-1025. https://doi.org/10.1021/ar800042p.
[75] J. Li, J. Peng, Y. Bai, G. Lai, X. Li, J. Organomet. Chem., 696 (2011) 2116-2121. https://doi.org/10.1016/j.jorganchem.2010.11.017.
[76] Y. Tian, E. Jürgens, D. Kunz, Chem. Commun., 54 (2018) 11340-11343. https://doi.org/10.1039/C8CC06503A.
[77] E.L. Kolychev, S. Kronig, K. Brandhorst, M. Freytag, P.G. Jones, M. Tamm, J. Am. Chem. Soc., 135 (2013) 12448-12459.
[78] M.O. Karataş, A. Di Giuseppe, V. Passarelli, B. Alıcı, J.J. Pérez-Torrente, L.A. Oro, I. Özdemir, R. Castarlenas, Organometallics, 37 (2018) 191-202. https://doi.org/10.1021/acs.organomet.7b00750.
[79] O.V. Zenkina, E.C. Keske, R. Wang, C.M. Crudden, Angew. Chem. Int., 50 (2011) 8100-8104. https://doi.org/10.1002/anie.201103316.
[80] J. Huang, E.D. Stevens, S.P. Nolan, Organometallics, 19 (2000) 1194-1197.
[81] J.H. Kim, S. Greßies, M. Boultadakis-Arapinis, C. Daniliuc, F. Glorius, ACS Catal., 6 (2016) 7652-7656. https://doi.org/10.1021/acscatal.6b02392.
[82] Y. Canac, C. Lepetit, M. Abdalilah, C. Duhayon, R. Chauvin, J. Am. Chem. Soc., 130 (2008) 8406-8413. https://doi.org/10.1021/ja801159v.
[83] R. Dorta, E.D. Stevens, S.P. Nolan, J. Am. Chem. Soc., 126 (2004) 5054-5055. https://doi.org/10.1021/ja049545+.
[84] N.M. Scott, R. Dorta, E.D. Stevens, A. Correa, L. Cavallo, S.P. Nolan, J. Am. Chem. Soc., 127 (2005) 3516-3526. https://doi.org/10.1021/ja043249f.
[85] W.B. Cross, C.G. Daly, Y. Boutadla, K. Singh, Dalton Trans., 40 (2011) 9722-9730. https://doi.org/10.1039/C1DT10753D.
[86] D. Ghorai, J. Choudhury, Chem. Commun., 50 (2014) 15159-15162. https://doi.org/10.1039/C4CC07170K.
[87] D. Ghorai, C. Dutta, J. Choudhury, ACS Catal., 6 (2016) 709-713. https://doi.org/10.1021/acscatal.5b02540.
[88] D. Ghorai, J. Choudhury, ACS Catal., 5 (2015) 2692-2696. https://doi.org/10.1021/acscatal.5b00243.
[89] R. Thenarukandiyil, J. Choudhury, Organometallics, 34 (2015) 1890-1897. https://doi.org/10.1021/acs.organomet.5b00157.
[90] R. Thenarukandiyil, H. Thrikkykkal, J. Choudhury, Organometallics, 35 (2016) 3007-3013. https://doi.org/10.1021/acs.organomet.6b00530.
[91] Q. Ge, B. Li, H. Songa, B. Wang, Org. Biomol. Chem., 13 (2015) 7695-7710. https://doi.org/10.1039/C5OB00823A.
[92] C. Segarra, E. Mas-Marzá, M. Benítez, J.A. Mata, E. Peris, Angew. Chem. Int. Ed., 51 (2012) 10841-10845. https://doi.org/10.1002/anie.201206175.
[93] A. McSkimming, G.E. Ball, M.M. Bhadbhade, S.B. Colbran, Inorg. Chem., 51 (2012) 2191-2203. https://doi.org/10.1021/ic202164v.
[94] M. Böhmer, G. Guisado-Barrios, F. Kampert, F. Roelfes, T.T.Y. Tan, E. Peris, F.E. Hahn, Organometallics, 38 (2019) 2120-2131. https://doi.org/10.1021/acs.organomet.9b00120.
[95] M. Böhmer, F. Kampert, T.T.Y. Tan, G. Guisado-Barrios, E. Peris, F.E. Hahn, Organometallics, 37 (2018) 4092-4099. https://doi.org/10.1021/acs.organomet.8b00642.
[96] R. Maity, A. Rit, C. Schulte to Brinke, C.G. Daniliuc, F.E. Hahn, Chem. Commun., 49 (2013) 1011-1013. https://doi.org/10.1039/C2CC37446C.
[97] B.K. Shaw, B.O. Patrick, M.D. Fryzuk, Organometallics, 31 (2012) 783-786. https://doi.org/10.1021/om201233e.
[98] H.P. Thomas, A.C. Marr, P.J. Morgan, G.C. Saunders, Organometallics, 37 (2018) 1339-1341. https://doi.org/10.1021/acs.organomet.8b00164.

[99] G. Lázaro, F.J. Fernández-Alvarez, J. Munárriz, V. Polo, M. Iglesias, J.J. Pérez-Torrente, L.A. Oro, Catal. Sci. Technol., 5 (2015) 1878-1887. https://doi.org/10.1039/C4CY01556Hv.
[100] W. Zhong, Z. Fei, R. Scopelliti, P.J. Dyson, Chem. Eur. J., 22 (2016) 12138-12144. https://doi.org/10.1002/chem.201602267.
[101] F. Aznarez, P.J. Sanz Miguel, T.T.Y. Tan, F.E. Hahn, Organometallics, 35 (2016) 410-419. https://doi.org/10.1021/acs.organomet.5b00993.
[102] F. Aznarez, W.-X. Gao, Y.-J. Lin, F.E. Hahn, G.-X. Jin, Dalton Trans., 47 (2018) 9442-9452. https://doi.org/10.1039/C8DT02212G.
[103] R.J. Rubio, G.T.S. Andavan, E.B. Bauer, T.K. Hollis, J. Cho, F.S. Tham, B. Donnadieu, J. Organomet. Chem., 690 (2005) 5353-5364. https://doi.org/10.1016/j.jorganchem.2005.05.007.
[104] G.T.S. Andavan, E.B. Bauer, C.S. Letko, T.K. Hollis, F.S. Tham, J. Organomet. Chem., 690 (2005) 5938-5947. https://doi.org/10.1016/j.jorganchem.2005.07.088.
[105] S.W. Reilly, G. Akurathi, H.K. Box, H.U. Valle, T.K. Hollis, C.E. Webster, J. Organomet. Chem., 802 (2016) 32-38. https://doi.org/10.1016/j.jorganchem.2015.11.010.
[106] J.-I. Ito, K. Sugino, S. Matsushima, H. Sakaguchi, H. Iwata, T. Ishihara, H. Nishiyama, Organometallics, 35 (2016) 1885-1894. https://doi.org/10.1021/acs.organomet.6b00239.
[107] J. Holmes, C.M. Pask, M.A. Fox, C.E. Willans, Chem. Commun., 52 (2016) 6443-6446. https://doi.org/10.1039/C6CC01650B.
[108] L. Benhamou, S. Bastin, N. Lugan, G. Lavigne, V. César, Dalton Trans., 43 (2014) 4474-4482. https://doi.org/10.1039/C3DT53089B.
[109] A. Labande, N. Debono, A. Sournia-Saquet, J.-C. Darana, R. Poli, Dalton Trans., 42 (2013) 6531-6537. https://doi.org/10.1039/C3DT50240F.
[110] N. Debono, J.-C. Daran, R. Poli, A. Labande, Polyhedron, 86 (2015) 57-63. https://doi.org/10.1016/j.poly.2014.04.050.
[111] A.P. da Costa, R. Lopes, J.M.S. Cardoso, J.A. Mata, E. Peris, B. Royo, Organometallics, 30 (2011) 4437-4442. https://doi.org/10.1021/om200523h.
[112] A.P. da Costa, M. Sanaú, E. Peris, B. Royo, Dalton Trans., (2009) 6960-6966.
[113] S.P. Downing, P.J. Pogorzelec, A.A. Danopoulos, D.J. Cole‐Hamilton, Eur. J. Inorg. Chem., 2009 (2009) 1816-1824. https://doi.org/10.1002/ejic.200801162.
[114] M. Prinz, M. Grosche, E. Herdtweck, W.A. Herrmann, Organometallics, 19 (2000) 1692-1694. https://doi.org/10.1021/om990804r.
[115] F.E. Hahn, B. Heidrich, T. Pape, A. Hepp, M. Martin, E. Sola, L.A. Oro, Inorganica Chim. Acta., 359 (2006) 4840-4846. https://doi.org/10.1016/j.ica.2006.07.010.
[116] A. Zanardi, E. Peris, J.A. Mata, New. J. Chem. , 32 (2008) 120-126. https://doi.org/10.1039/B707280E.
[117] C.Y. Tang, W. Smith, D. Vidovic, A.L. Thompson, A.B. Chaplin, S. Aldridge, Organometallics, 28 (2009) 3059-3066. https://doi.org/10.1021/om9000082.
[118] C.Y. Tang, A.L. Thompson, S. Aldridge, J. Am. Chem. Soc., 132 (2010) 10578-10591. https://doi.org/10.1021/ja1043787.
[119] C.Y. Tang, N. Phillips, M.J. Kelly, S. Aldridge, Chem. Commun., 48 (2012) 11999-12001. https://doi.org/10.1039/C2CC35947B.
[120] G. Sipos, A. Ou, B.W. Skelton, L. Falivene, L. Cavallo, R. Dorta, Chem. Eur. J., 22 (2016) 6939-6946. http://dx.doi.org/10.1002/chem.201600378.
[121] G. Sipos, P. Gao, D. Foster, B.W. Skelton, A.N. Sobolev, R. Dorta, Organometallics, 36 (2017) 801-817. https://doi.org/10.1016/j.ccr.2017.10.019.
[122] P. Gao, G. Sipos, D. Foster, R. Dorta, ACS Catal., 7 (2017) 6060-6064. https://doi.org/10.1021/acscatal.7b02508.
[123] P. Gao, D. Foster, G. Sipos, B.W. Skelton, A.N. Sobolev, S.A. Moggach, R. Dorta, Organometallics, 38 (2019) 3568-3581. https://doi.org/10.1021/acs.organomet.9b00414.

[124] P. Gao, D. Foster, G. Sipos, B.W. Skelton, A.N. Sobolev, R. Dorta, Organometallics, 39 (2020) 556-573. https://doi.org/10.1021/acs.organomet.9b00770.
[125] F. Hanasaka, Y. Tanabe, K. Fujita, R. Yamaguchi, Organometallics, 25 (2006) 826-831. https://doi.org/10.1021/om050723x.
[126] Y. Tanabe, F. Hanasaka, K. Fujita, R. Yamaguchi, Organometallics, 26 (2007) 4618-4626. https://doi.org/10.1021/om7004589.
[127] N.M. Scott, V. Pons, E.D. Stevens, D.M. Heinekey, S.P. Nolan, Angew. Chem. Int. Ed., 44 (2005) 2512-2515. https://doi.org/10.1002/anie.200463000.
[128] G.C. Fortman, H. Jacobsen, L. Cavallo, S.P. Nolan, Chem. Commun., 47 (2011) 9723-9725. https://doi.org/10.1039/C1CC13492B.
[129] N. Phillips, C.Y. Tang, R. Tirfoin, M.J. Kelly, A.L. Thompson, M.J. Gutmann, S. Aldridge, Dalton Trans., 43 (2014) 12288-12298. https://doi.org/10.1039/C4DT01398K.
[130] J. Navarro, O. Torres, M. Martín, E. Sola, J. Am. Chem. Soc., 133 (2011) 9738-9740. https://doi.org/10.1021/ja204522e.
[131] O. Torres, M. Martin, E. Sola, Organometallics, 28 (2009) 863-870. https://doi.org/10.1021/om800965y.
[132] J.E. Wheatley, C.A. Ohlin, A.B. Chaplin, Chem. Commun., 50 (2014) 685-687. https://doi.org/10.1039/C3CC48015A.
[133] M. Benítez, E. Mas-Marzá, J.A. Mata, E. Peris, Chem. Eur. J., 17 (2011) 10453-10461. https://doi.org/10.1002/chem.201101187.
[134] M. Viciano, M. Feliz, R. Corberán, J.A. Mata, E. Clot, E. Peris, Organometallics, 26 (2007) 5304-5314. https://doi.org/10.1021/om7006979.
[135] R. Corberán, M. Sanaú, E. Peris, Organometallics, 25 (2006) 4002-4008. https://doi.org/10.1021/om060343r.
[136] R. Corberán, M. Sanaú, E. Peris, J. Am. Chem. Soc., 128 (2006) 3974-3979. https://doi.org/10.1021/ja058253l.
[137] S. Semwal, I. Mukkatt, R. Thenarukandiyil, J. Choudhury, Chem. Eur. J., 23 (2017) 13051-13057. https://doi.org/10.1002/chem.201785364.
[138] Y. Han, Z. Tian, S. Zhang, X. Liu, J. Li, Y. Li, Y. Liu, M. Gao, Z. Liu, J. Inorg. Biochem, 189 (2018) 163-171. https://doi.org/10.1016/j.jinorgbio.2018.09.009.
[139] M. Mondal, T.K. Ranjeesh, S.K. Gupta, J. Choudhury, Dalton Trans., 43 (2014) 9356-9362. https://doi.org/10.1039/C4DT00551A.
[140] S.K. Gupta, J. Choudhury, Dalton Trans., 44 (2015) 1233-1239. https://doi.org/10.1039/C4DT03161J.
[141] Z.G. Specht, D.B. Grotjahn, C.E. Moore, A.L. Rheingold, Organometallics, 32 (2013) 6400-6409. https://doi.org/10.1021/om400758b.
[142] R. Maity, H. Koppetz, A. Hepp, F.E. Hahn, J. Am. Chem. Soc., 135 (2013) 4966-4969. https://doi.org/10.1021/ja401546h.
[143] R. Maity, A. Rit, C. Schulte to Brinke, J. Kösters, F.E. Hahn, Organometallics, 32 (2013) 6174-6177. https://doi.org/10.1021/om400921c.
[144] F. Aznarez, M. Iglesias, A. Hepp, B. Veit, P.J.S. Miguel, L.A. Oro, G.-X. Jin, F.E. Hahn, Eur. J. Inorg. Chem., (2016) 4598-4603. http://dx.doi.org/10.1002/ejic.201600922.
[145] T.T.Y. Tan, F.E. Hahn, Organometallics, 38 (2019) 2250-2258. https://doi.org/10.1021/acs.organomet.9b00184.
[146] R.N.O. Yáñez, A. Hepp, T.T.Y. Tan, F.E. Hahn, Organometallics, 39 (2020) 344-352. https://doi.org/10.1021/acs.organomet.9b00759.
[147] A. Majumder, R. Naskar, P. Roy, R. Maity, Eur. J. Inorg. Chem., (2019) 1810-1815. https://doi.org/10.1002/ejic.201801570.

[148] J. Lin, N.-Y. Chau, J.-L. Liao, W.-Y. Wong, C.-Y. Lu, Z.-T. Sie, C.-H. Chang, M.A. Fox, P.J. Low, G.-H. Lee, Y. Chi, Organometallics, 35 (2016) 1813-1824. https://doi.org/10.1021/acs.organomet.6b00205.
[149] N. Hellou, M. Srebro-Hooper, L. Favereau, F. Zinna, E. Caytan, L. Toupet, V. Dorcet, M. Jean, N. Vanthuyne, J.A.G. Williams, L. Di Bari, J. Autschbach, J. Crassous, Angew. Chem. Int. Ed., 56 (2017) 8236-8239. https://doi.org/10.1002/ange.201704263.
[150] S.K. Gupta, A. Haridas, J. Choudhury, Chem. Eur. J., 23 (2017) 4770-4773. https://doi.org/10.1002/chem.201700668.
[151] S. Aghazada, A.J. Huckaba, A. Pertegas, A. Babaei, G. Grancini, I. Zimmermann, H. Bolink, M.K. Nazeeruddin, Eur. J. Inorg. Chem., (2016) 5089-5097. https://doi.org/10.1002/ejic.201600971.
[152] T.-Y. Li, X. Liang, L. Zhou, C. Wu, S. Zhang, X. Liu, G.-Z. Lu, L.-S. Xue, Y.-X. Zheng, J.-L. Zuo, Inorg. Chem., 54 (2015) 161-173. https://doi.org/10.1021/ic501949h.
[153] B. Liu, M.A. Jabed, J. Guo, W. Xu, S.L. Brown, A. Ugrinov, E.K. Hobbie, S. Kilina, A. Qin, W. Sun, Inorg. Chem., 58 (2019) 14377-14388. https://doi.org/10.1021/acs.inorgchem.9b01678.
[154] B. Liu, S. Monro, M.A. Jabed, C.G. Cameron, K.L. Colón, W. Xu, S. Kilina, S.A. McFarland, W. Sun, Photochem. Photobiol. Sci., 18 (2019) 2381-2396. https://doi.org/10.1039/C9PP00142E.
[155] Z. Chen, S. Suramitr, N. Zhu, C.-L. Ho, S. Hannongbua, S. Chen, W.-Y. Wong, J. Mater. Chem. C, 8 (2020) 2551-2557. https://doi.org/10.1039/C9TC05779J.
[156] V. Adamovich, S. Bajo, P.T. Boudreault, M.A. Esteruelas, A.M. López, J. Martín, M. Oliván, E. Oñate, A.U. Palacios, A. San-Torcuato, J.-Y. Tsai, C. Xia, Inorg. Chem., 57 (2018) 10744-10760. https://doi.org/10.1021/acs.inorgchem.8b01367.
[157] C.H. Hsieh, F.I. Wu, C.H. Fan, M.J. Huang, K.Y. Lu, P.Y. Chou, Y.H.O. Yang, S.H. Wu, I.C. Chen, S.H. Chou, Chem. Eur. J., 17 (2011) 9180-9187. https://doi.org/10.1002/chem.201100317.
[158] Y. Zhou, J. Jia, W. Li, H. Fei, M. Zhou, Chem. Commun., 49 (2013) 3230-3232. https://doi.org/10.1039/C3CC40845K.
[159] L.M. Cañada, J. Kölling, T.S. Teets, Polyhedron, 178 (2020) 114332. https://doi.org/10.1016/j.poly.2019.114332.
[160] H. Na, L.M. Cañada, Z. Wen, J.I.-C. Wu, T.S. Teets, Chem. Sci., 10 (2019) 6254-6260. https://doi.org/10.1039/C9SC01386E.
[161] M. Raynal, R. Pattacini, C.S.J. Cazin, C. Vallée, H. Olivier-Bourbigou, P. Braunstein, Organometallics, 28 (2009) 4028-4047. https://doi.org/10.1021/om900226c.
[162] W. Zuo, P. Braunstein, Organometallics, 29 (2010) 5535-5543. https://doi.org/10.1021/om100496x.
[163] W. Zuo, P. Braunstein, Organometallics, 31 (2012) 2606-2615. https://doi.org/10.1021/om200444q.
[164] W. Zuo, P. Braunstein, Dalton Trans., 41 (2012) 636-643. https://doi.org/10.1039/C1DT11511A.
[165] M. Jagenbrein, A.A. Danopoulos, P. Braunstein, J. Organomet. Chem., 775 (2015) 169-172. https://doi.org/10.1016/j.jorganchem.2014.05.035.
[166] M. Raynal, C.S.J. Cazin, C. Vallée, H. Olivier-Bourbigou, P. Braunstein, Chem. Commun., (2008) 3983-3985. https://doi.org/10.1039/B808806C.
[167] A.R. Chianese, A. Mo, N.L. Lampland, R.L. Swartz, P.T. Bremer, Organometallics, 29 (2010) 3019-3026. https://doi.org/10.1021/om100302g.
[168] S.M.M. Knapp, S.E. Shaner, D. Kim, D.Y. Shopov, J.A. Tendler, D.M. Pudalov, A.R. Chianese, Organometallics, 33 (2014) 473-484. https://doi.org/10.1021/om400786r.

[169] K.M. Schultz, K.I. Goldberg, D.G. Gusev, D.M. Heinekey, Organometallics, 30 (2011) 1429-1437. https://doi.org/10.1021/om101024x.
[170] L.-H. Chung, H.-S. Lo, S.-W. Ng, D.-L. Ma, C.H. Leung, C.-Y. Wong, Sci. Rep., 5 (2015) 15394. https://doi.org/10.1038/srep15394.
[171] L. González-Sebastián, A.B. Chaplin, Inorg. Chim. Acta, 460 (2017) 22-28. https://doi.org/10.1016/j.ica.2016.08.006.
[172] H.-H. Kuo, Z.-l. Zhu, C.-S. Lee, Y.-K. Chen, S.-H. Liu, P.-T. Chou, A.K.-Y. Jen, Y. Chi, Adv. Sci., 5 (2018) 1800846. https://doi.org/10.1002/advs.201800846.
[173] V. Adamovich, P.-L.T. Boudreault, M.A. Esteruelas, D. Gómez-Bautista, A.M. López, E. Oñate, J.-Y. Tsai, Organometallics, 38 (2019) 2738-2747. https://doi.org/10.1021/acs.organomet.9b00265.
[174] M.A. Esteruelas, A.M. López, E. Oñate, A. San-Torcuato, J.-Y. Tsai, C. Xia, Inorg. Chem., 57 (2018) 3720-3730. https://doi.org/10.1021/acs.inorgchem.7b02993.
[175] N. Darmawan, C.-H. Yang, M. Mauro, M. Raynal, S. Heun, J. Pan, H. Buchholz, P. Braunstein, L. De Cola, Inorg. Chem., 52 (2013) 10756-10765. https://doi.org/10.1021/ic302695q.
[176] A.A. Danopoulos, D. Pugh, J.A. Wright, Angew. Chem. Int. Ed., 47 (2008) 9765-9767. https://doi.org/10.1002/ange.200804573.
[177] M.A. Esteruelas, A.M. López, E. Oñate, A. San-Torcuato, J.-Y. Tsai, C. Xia, Organometallics, 36 (2017) 699-707. https://doi.org/10.1021/acs.organomet.6b00891.
[178] P.B. Hitchcock, M.F. Lappert, P. Terreros, J. Organomet. Chem., 239 (1982) C26-C30. https://doi.org/10.1016/S0022-328X(00)95275-6.
[179] T. Sajoto, P.I. Djurovich, A. Tamayo, M. Yousufuddin, R. Bau, M.E. Thompson, Inorg. Chem., 44 (2005) 7992-8003. https://doi.org/10.1021/ic051296i.
[180] J. Lee, H.-F. Chen, T. Batagoda, C. Coburn, P.I. Djurovich, M.E. Thompson, S.R. Forrest, Nat. Mater., 15 (2016) 92-99. https://doi.org/10.1038/nmat4446.
[181] Z. Chen, L. Wang, S. Su, X. Zheng, N. Zhu, C.-L. Ho, S. Chen, W.-Y. Wong, ACS Appl. Mater. Inter., 9 (2017) 40497-40502. https://doi.org/10.1021/acsami.7b09172.
[182] Y.-J. Cho, S.-Y. Kim, J.-H. Kim, J. Lee, D.W. Cho, S. Yi, H.-J. Son, W.-S. Han, S.O. Kang, J. Mater. Chem. C, 5 (2017) 1651-1659. https://doi.org/10.1039/C6TC04757B.
[183] A.K. Pal, S. Krotkus, M. Fontani, C.F.R. Mackenzie, D.B. Cordes, A.M.Z. Slawin, I.D.W. Samuel, E. Zysman-Colman, Adv. Mater., 30 (2018) 1804231. https://doi.org/10.1002/adma.201804231.
[184] G. Sarada, A. Maheshwaran, W. Cho, T. Lee, S.H. Han, J.Y. Lee, S.-H. Jin, Dyes Pigm., 150 (2018) 1-8. https://doi.org/10.1016/j.dyepig.2017.11.011.
[185] A.D. Ibrahim, S.W. Entsminger, L. Zhu, A.R. Fout, ACS Catal., 6 (2016) 3589-3593. https://doi.org/10.1021/acscatal.6b01091.
[186] E.B. Bauer, G.T.S. Andavan, T.K. Hollis, R.J. Rubio, J. Cho, G.R. Kuchenbeiser, T.R. Helgert, C.S. Letko, F.S. Tham, Org. Lett., 10 (2008) 1175-1178. https://doi.org/10.1021/ol8000766.
[187] S.W. Reilly, H.K. Box, G.R. Kuchenbeiser, R.J. Rubio, C.S. Letko, K.D. Cousineau, T.K. Hollis, Tetrahedron Lett., 55 (2014) 6738-6742. https://doi.org/10.1016/j.tetlet.2014.09.107.
[188] G.C. Fortman, A.M.Z. Slawin, S.P. Nolan, Organometallics, 30 (2011) 5487-5492. https://doi.org/10.1021/om2007437.
[189] H.R. Park, Y. Ha, Molecular Crystals and Liquid Crystals, 538 (2011) 67-74. 10.1080/15421406.2011.563645.
[190] E. Longhi, L. De Cola, Iridium(III) Complexes for OLED Application, in: Iridium(III) in Optoelectronic and Photonics Applications, 2017, pp. 205-274. https://doi.org/10.1002/9781119007166.ch6.

[191] L.F. Gildea, J.A.G. Williams, Iridium and platinum complexes for OLEDs, in: A. Buckley (Ed.) Organic Light-Emitting Diodes (OLEDs), Woodhead Publishing, 2013, pp. 77-113. https://doi.org/10.1533/9780857098948.1.77.